

Chapter 1. Outline of Geophysical Prospecting (See Fig. II-2)

The Iscay Cruz ore deposits are lead-zinc replacement deposits with host rock of limestone in the Santa formation.

The outcrop of deposits comprise iron-quartz gossan containing lead and zinc oxide disseminated lead and zinc sulfide. Mineralized zones from the first to the seventh are recognized along its length of about 12 km. About 400 meters west of the fifth mineralized zone lies Chupa ore deposit in the Pariahuanca formation.

Prospecting by induced polarization (IP) method using dipole-dipole configuration was carried out all over the above region in 1980.

Electromagnetic (EM) methods utilizing induction and VLF were also employed on some of the survey lines. These surveys revealed 3 remarkable FE (frequency effect) anomaly zones; No.1 anomaly zone in Chambre de Limpe, No.2 anomaly zone in the surrounding area of Chupa Mine, and No.3 anomaly zone in Antapampa. Among them, the following sectors were considered to require further prospecting, and were subjected to the survey in 1981:

(1) No.2 anomaly zone lying between Chupa Mine and Chunsha Punta:

EM was employed here to estimate the underground conductor since the ground surface is covered with talus and there are some topographical restrictions.

(2) No.3 anomaly zone in Antapampa: On the surface of this sector, non mineralized limestone and black gossans are distributed to the south of it. Partly because of the sparse setting of the survey lines, estimation concerning the size of the underground mineralized zone had been inconclusive. IP and EM methods on survey lines crossing over the Santa formation were employed to clarify the status of the mineralized

zone.

Survey lines subjected to IP method and EM method using VLF are as follows:

survey line	length	IP		EM		remarks
		electrode spacing	electrode separation index	station spacing	number of stations	
I	1.3 km			50 m	27	No.2 anomaly zone, N72°30'E
J	1.1			"	23	"
K	1.1			"	23	"
L	1.1			"	23	"
M	1.5			"	31	No.3 anomaly zone, N72°00'E
N	1.2			"	25	"
O	1.5	a = 100 m	n = 1 - 5	"	31	"
P	1.2	"	"			"
Q	1.3	"	"			"
R	1.3	"	"			"
S	1.2	"	"	50 m	25	"
T	1.5	"	"			"
U	2.5	"	"			along the Santa formation
Total	17.8	IP: 10.5 km		EM: 10 km		along the Santa formation

In addition, inductive EM survey (0.65 km) was executed on Line M. In-line configuration was selected. Transmitter-receiver distance was 200 feet.

Chapter 2. Methods of Prospecting and Data Analysis

Methods of prospecting and data analysis used in this survey were the same as those in the 1980 survey. The report of the year 1980 presents detailed descriptions of them.

Chapter 3. Results of Survey

3-1 Geology of the Surveyed Area

3-1-1 Geology and Geological Structure of Iscay Cruz Area

Sedimentary rocks of Cretaceous era, divided into the formations of Oyon, Chimu, Santa, Carhuaz, and Farrat in ascending order are distributed in Iscay Cruz area. Limestone of the upper layers are divided into the formations of Pariahuanca, Chulec, Pariatambo, Jumasha, Celendin, and Casapalca red formation in ascending order. Stock or dike form quartz porphyry, dacite, porphyrite, etc. are intruding. Sedimentary rocks generally strike in the NNW-SSE direction with dips varying between 70°W and 80°E.

3-1-2 Iscay Cruz Ore Deposits

Iscay Cruz ore deposits are embedded in the Santa formation in the west wing of the anticlinal structure which forms the axial trend lying on the Chimu formation. The Santa formation ranges in thickness from 40 to 80 meters.

Some faults and fissures run in the same direction as the trend of formation.

The ore deposits are embedded in carbonate rocks and consists of iron-quartz gossan, disseminated lead, zinc sulfides, skarn etc. The deposits are developed intermittently from the first mineralized zone at the northern end down to the seventh at the southern end.

The following describes the sixth and the seventh mineralized zones that were subject to this year's survey:

The sixth mineralized zone. An outcrop of black gossan is recognized from 0.5 to 0.6 km south of Cunsha Punta Pass. Sphalerite and pyrite are

concentrated in this gossan. Remarkably brecciated black gossan is found 0.4 km to the south of this outcrop. Between these are intermittent outcrops of limestone and dolostone spotted with small gossan.

The seventh mineralized zone: In the western mountainside of Antapampa, black gossan is 30 m wide and 250 m long to form the southernmost end of the Iscay Cruz mineralized zone. This gossan comprises quartz and goethite, and accompanying hematite. The northern sector of this gossan is limestone with small gossan, and is cut by a fault that runs in parallel to the strike of the formations. Along the fault is a recent conglomerate developed on the Santa formation.

3-2 IP Measurement with Dipole-Dipole Configuration

Profiles of AR (apparent resistivity), FE (frequency effect), and MF (metal factor) are reproduced in Pl. II-2-1 to Pl. II-2-7 by each survey line.

3-2-1 AR (apparent resistivity) Measurement

The apparent resistivity values range from 1 ohm m to over 9,000 ohm m. The measured values are classified into 5 reasonable ranges for convenience of analysis as shown below:

10 ohm m	40 ohm m	150 ohm m	650 ohm m	
UL	VL	L	M	H

Explanation is given in the following on the apparent resistivity measured on each survey line:

(1) Line 0 (See Pl. II-2-1)

Low (L) and lower ARs are detected in a "pant-legs" pattern centering on the shallow underground near the station 10.

This is an extremely low AR zone, lower than that detected near stations 65 - 70 on Line A in 1980 by a factor of about 1/5, and part of which shows ultra-low (UL) apparent resistivity.

Medium (M) and high (H) apparent resistivities are detected to the east and west along this zone.

This low AR zone is centered on a region where the Quaternary period sediment is distributed on the ground surface. Existence of limestone that belongs to the Santa formation is suggested by geological survey to the west and underneath the sediment of the Quaternary period. The medium and high AR zones correspond in situation, most probably, to the Chimu, Carhuaz, and Farrat formations.

(2) Line P (See Pl. II-2-2)

The values of AR along this line are similar to those along Line O.

Low (L) and lower ARs are found in a pant-legs pattern centered shallow underground near station 7.

Medium (M) ARs are detected to the east and west along this low AR zone.

The low AR zone is somewhat deeper than that on Line O. Limestone of the Santa formation and sediment of the Quaternary period is distributed on the surface. Since the Quaternary period sediment generally occurs only near the ground surface, the low AR zone is considered to correspond in situation to limestone of the Santa formation and its vicinity. The medium AR zone is considered to correspond in situation to the Chimu and Carhuaz formations.

(3) Line Q (See Pl. II-2-3)

Low (L) and lower ARs are detected near stations 5 to 9. The VL AR zone is deeper than those measured on Line O and Line P, and its size is about half of them.

Medium (M) ARs are detected to the east and west along this low AR zone.

This low AR zone corresponds in situation mainly to the Santa formation, Chimu formation, Carhuaz formation, and the Quaternary-period sediment. The medium AR zones are considered to correspond in situation to the Chimu and Carhuaz formations.

(4) Line B (See Pl. II-2-2 in 1980's report)

This survey line is located between Line Q and Line R and was surveyed in 1980. A part of the report of the former year is represented here to facilitate reference:

On the whole, low (L) AR is distributed widely, though medium (M) or higher (H) AR is observed near the surface ground of stations 3 - 4, 5 - 6, and 13 - 14. Medium to low (M-L) AR in the western sector of survey line to the west of station 4 is distributed corresponding to the Farrat formation, the Pariahuanca formation, etc. The low AR to the west of station 4 is distributed corresponding to the Carhuaz formation, the Santa formation, and the Chimu formation, while the medium AR detected near stations 13 - 14 is considered to correspond in locality to the Chimu formation because the location of the medium AR coincides with the position of the outcrop of quartzite observed on the surface ground. The result of the 1980 geological survey confirmed the existence of black gossan and skarn zone within the Santa formation near stations 9 - 10.

(5) Line R (See Pl. II-2-4)

The ARs detected on this line are similar to those on Lines O and P.

Low (L) ARs are detected in deep underground near stations from 4 to 11.

To the east and the west along this low AR zone are detected medium (M)

and high (H) ARs.

Localized occurrence of ultra-low (UL) ARs is detected in the shallow underground near station 5.

The low AR zone coincides with the deep underground of the area where the Carhuaz, Santa, and Chimu formations are distributed on the ground surface. The zone extends upward, especially where the Santa formation is distributed. The pattern of this low AR zone suggests a vertical-plate structure with low resistivity in the Santa formation and its close vicinity. The same pattern is recognized on Lines O and P as well.

The medium to high AR zone is considered to correspond in locality to the Chimu and Carhuaz formations.

(6) Line S (See Pl. II-2-5)

The ARs detected on this line are similar to those on Line B.

Low (L) ARs are detected in the shallow underground near stations 2, 5, and 6. In addition, the low ARs are found almost uniformly in the deep underground.

Medium (M) ARs are obtained in the westernmost part of the line, in the shallow underground near station 4, and in the shallow underground from station 7 to the easternmost part of the line.

The pattern of the low AR zone suggests the occurrence of a vertical-plate structure with low resistivity in the Carhuaz formation around stations 5 and 6. The Santa formation is exposed around stations 7 and 8. Since the ARs in this neighbourhood are higher in the shallow underground and lower in the deep, a low-resistivity-responding body in the deep underground is inferred.

(7) Line T (See Pl. II-2-6)

The ARs detected on this line are similar to those on Lines B and S.

Low (L) ARs are detected from the shallow underground near station 8 to the deep underground near stations 6 - 12.

Medium (M) ARs are obtained to the east and to the west along this low AR zone.

Distribution of the low AR zone suggests a vertical-plate structure with low resistivity to the east of the Carhuaz formation. The medium AR zone is considered to correspond in locality to the Chimu and Carhuaz formations. The Santa formation is exposed from station 10 to station 11. A low-resistivity-responding body in the deep underground is suggested by the observation that the ARs in this area are higher in the shallow underground and lower in the deep.

(8) Line U (See Pl. II-2-7)

This line is set on the Santa formation in parallel to a part of Line A that was surveyed in 1980, and intersects Lines O - T in about the middle.

A low AR zone including ultra-low (UL) ARs are detected from station 5 to station 11.

Medium (M) ARs are detected to the south and to the north along this low AR zone.

The higher AR is obtained at the southern station from station 7. The depth of the low AR becomes deeper in the same manner. These results are in accordance with our findings that the southern line of Lines O - T shows higher ARs and deeper location of low ARs.

This line has similar distribution of ARs to Line A that was surveyed in 1980. Extent of very low (VL) and ultra-low (UL) ARs are wider in this low AR zone than that on Line A.

ARs on Line U in parallel to the strike of the formations are somewhat different from those on Lines O - T that are set across the

strike of the formations.

The reason would be that the extension of the low-resistivity-responding body may coincide with the strike of the formations.

That causes an electric unisotropy in the ground.

The general trend expected from the above results is shown in panel diagram, Pl. II-5-1, and maps of AR distribution, Pl. II-3-3 and II-3-4. In Antapampa, the trend of AR distribution of the Lines O-T is relatively similar. In particular, Lines O, P, and R share a common trend, and so do Lines B, S, and T. A low AR zone (referred to as the No. 3 Central AR anomaly zone) corresponding in locality to a part of the Chimu formation, the Santa formation, and a part of the Carhuaz formation is detected around the middle of each of the above lines. To the east and to the west along this low AR zone are medium to high AR zones corresponding in locality to the Chimu and Carhuaz formations. The lines from O to T show a tendency for the location of the low AR zone to become deeper. The more southern line shows higher values of AR. These results are in accordance with results obtained in Lines A and U.

3-2-2 FE (frequency effect) measurement

The maximum value of measured FE is over 10%. The values are classified into reasonable ranges for convenience of analysis:

	2%	3%	4%	5%	6%
Background	W	M	S	S	VS

The following gives descriptions for FE anomalies detected on each survey line:

(1) Line O (See Pl. II-2-1)

Medium (M) FE anomaly including strong (S) FE anomaly detected around the middle of the line. A region from the deep underground at station 6 to the shallow underground at station 9 is the center of the anomaly. This FE anomaly is distributed somewhat more widely to the west in comparison with the low AR zone that shows 10 ohm m or less of AR.

Weak (W) FE anomaly was detected to the west of the survey line.

The FE anomaly zone detected around the middle of the line coincides with the region where the Quaternary period sediment and a part of the Carhuaz formation are exposed on the surface. This FE anomaly zone is considered to correspond in locality to the Santa and Carhuaz formations according to the results of geological survey that suggest the occurrence of the Santa formation to the west and underneath the Quaternary period sediment.

The weak FE anomaly to the east of the line is detected in the area where the Quaternary period sediment and the Chimu formation are exposed on the surface. This anomaly may be due to the alteration of the Oyon formation that is supposed to lie under the Chimu formation and the Quaternary period sediment. Another possibility is that the anomaly is caused by the intrusion of igneous rocks such as those seen along the Lines I and J. Since there is no outcrop in the vicinity of the Line O, these speculations are not confirmed.

(2) Line P (See Pl. II-2-2)

Very strong (VS) FE anomaly is detected in the shallow underground near station 6 in the middle sector along the line. Including this anomaly, strong (S) and medium (M) FE anomalies extend to the deep underground near stations 3 - 9. Extent of this anomaly zone is less wider than that on Line O.

Medium (M) FE anomaly is detected in the easternmost end of the line.

The FE anomaly zone in the middle of the line coincides well with the low AR zone that shows 10 ohm m or less of AR. The fact indicates the occurrence of a responding body that has a low resistivity and strong FE. This FE anomaly is detected in an area where the Santa formation is predominant accompanying the Quarternary period sediment and the Carhuaz formation on the ground surface. The anomaly zone corresponds in locality to the Santa formation and a part of the Carhuaz formation.

The weak FE anomaly is detected in an area where the Quarternary period sediment and the Chimu formation are distributed on the surface.

(3) Line Q (See Pl. II-2-3)

Medium (M) FE anomaly including strong (S) FE anomaly is detected near stations 4 - 10 in the middle sector along the line. Extent of this anomaly is almost the same as that on Line P.

Weak (W) FE anomaly is detected in the easternmost end of the line.

The weak FE anomaly in the middle of the line is detected in the shallow underground in an area where a part of the Santa formation and a part of the Carhuaz formation are exposed on the surface. It spreads to the shallow underground where the Santa formation is distributed. Distribution of this FE anomaly has a pattern that suggests a strong FE structure of vertical plate type located in the Santa formation and its close vicinity.

The weak FE anomaly in the easternmost end of the line is detected in an area where the Chimu formation is exposed on the surface.

(4) Line B (See Pl. II-2-2 in 1980's report)

Medium (M) FE anomaly including strong (S) FE anomaly is detected near stations 6 - 10 at the middle of the line.

A small medium (M) FE anomaly zone including strong (S) FE anomaly

is detected near station 13 in the eastern sector of the line.

This FE anomaly is stronger than those on Lines O, P, and Q.

The FE anomaly zone in the middle of the line is detected in an area where the ground surface is covered with the Santa formation and a part of the Carhuaz formation. The eastern FE anomaly zone is detected where the surface is covered with the Chimu formation. The close location of these two FE anomaly zones complicate the discernment of whether they are independent or parts of a zone.

Geological survey found a minor outcrop of scarn and black gossan in the Santa formation near stations 9 and 10. The FE anomaly zone in the middle of the line may correspond to this scarn and gossan.

(5) Line R (See Pl. II-2-4)

Strong (S) and medium (M) FE anomalies including very strong (VS) FE anomaly are detected near stations 4 - 9 from the western to central part of the line. Strong (S) FE anomaly near station 5 corresponds to the ultra-low AR and is considered to be a localized anomaly near the ground surface.

Weak (W) FE anomaly is detected in the easternmost end of the line.

The FE anomaly zone lying from the western to central part of the line coincides with an area where the Santa formation and the Carhuaz formation are exposed on the surface. This FE anomaly zone is centered on the Carhuaz formation rather than the Santa formation, and is considered to correppond in locality mainly to the Carhuaz formation.

The weak FE anomaly zone in the easternmost end of the line is detected in a region where the surface is covered with the Chimu formation.

(6) Line S (See Pl. II-2-5)

Weak (W) FE anomaly and stronger FE anomalies are detected over a wide area ranging from the deep underground of station 4 to the

easternmost end of the line. This FE anomaly has strong (S) FE anomaly including very strong (VS) FE anomaly in the deep underground near stations 6 and 7 at the central part of the line. The anomaly also has strong (S) FE anomaly in the shallow underground in the easternmost end of the line.

This FE anomaly is found in an area where the Quarternary sediment, the Santa formation, and the Carhuaz formation are exposed on the surface. The strong (S) and stronger FE anomaly is considered to correspond in locality to the Chimu formation and the deep underground of the Santa formation.

(7) Line T (See Pl. II-2-6)

Strong (S) FE anomaly zone including very strong (VS) FE anomaly and medium FE anomaly zone (M) are detected in a wide area from station 5 to station 13 at the middle of the line.

This FE anomaly is found in an area where the Chimu formation, the Quarternary sediment, the Santa formation, and the Carhuaz formation cover the ground surface. This FE anomaly is considered to correspond to them.

It is not discerned whether the FE anomaly detected around the eastern end of Lines O - S is included in the anomaly detected in the middle of Line T or the anomaly is further shifted to the east of Line T.

(8) Line U (See Pl. II-2-7)

Strong (S) FE anomaly and medium (M) FE anomaly including weak (W) FE anomaly are detected from the northern end of the line to near station 22 on the southern part of the line.

The distribution of FE on this line is similar to that on Line A surveyed in 1980. Values of FE are somewhat weaker on Line U than on Line A.

The FE distribution on Line U was compared with those of the 7 lines intersecting it. The FE values at their intersecting points are in accordance with those for Lines O, P, and Q. For Lines B, R, S, and T, the values on Line U are generally smaller than corresponding values on the intersecting lines. This may be explained by the unisotropy in the detection of a responding body when the survey line is set across the body and when it is set in parallel to the body.

The above results are shown in a panel diagram, Pl. II-5-1, and plain figures, Pl. II-3-1 and II-3-2, to describe the general trend. In Antapampa, the trend of FE was similar among Lines O - T.

A strong FE anomaly zone (No.3 central FE anomaly zone) is detected in the middle areas of Lines O - T, which is considered to correspond in locality to a part of the Chimu formation, a part of the Santa formation, and a part of the Carhuaz formation. A weak FE anomaly zone (No.3 eastern FE anomaly zone) is detected at the ends of Lines O - T, which is considered to correspond to localized alteration of parts of the Chimu formation and the Oyon formation, or igneous intrusion into these formations.

The FE values in the central FE anomaly zone have a wide variety among the lines from Line O, the most northern, to Line T, the most southern. Shapes of the contour lines suggest the occurrence of an FE responding body near the ground surface beneath Lines O and P, the northern ones. The body seems deeper under the other survey lines. Small outcrops of scarn and black gossan are observed near stations 9 - 10 on Line B and near station 8 on Line R in the Santa formation. The shallow underground of these areas generally have medium (M) FE anomaly with FEs stronger than those in the deep underground. This observation indicates that mineralization and alteration are stronger in the deeper parts.

3-2-3 MF (metal factor) Measurement

The maximum value of MF obtained is over 4,000. The MF values are classified into the following ranges for the convenience of analysis:

	10	50	100	200	500	
background	W	M	S	VS	VS	

Description is given in the following on the MFs observed on each survey line:

(1) Line O (See Pl. II-2-1)

MF anomaly including very strong (VS) MF anomaly is detected from the middle to eastern parts of the line. Wide areas show MFs of 1,000 or more. This zone is the most predominant one in the surveyed area. The strong FEs and the corresponding low ARs suggest the occurrence of sulfides.

(2) Line P (See Pl. II-2-2)

Weak (W) or stronger MF anomaly including very strong (VS) MF anomaly are detected in a wide range extending over the east and west centered on the middle part of the line. Very strong MF anomaly more than 500 corresponds to a pant-legs pattern of strong FE anomaly and very low AR.

(3) Line Q (See Pl. II-2-3)

Weak (W) MF anomaly is detected in a wide range extending to the east and west centered on stations 6 - 7. Medium (M) or stronger MF anomaly is detected from station 6 to the eastern end of the line.

(4) Line B (See Pl. II-2-2 in the 1980 report)

Strong (S) MF anomaly of a small scale is detected near the stations 8 - 11 about 200 meters deep in the ground, corresponding to strong (S) FE anomaly and low (L) AR.

An outcrop of scarn is found on the ground surface near station 9.

(5) Line R (See Pl. II-2-4)

Strong (S) and medium (M) MF anomalies are observed in the deep underground near stations 4 - 9. The MF anomaly at the middle of the line is about the same scale as those on Lines Q and B.

The strong (S) MF anomaly near station 5 is caused by localized anomaly due to strong FE anomaly and very low AR.

(6) Line S (See Pl. II-2-5)

Medium (M) MF anomaly is detected in the deep underground near stations 5 - 9.

(7) Line T (See Pl. II-2-6)

Medium (M) MF anomaly is detected in the deep underground near stations 8 - 10.

(8) Line U (See Pl. II-2-7)

Strong (S) and medium (M) MF anomalies including very strong (VS) MF anomaly are detected near stations 4 - 12.

The MF distribution on Line U was compared with those on the lines intersecting it. The MF values at the intersecting points are in accordance with those for Lines O, P, and Q. The MF values on Line U tend to be smaller than corresponding values on Lines B, R, S, and T.

The general trend of MF is shown in plain figures Pl. II-3-5 and Pl. II-3-6. Strong MF anomaly including very strong MF anomaly is observed on Lines O and P. Generally, the more southern line has a smaller MF. Especially, Line T has only medium MF anomaly on a small scale. This tendency is caused by the difference in AR rather than in FE, and corresponds to the observation that the more southern line shows the higher AR.

3-3 EM Measurement

The in-phase and out-of-phase components detected by VLF method are shown in Pl. II-4-1 and Pl. II-4-2.

A radio station which is located in the strike direction of the expected conductor should be selected for this prospecting method. The NAA station (USA, 17.8 kHz) was selected through preliminary measurements by receiving the signal from several stations on some survey lines.

The followings are the description on the in-phase and out-of-phase components detected on each survey line:

(1) Line I (See Pl. II-4-1)

In-phase response was between +20% and +30% on the western part of the line, negative with a minimum of -49% on the middle part, positive with a maximum of +63% on the eastern part, and negative the further eastern part. Small negative response and positive response are obtained near stations 4 - 4.5.

The out-of-phase component generally has small variation in response. Inversion is seen near stations 3.5, 4.5, and 12, corresponding to the inversion of in-phase response.

These results indicate the occurrence of a conductor near stations 3.5 - 4.5 and 12.

(2) Line J (See Pl. II-4-1)

Both in-phase and out-of-phase components are similar to those on Line I.

In-phase response was positive over +20% on the western part of the line, negative with a minimum of -41% at the middle part, positive with a maximum of +54% at the station 9.5 on the eastern part, and negative on the further eastern part. Near station 4 is an increase of

negative response toward the positive direction.

Out-of-phase response has small variation. Inversion is seen near stations 2.5 and 11, corresponding to inversion of in-phase response.

These results suggests the occurrence of conductors near stations 1.5 - 4 and 11.

(3) Line K (See Pl. II-4-1)

In-phase component is negative to the west of station 7.5 and positive to the east of it. Near stations 4 - 5 was a decrease in negative response from the maximum of -7% to the minimum of -32%.

Out-of-phase shows inversion from negative to positive near station 3.5.

Conductor is presumed near stations 4 - 5.5.

(4) Line L (See Pl. II-4-1)

Both components are similar to those on Line K.

In-phase response is negative on the western part of the line and positive on the eastern part. Near stations 3.5 - 5.5 is a decrease in negative response from a maximum of 0% to a minimum of -38%.

Out-of-phase response shows inversion from negative to positive near station 2.5 and from positive to negative near station 4.

The results suggest the occurrence of a conductor near the stations 3.5 - 5.5.

(5) Line M (See Pl. II-4-2 and Fig. II-3)

In the middle part of this line, the Santa formation and other formations are covered with the Quarternary sediment; there are no outcrops. EM method was employed here in addition to VLF method to obtain a sufficient amount of data.

Fig. II-3 shows the data from VLF, difference between the successive two values from west to east, and the data of EM measurements using

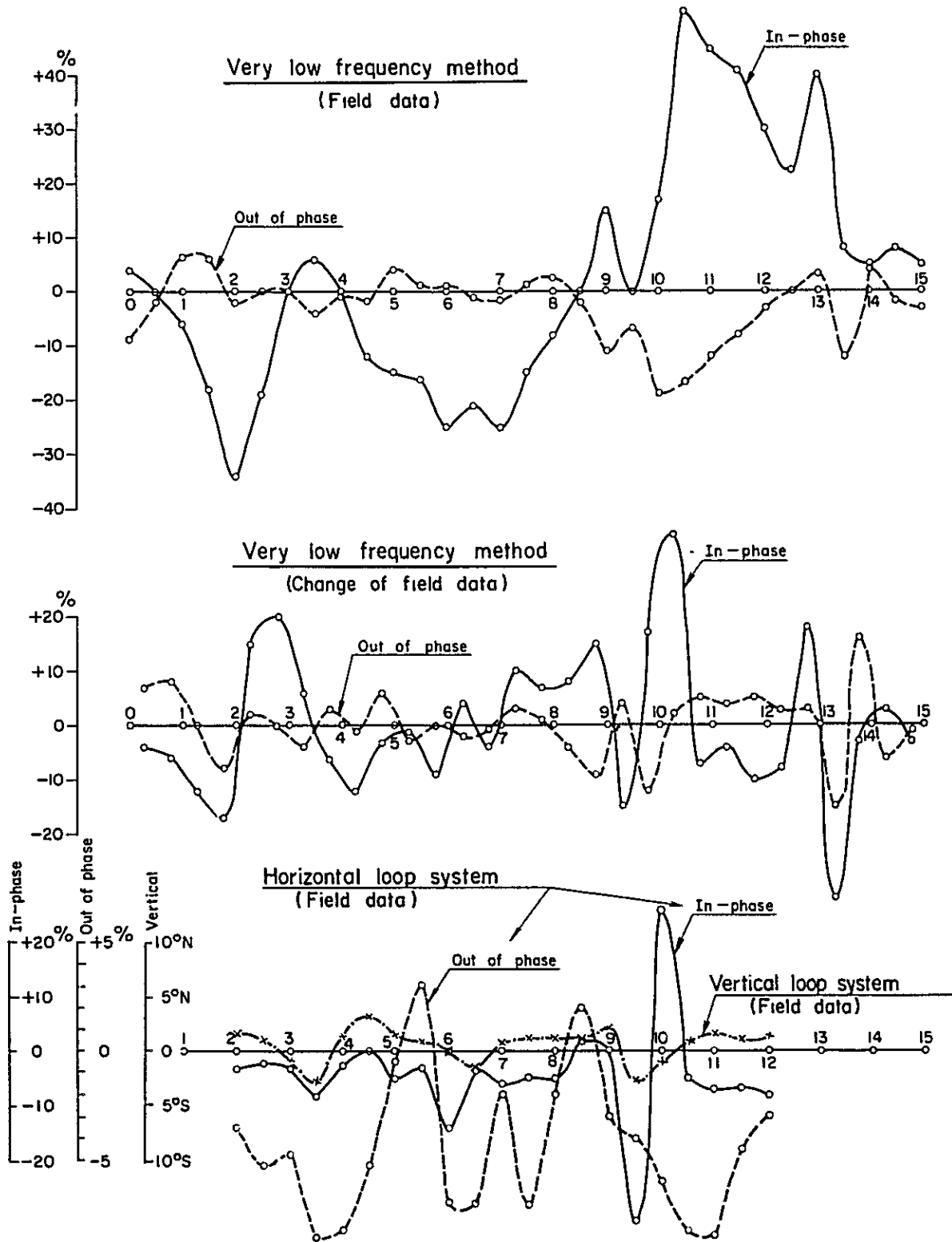


Fig. II-3 Profiles of electromagnetic field curves on Line-M

induction method.

For VLF, the in-phase component changes with a shorter cycle than that on Lines I, J, K, and L. The values of the in-phase response and its change indicate the following anomalies:

Inversion from positive to negative near stations 4 - 6. Areas near stations 9 - 9.5, 10.5 - 12.5, and 13 - 14, where the positive response shows a maximum to the west and a minimum to the east.

Out-of-phase response shows inversion from negative to positive near stations 3.5 - 5, 12.5, and 13.5 - 14. Near stations 9 - 9.5, the negative response shows the minimum to the west and the maximum to the east on the line.

Induction method with horizontal loop system detects minimum values in in-phase component at the stations 3.5, 6, and 9.5. Minimum values in out-of-phase response are found at stations 3.5, 6 - 6.5, 7.5, and 10.5 - 11. The method with vertical loop system detects changes toward the dips near stations 3, 4, 6, 7, 9, and 10.5.

Occurrence of conductor is inferred near stations 3.5 - 4.5 and 9 - 9.5 where both VLF method and induction method detect anomaly. In addition, VLF method suggests the occurrence of conductor near stations 10.5 - 12.5 and 13 - 14. Induction method suggests conductor near stations 6 - 7.

(6) Line N (See Pl. II-4-2)

The in-phase component varies in a short cycle similar to that on Line M. The following anomalies are found at the in-phase component:

Around stations 1 and 10, where western positive response showed inversion to eastern negative response; near stations 7 - 7.5 and 8 - 8.5, where positive response showed a maximum to the west and a minimum to the east on the line; in the area from station 1 to station

6.5 where the response is negative there are small areas that show a maximum to the west and a minimum to the east on the line.

Out-of-phase response shows inversion near stations 4 and 10.5. A pattern similar to in-phase response is seen near stations 7 - 7.5 and 8 - 8.5.

The results suggest the occurrence of conductor near stations 1, 7 - 7.5, 8 - 8.5, and 10.5.

Small conductors are inferred near the stations 2 - 2.5, 3 - 3.5, and 4 - 4.5.

(7) Line O (See Pl. II-4-2)

The following anomalies are found at the in-phase component:

Near stations 2.5, 10, and 13-14.5, where western positive response is inverted to eastern negative response; near station 8, where negative response shows a maximum to the west and a minimum to the east on the line.

Out-of-phase component shows inversion near stations 7, 9, 13, and 14. The inversion from western negative response to eastern positive response near station 14 corresponds to inversion in in-phase response.

Occurrence of conductors is presumed near stations 2.5, 8, 10, and 13 - 14.5.

(8) Line S (See Pl. II-4-2)

In-phase response is negative at the middle part of the line and positive on the eastern and western part. The following anomalies are found at the in-phase component:

Near station 1.5, where western positive response is inverted to eastern negative response. Near station 5 and 8, where a maximum is seen to the west and a minimum to the east on the line. In the eastern part, a maximum of station 11 drops toward the east, although the response

is not completely understood in this area because of its location at an end of the line.

The out-of-phase component largely shows the same trend as in-phase response.

The conductor is expected near station 1.5. Small conductors are presumed near stations 5 and 8.

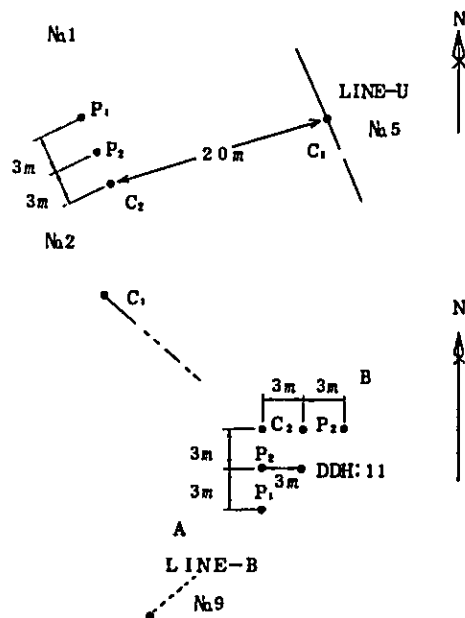
3-4 In-situ Measurement and Laboratory Work

3-4-1 In-situ Measurement

In-situ measurements were executed near station 5 on Line U and near station 9 on Line B in the vicinity of DDH-11. The results are shown in Table II-1.

Table II-1 Results of in situ measurement

Point of measurement	FE (%)	AR (Ωm)	Note
No 1	0	886	Carhuaz F.
No 2 A	4.2	350	Santa F.
No 2 B	4.4	203	Santa F.



3-4-2 Laboratory Measurement

Laboratory measurements were made on 34 samples. The sum of the samples studied comes to 86 as the 52 samples were studied in 1980. The results are shown in Table II-2 classified by formation. Fig. II-4 shows the relation between resistivity and FE, including 1980 data.

We point out the followings on laboratory measurements:

- (1) Samples with strong FE are magnetite, pyrite, hematite, and gossan. Most of them belong to the Santa formation. Some belong to the Carhuaz and Pariahuanca formations.
- (2) The Chimu, Santa, and Carhuaz formations are not discernable from each other by resistivity and FE.
- (3) The Farrat formation presents somewhat lower resistivity than the above formations, although the conclusion is not confirmed because of the small number of samples.

These results show that although it is difficult to identify the formation by resistivity and FE, ore and minerals in the Santa formation are able to be identified distinctly by resistivity and FE.



Table II-2 Results of Laboratory Measurement

Rock group	Collecting point	FE (%)	AR (Ωm)	Note
Cm	I 8.5	0.9	3,560	quartzite
	J 6.5	0.2	7,650	"
	K 8	0.1	9,970	"
	L 8	0.8	1,490	"
	M 12	0.1	3,890	"
	O 10	0.1	13,900	"
	P 7	0.2	30,100	"
	Q 9	0.1	3,390	"
	S 10	0.8	11,500	"
	T 12	0.9	13,900	"
St	B 9-1	25	490	hematite, siderite, dolomi , gossan
	B 9-2	11	230	" "
Cz	I 1	0.5	152	calcareous shale
	I 2-1	1.1	1,120	limestone
	I 2-2	0.5	6,250	silicified shale
	I 3	2.0	726	limestone
	I 4	25	350	Cu, pyrite garnet skarn
	I 5-1	3.8	838	pyrite garnet skarn
	I 5-2	0.7	11,300	sandstone
	K 1.5	1.1	1,390	sandstone
	M 5.5	2.6	732	silicified sandstone
	P 5-1	4.4	349	sandstone
	P 5-2	3.3	658	limonite, sandstone
	Q 5-1	1.2	37,800	shale
	Q 5-2	2.2	1,190	dolomite
	R 7-1	2.3	2,400	dolomite
	R 7-2	1.9	6,350	calcareous shale
	S 6	2.2	3,820	dolomitic limestone
	T 9	0.8	38,700	limestone
U 7	0.2	6,390	sandstone	
Fr	M 4	2.9	568	limonite, sandstone
	O 1	2.4	182	calcareous limestone
Ph	N 0	9.5	206	black gossan
Cl	M 2	0.9	3,250	limestone

Cm ; Chimu Formation
 St ; Santa "
 Cz ; Carhuaz "
 Fr ; Farrat "
 Ph ; Pariahuanca "
 Cl ; Chulec "

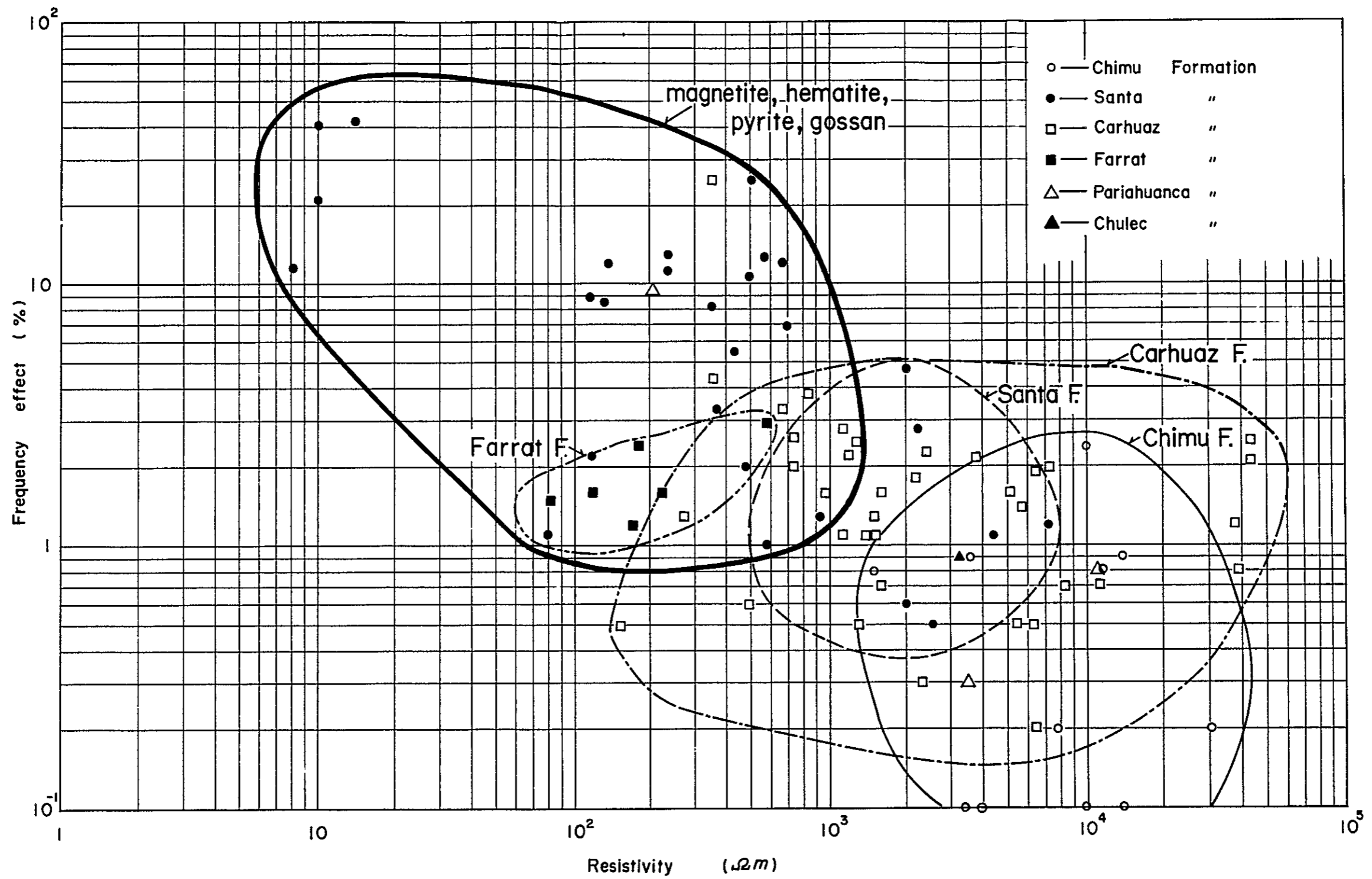


Fig. II - 4 Correlation between AR and FE of laboratory measurements



Chapter 4. Results of Analysis

4-1 IP Measurement with Dipole-Dipole Configuration

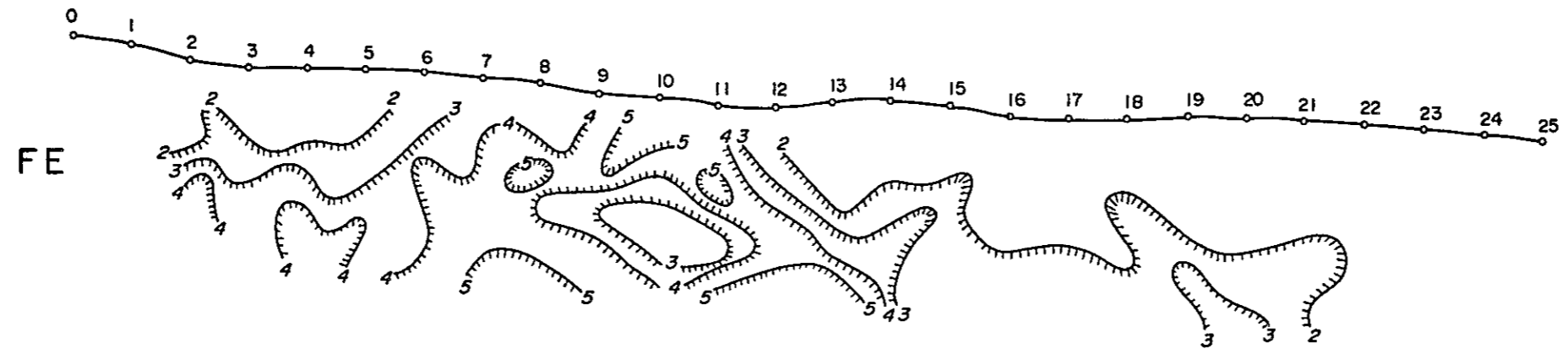
4-1-1 EM Coupling Effect

AS the result of IP measurement, extremely low apparent resistivities (ARs) are obtained on some survey lines. This implies the possibility that recorded FE values are enhanced by electromagnetic (EM) coupling effect. We tried to eliminate the EM coupling effect by the J.S. Sumner method (See References). There may be considerable error because his computation is intended to be applied to semi-infinite homogeneous medium and because we assume apparent resistivity to represent the precise resistivity of the medium. Despite that the approximation must be valid in understanding and analyzing the trend. Fig. II-5 shows the result of the computation to eliminate EM coupling effect carried out on Line U, as the representative of the survey lines that have a wide variation in ARs and are proved to have FE anomaly.

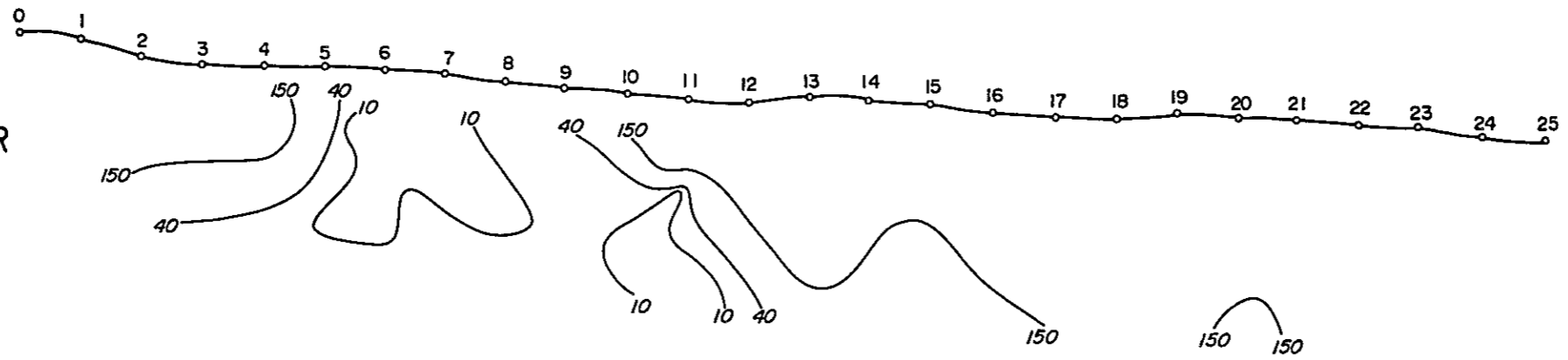
Consideration is given in the following on the influence of EM coupling effect to FE measurement, taking Line U as an example:

- (1) EM coupling effect may be neglected for FE values at $n = 1$.
- (2) For FE values at $n = 4$ and $n = 5$, the influence of EM coupling is considerably large. Since the method of correction is not so rigorous, the conclusion should be qualitative.
- (3) Contour lines in FE cross-section have a tendency to expand in deeper regions before correction. The lines in these regions become narrower after correction.
- (4) Comparing the cross-sections before and after the correction of EM coupling effect, it is seen that the presumed scale and location

Field data



AR



Corrected EM Coupling

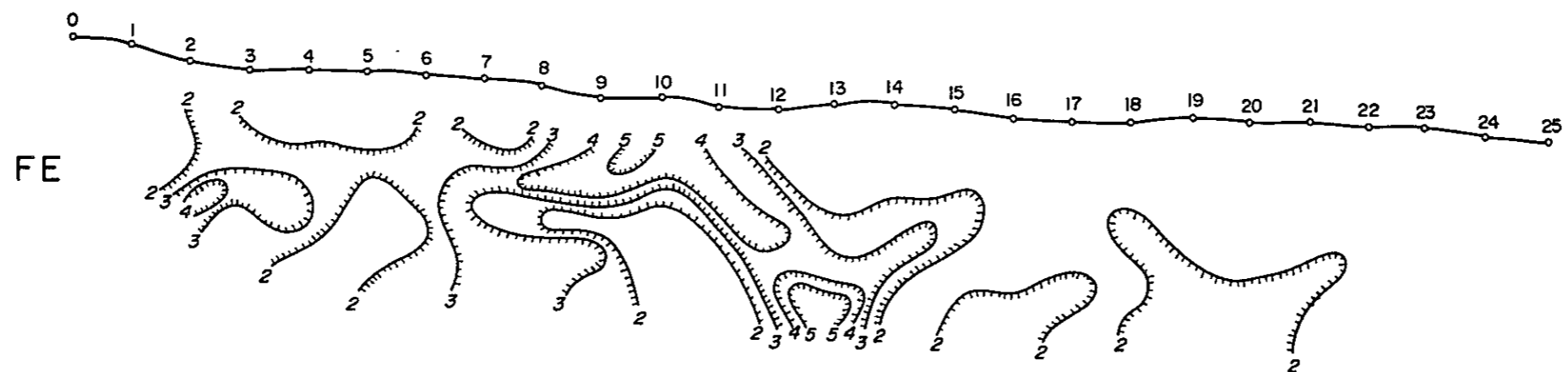
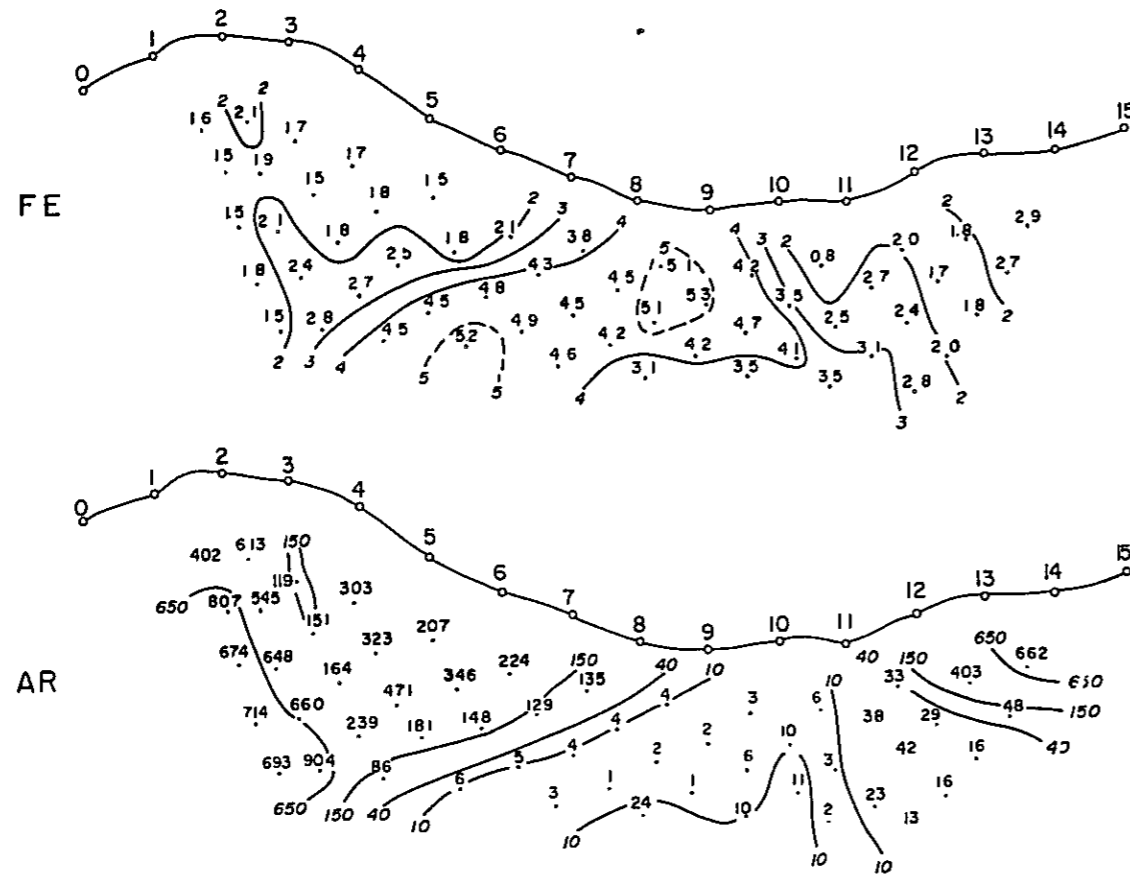
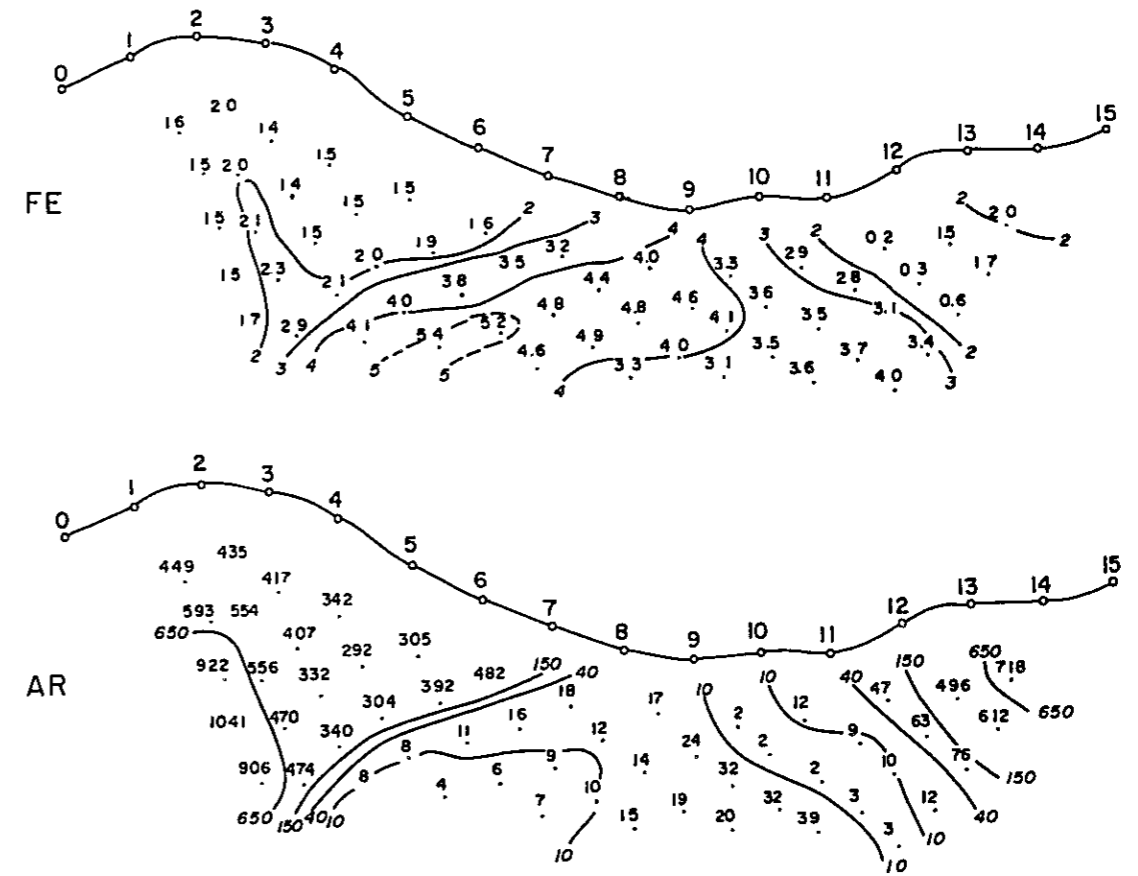


Fig. II - 5 Correction of EM coupling on Line - U

Field Data



Results of Simulation



Model

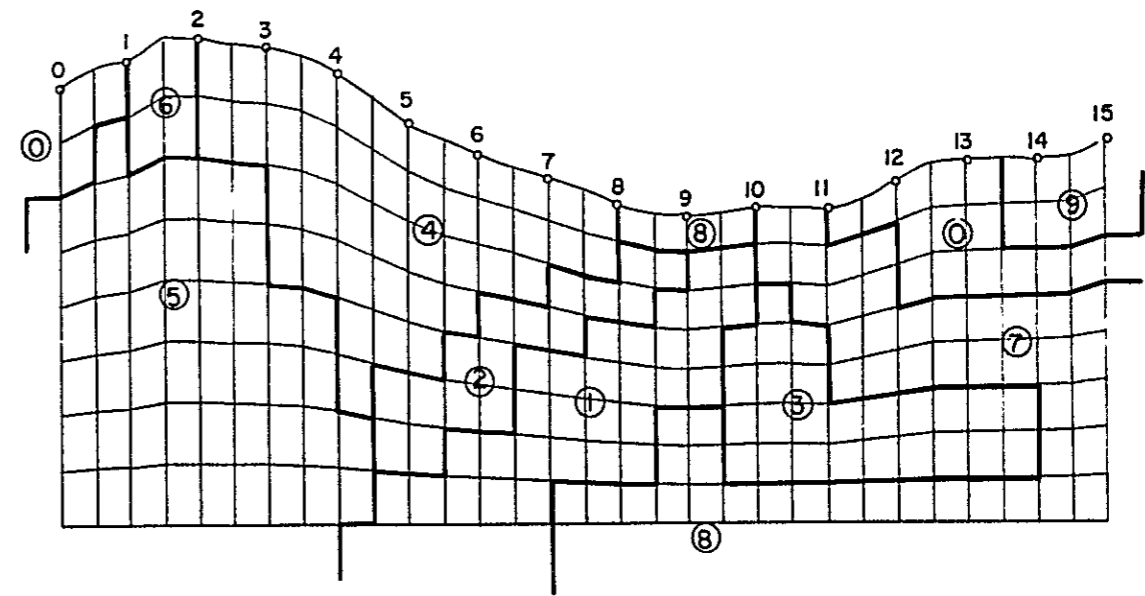


Fig. II - 6 Field Results and Results of Computer Modeling on Line - O

	①	②	③	④	⑤	⑥	⑦	⑧	⑨	
AR, nm	400	5	150	5	350	800	400	30	5	800
FE %	1.5	6.0	5.0	0.5	1.5	1.5	2.2	0.5	3.0	2.5

of the responding body have little discrepancy.

4-1-2 FE Anomalies in Antapampa

Model simulation on parts of Lines A and B are given in the 1980 report. This time, the simulation on Lines O and S was carried out to clarify the status of the IP responding bodies. Fig. II-6 shows the values calculated on Line O and its model, which correspond fairly well to the observed values. Another example is shown in Fig. II-7 on Line S.

(1) Line O (See Fig. II-6)

Responding bodies 1 (resistivity 5 ohm m, FE 6%) and 2 (resistivity 150 ohm m, FE 5%) represent the ones that present a strong FE indication at the middle of the survey line. They produce good approximation. Both are to dip westward and located under responding body 8 (resistivity 5 ohm m, FE 3%) that lies close to the ground surface. To the east of them are responding bodies 3 and 8 (resistivity 5 ohm m, FE 0.5 - 3%). This region corresponds to the range where the Chimu formation, the Carhuaz formation, and the Quarternary sediment are distributed on the surface. The Santa formation is distributed near station 8.5 by a small scale and is assumed to extend underneath station 9. This region is, therefore, considered to correspond in locality to the Santa formation, a part of the Carhuaz formation.

Responding bodies 0, 7, and 9 (resistivity 30 - 800 ohm m, FE 0.5 - 2.5%) on the eastern part of the survey line correspond to the range where the Quarternary sediment, the Chimu formation, and the Oyon formation are distributed on the surface. Responding body 9 (resistivity 800 ohm m, FE 2.5%) is considered to correspond to alteration of a part

of the Chimu formation and the Oyon formation, or intruding igneous rock.

Responding bodies 4, 5, and 6 (resistivity 350 - 800 ohm m, FE 1.5 - 2.2%) on the western part of the survey line correspond to the range where the Carhuaz formation and the Santa formation are exposed on the ground surface.

Since the influence of EM coupling effect is suspected when FE is measured at $n = 4$ or $n = 5$ and AR is smaller than about 40 ohm m, the FE values in responding body 8 and the deeper part of responding body 1 would be weaker than the values obtained through model simulation.

(2) Line S (See Fig. II-7)

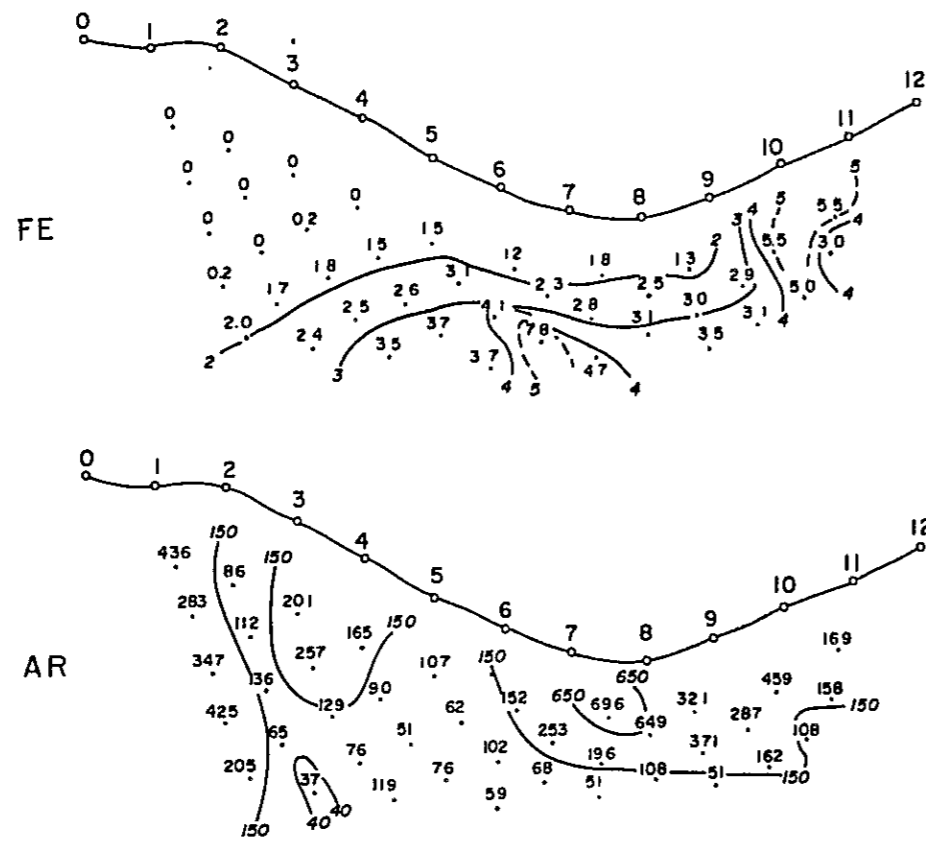
Responding bodies 1 (resistivity 30 ohm m, FE 6%) and 2 (resistivity 40 ohm m, FE 4%) represent ones that show a strong FE indication at the middle of the survey line. They produce good approximation. Responding body 2 is located deep beneath responding body 1. This region corresponds to an area where the Santa formation, the Carhuaz formation, and the Quarternary sediment are distributed on the ground surface.

Responding bodies 5, 6, and 7 (resistivity 80 - 500 ohm m, FE 1.5 - 5%) correspond to an area where the Chimu formation is distributed on the surface. Responding body 6 (resistivity 450 ohm m, FE 5%) is considered to correspond to alteration of part of the Chimu formation or intruding igneous rock such as seen on Line O.

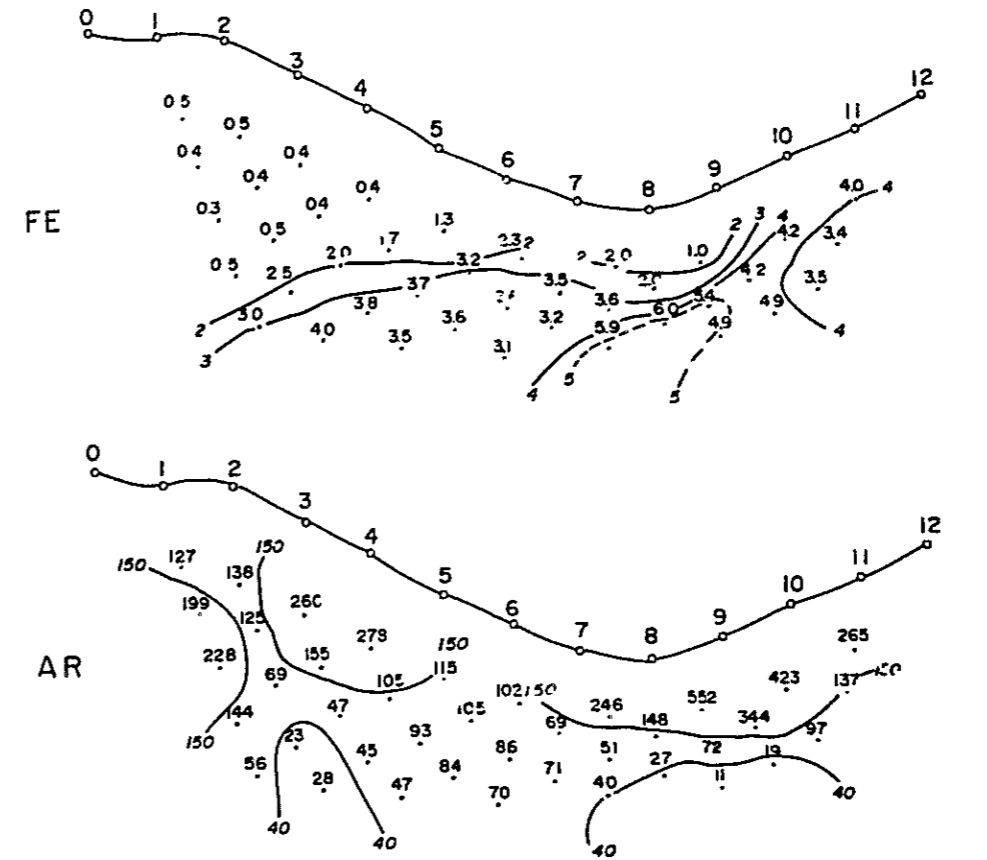
Responding bodies 0, 3, and 4 (resistivity 100 - 350 ohm m, FE 0.5%) at the western part of the line correspond to the range where the Carhuaz formation and the Santa formation are distributed on the ground surface.

The region where ARs are about 40 ohm m or less is of a limited extent. So, the influence of EM coupling effect is negligible.

Field Data



Results of Simulation



Model

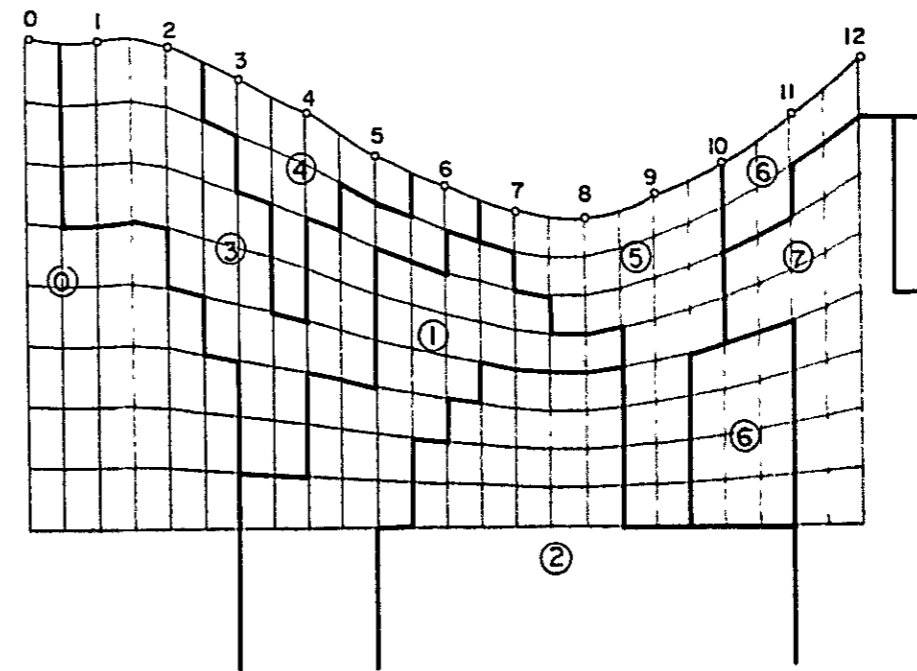


Fig. II-7 Field Results and Results of Computer Modeling on Line = S

	①	②	③	④	⑤	⑥	⑦	
AR.m	350	30	40	100	300	500	450	80
FE %	0.5	6.0	4.0	0.5	0.5	1.5	5.0	3.0

4-2 Analysis of EM Measurement Results

4-2-1 Correlation between EM Measured with VLF and AR

The results of AR measurement and EM measurement on Lines O and S are comparatively shown in Pl. II-6.

(1) Line O (See Pl. II-6)

Results of EM measurement suggests the existence of conductors near stations 2.5, 10, and 13 - 14.5. Comparison with the results of AR measurement indicates that the vicinity of station 2.5 corresponds to the region which is supposed to have a low resistivity body with ARs of 150 ohm m or less. The vicinity of stations 8 and 10 coincide with the two ends of the region where an ultra-low resistivity body is presumed. Being at the end of the survey line, comparison in the vicinity of stations 13 - 14.5 is difficult. The results are in concordance with the model simulation on IP shown in Fig. II-6.

(2) Line S (See Pl. II-6)

Results of EM measurements suggests the existence of conductors near stations 1.5, 5, and 8. Comparison with the results of AR measurement indicates that the vicinity of station 1.5 and 5 correspond to the region where the occurrence of bodies with resistivities of lower than 150 ohm m is inferred. The vicinity of station 8 corresponds to the region where a body with resistivities of 400 ohm m or less is expected to occur in a body with resistivities of 400 - 650 ohm m.

Similar correspondence can be seen on Line E on Pl. II-5-1 and Line C on Pl. II-5-2, in the 1980 report.

Comparing the results of AR measurement and those of EM measurement, the good coincidence of the values at $n = 1$ assures that the results of EM measurement can be utilized effectively in presuming the existence

of conductors up to about 100 meters deep in the ground.

4-2-2 EM Anomalies in Chupa Mine, Cunsha Punta, and Antapampa

In the area subjected to this survey, as described above, the results of EM measurement can be utilized effectively in estimating the occurrence of conductors up to 100 meters deep in the ground. This means that EM measurement is influenced strongly by localized anomaly in the shallow underground. It is known that sedimentary rocks in Chupa Mine, Cunsha Punta, and Antapampa generally lie in a NNW-SSE direction with dips varying between 70°W and 80°E, and that some faults and fissures run in parallel to the lay of the formations and some across. Geological structure should be noted as well as the trend of FE profiles to indicate the conductors. Continuous conductors are expected qualitatively in the following five regions, contrasting with the values of in-phase and out-of-phase components on neighbouring survey lines pointing at the clarity of anomalies, and considering the geological structure:

- (1) The area connecting the vicinity of stations 3.5 - 4.5 on Line I and the vicinity of stations 1.5 - 4 on Line J:

The Carhuaz formation is distributed on the ground surface. At the eastern end of this area where a conductor is expected, an occurrence of the Santa formation under the cover of talus is assumed. The conductor expected here corresponds to a part of the Carhuaz formation and predictable Santa formation.

It is possible that this conductor continues to the north to the conductor expected near station 10 on Line C.

The area where this conductor is expected is hereafter referred to as the No.1 EM anomaly zone.

- (2) The area connecting the vicinity of stations 4 - 5.5 on Line K

and the vicinity of stations 3.5 - 5.5 on Line L:

The Chimu formation is distributed on the ground surface, and the existence of the Santa formation is supposed as well. The conductor presumed here may correspond to the Santa formation as well as a part of the Chimu formation.

The area where this conductor is expected is hereafter referred to as the No.2 EM anomaly zone.

- (3) The area connecting the vicinity of stations 9 - 9.5 on Line M, the vicinity of stations 7 - 7.5 and 8 - 8.5 on Line N, and the vicinity of stations 8 and 10 on Line O:

The Quarternary sediment is distributed on the surface, and the existence of the Santa formation is supposed as well. The conductor presumed here is considered to correspond to the Santa formation. The area where this conductor is expected is hereafter referred to as the No.3 EM anomaly zone.

- (4) The area connecting the vicinity of station 12 on Line I and the vicinity of station 11 on Line J:

The Chimu formation is distributed on the ground surface, and the intrusion of igneous rock is apparent. Conductor presumed here is considered to correspond to igneous intrusion.

The area where this conductor is expected is hereafter referred to as the No.4 EM anomaly zone.

- (5) The area connecting the vicinity of stations 3.5 - 4.5 on Line M, the vicinity of station 1 on Line N, and the vicinity of station 2.5 on Line O:

The Carhuaz formation and the Farrat formation are distributed on the ground surface. The conductor presumed here corresponds to a part of the Carhuaz formation and a part of the Farrat formation.

The area where this conductor is expected is hereafter referred to as the No.5 EM anomaly zone.

Some EM anomaly zones are observed in addition to the above ones. These correspond to the Chimu formation and a part of the Carhuaz formation. Their continuity is not certified.

4-3 Comparison with Drilling Exploration

Drillings were performed at twelve spots (DDH-1 ~ DDH-12) in the area during 1980 and 1981. The locations are shown in Fig. 6, Geological Survey, Part I. Columnar profiles are reproduced in the section of Boring Works, Part III in the 1980 and 1981 reports. The followings are results of comparison between geophysical prospecting and drilling surveys:

(1) Limpe District

DDH-3, 4, 5, and 6 were drilled near stations 64, 66, 69, and 72 on Line A, respectively. Mineralized zones mainly comprising lead and zinc were detected. Referring to Pl. II-2-1 in the 1980 report, extremely good correspondence is recognized between the mineral-rich areas in these mineralized zones and the anomaly zones with FEs of 4% or more, ARs of 15 ohm m or less, and MFs of 100 or more.

(2) Surrounding Area of Chupa Mine District

DDH-7 was drilled near station 10 on Line C. Referring to Pl. II-2-3 in the 1980 report, extremely good correspondence is seen between the mineral-rich part of the mineralized zone and the anomaly zone with FEs of 4% or more, ARs of 15 ohm m or less, and MFs of 100 or more, similar to the Limpe District.

(3) Antapampa District

DDH-11 and DDH-12 were performed near station 9 on Line B and near station 7 on Line R, respectively. The comparison with Pl. II-2-2 in the 1980 report and Pl. II-2-4 in the 1981 report indicates that, although mineralization at DDH-11 is weak, it largely corresponds to the area on Line B where FEs are 3% or more, ARs are about 150 ohm m, and MFs are 50 or more. Detection of an IP-responding body, in a shallow underground distant from the survey line, is inferred. The survey at DDH-12 shows good correspondence between mineral-rich area in the mineralized zone and an area where FEs of 4% or more, ARs of 25 ohm m or more, and MFs of 100 or more are obtained.

The above results show that extremely good correspondence is seen between the mineral-rich areas in mineralized zones and anomaly zones with FEs of 4% or more, ARs of 15 to 25 ohm m, and MFs of 100 or more. As the present survey detected such IP indications on the central parts of Lines O and P, drilling surveys in these areas is advisable.

Chapter 5. The Underground Structure Inferred from
the Results of Geophysical Prospecting by
IP and EM (See Pl. II-5-2 and Fig. II-8)

The cross section of IP responding body structure of No.3 FE anomaly zone in Antapampa is shown in Pl. II-5-2. The picture was produced based on the IP profiles along Lines B, O, and S that were subjected to computer-simulation in 1980, 1981, and 1981, respectively. The geological structure was taken in account as well. Fig. II-8 presents the planar distribution of EM anomaly zones and IP responding bodies including the data of the 1980 survey. The EM anomaly zones are the ones detected on EM measurement. The IP responding bodies are the ones inferred through model simulation.

For Lines T and O, the FE responding body which presents strong FE anomaly in the middle parts of the lines (No. 3 central FE anomaly zone) continues from north to south, corresponding to the Santa formation, a part of the Chimu formation, and a part of the Carhuaz formation. This is a large-scale responding body extending about 1500 meters long. It may further extend to the south.

Pyrite is observed abundantly in the middle part of Line O. Black gossan containing hematite and goethite is observed in the vicinity of stations 9 - 10. This FE responding body is presumed to correspond to ore and minerals occurring along the Santa formation. Electrical properties of the responding body are: Resistivity is extremely small (5 ohm m, FE 6%) on Line O, the northern one, and higher (30 ohm m, FE 6%) on Line S the southern one. This may be attributed to the difference in the quantity of sulfides and the degree of alteration.

FE responding body presenting weak FE indication on the eastern

part of Lines O - S (No.3 eastern FE anomaly zone) shows continuity from north to south, corresponding to the Chimu formation and a part of the Oyon formation. It may be concluded that this responding body corresponds to the Chimu formation and alteration of a part of the Oyon formation. Another possibility is that the responding body is reflecting the intrusion of igneous rock. This is indicated by the igneous intrusion in the eastern part of Lines I and J that forms a sheet in the NNW-SSE direction.

A presumed conductor continues from Chupa Mine and Cunsha Punta to Antapampa in N-S direction, oriented along the strike of the Santa formation (No.1 - No.3 EM anomaly zones). In this area, the rocks with especially low resistivity are confined mainly to magnetite, hematite, pyrite, and gossan that belong to the Santa formation, as shown by laboratory measurements. This implies that the EM anomaly zone is the continuity of the Santa formation. It is considered that the central FE responding body is located near the ground surface in the eastern part and extends with westward dip, since the No.3 EM anomaly zone is identical to the east end of the FE responding body presenting the No.3 central FE anomaly zone, since EM anomaly implies the occurrence of comparatively shallow conductor and FE responding body in the central part has low resistivities. This conclusion coincides with the geological observations on the Santa formation.

For No.4 and No.5 anomaly zones, a definite underground structure has not been determined because they are located at the end of the survey lines. Correspondences are expected between No.4 EM anomaly zone and the igneous intrusion and between No.5 EM anomaly zone and the Pariahuanca formation and a part of the Farrat formation. Since Chupa Mine is embedded in the Pariahuanca formation, the No.5 EM anomaly zone is considered to correspond to some mineralization or alteration.

Chapter 6. Conclusion and Guidance for
Future Exploration (See Fig. II-8)

6-1 Conclusion

We summarize the results of the 1981 geophysical prospecting using IP and EM methods.

- (1) Notable FE anomaly zones in this area are the following 2 zones:
 - i) No.3 central FE anomaly zone corresponding to the Santa formation, a part of the Chimu formation, and a part of the Carhuaz formation in Antapampa.
 - ii) No.3 eastern FE anomaly zone corresponding to the Chimu formation and a part of the Oyon formation in Antapampa.
- (2) Notable EM anomaly zones in this area are the following 5 zones classified into 3 groups:
 - i) No.1 - No.3 EM anomaly zones detected largely along the strike of the Santa formation from Chupa Mine and Cunsha Punta to Antapampa.
 - ii) No.4 EM anomaly zone considered to correspond to igneous intrusion into the Chimu formation.
 - iii) No.5 EM anomaly zone considered to correspond to the Pariahuanca formation and a part of the Farrat formation.

Description is given in the following on the properties of each FE anomaly zone:

(a) No.3 central FE anomaly zone

This anomaly zone located on Lines O and T has fairly strong FEs of 3% or more. Comparatively low ARs of 150 ohm m or less are obtained. FEs of 10% or more and ARs of 10 ohm m or less are obtained in limited areas.

FE responding body corresponds in locality to the Santa formation, a part of the Chimu formation, and a part of the Carhuaz formation. It is related strongly to the Santa formation where gossan is recognized containing pyrite as well as hematite and goethite. This responding body extends for 1500 meters and has a possibility of further continuation to the south.

(b) No.3 eastern FE anomaly zone

This anomaly zone located on Lines O and S has FEs of 2% or more and ARs of several hundreds ohm m.

FE responding body is considered to correspond in locality to parts of the Chimu formation and the Oyon Formation. Correspondence to the alteration of a part of these formations or igneous intrusion is suspected.

6-2 Guidance for Future Exploration

(1) No.3 central FE anomaly zone in Antapampa has a possibility of further continuation to the south. This survey showed that FE anomaly is difficult to detect unless the survey lines are set on the FE responding body where the lines are set in parallel to the strike of the formations. Further IP survey should be executed with survey lines (e.g., seven 1.5-km lines) crossing the strike of the formations. Surveyed area should be extended to the south by about 1500 meters.

(2) Further prospecting should be conducted in the No.3 central FE anomaly zone with drilling survey to estimate the scale of mineralized zone, to examine its electric properties, and to determine the source of anomaly.

(3) EM measurement in the region ranging from Chupa Mine and Cunsha Punta to Antapampa detected a conductor in the Santa formation. There are areas with similar geological environment to the east and to the west

of the area surveyed here. These areas also have the Santa formation distributed over them. It would be profitable to take EM measurements in a wide area with survey lines (e.g., thirty 1.5-km lines) intersecting the strike of the formations to detect the conductors, on the basis of this successful experience.

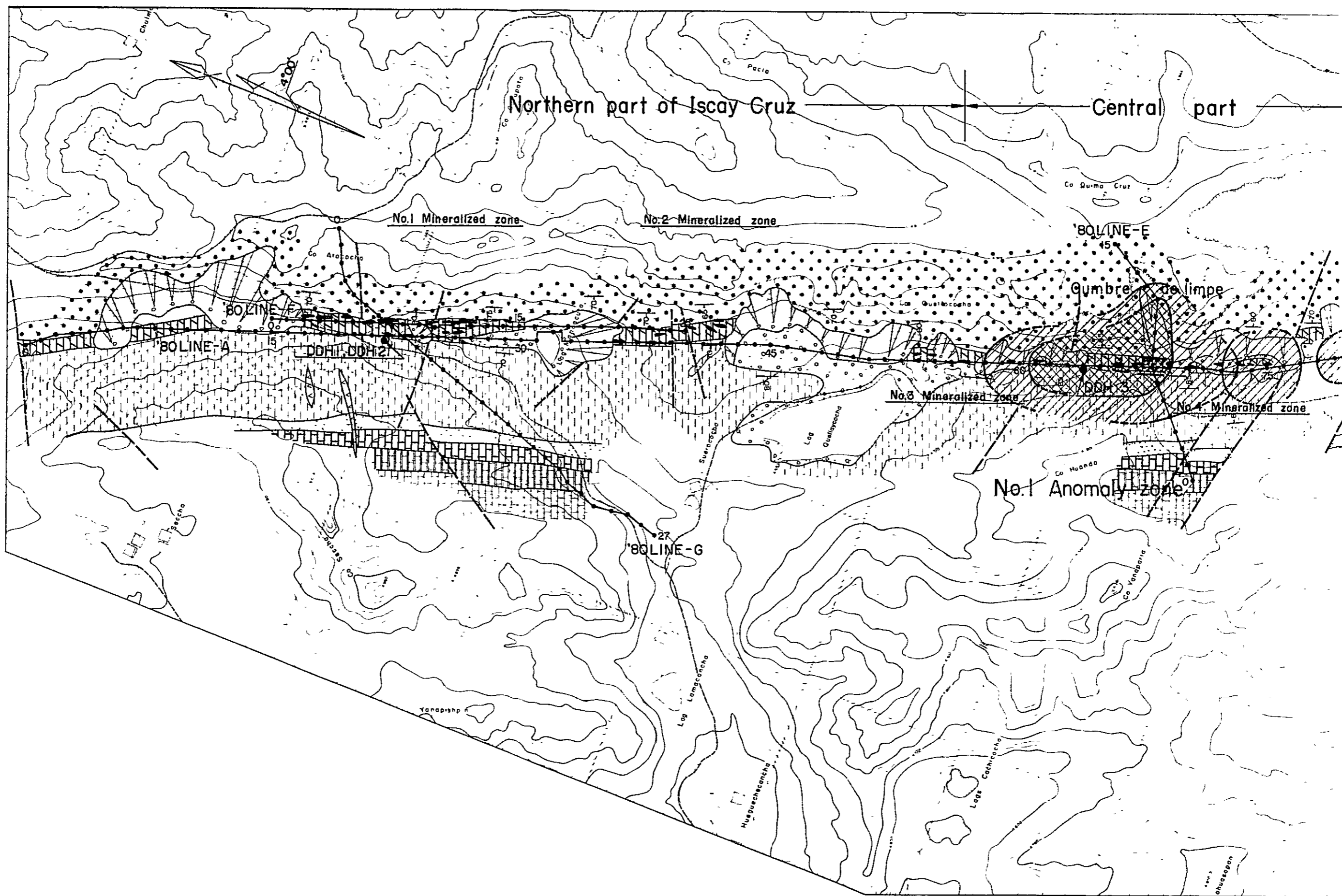
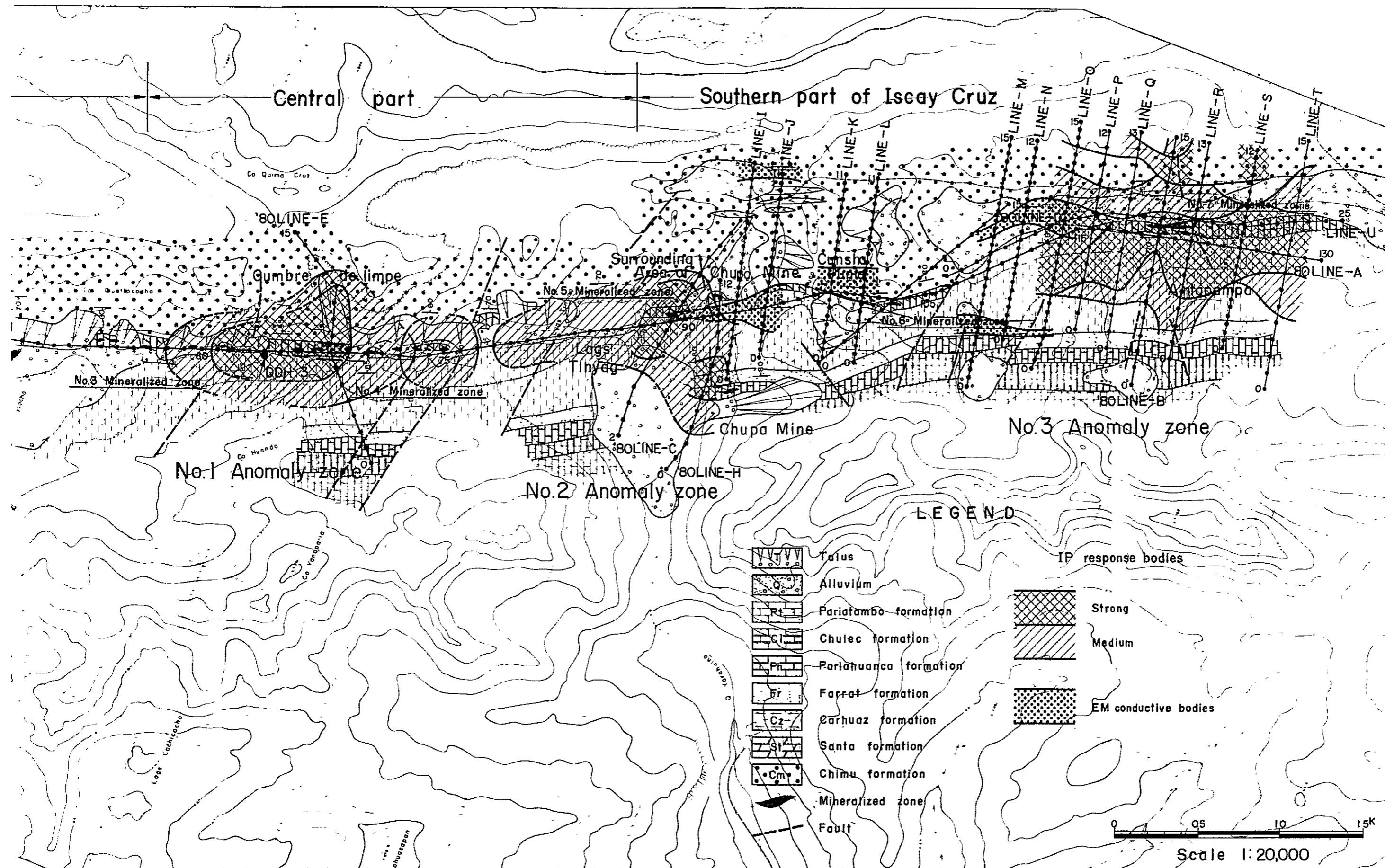


Fig II-8 Relationship between geology and the local



Relationship between geology and the location of the IP and EM anomalies

REFERENCES

- Summer, J.S. 1976, Principles of Induced polarization for geophysical exploration
- M.M.A. 1980, Republic of Peru report on geological survey of the Oyon Area phase I
- M.M.A. 1981, Republic of Peru report on geological survey of the Oyon Area phase II

PARTICULARS
PART III
DRILLING EXPLORATION

PART III DRILLING EXPLORATION

CONTENTS

Chapter 1	Outline of Diamond Drilling	III - 5
1-1	Purpose of the Survey	III - 5
1-2	Outline of Operation	III - 5
1-3	Core Evaluation and Analysis Works	III - 6
Chapter 2	Diamond Drilling Works	III - 8
2-1	Access Road for Transporting Equipment & Materials	III - 8
2-2	Location of the Drill Holes	III - 8
2-3	Preparatory Works	III - 9
2-4	Drilling Works	III - 10
2-5	Mobilization and Demobilization	III - 19
2-6	Progress Records	III - 20
Chapter 3	Geology and Mineralization of the Drill Holes ...	III - 21
3-1	DDH-4	III - 21
3-2	DDH-5	III - 22
3-3	DDH-6	III - 23
3-4	DDH-7	III - 24
3-5	DDH-8	III - 26
3-6	DDH-9	III - 26
3-7	DDH-10	III - 28
3-8	DDH-11	III - 29
3-9	DDH-12	III - 30
3-10	Summary of Drilling Exploration	III - 31

LIST OF FIGURES

Fig. III-1	Progress record of diamond drilling, DDH-4
Fig. III-2	Progress record of diamond drilling, DDH-5
Fig. III-3	Progress record of diamond drilling, DDH-6
Fig. III-4	Progress record of diamond drilling, DDH-7
Fig. III-5	Progress record of diamond drilling, DDH-8
Fig. III-6	Progress record of diamond drilling, DDH-9
Fig. III-7	Progress record of diamond drilling, DDH-10
Fig. III-8	Progress record of diamond drilling, DDH-11
Fig. III-9	Progress record of diamond drilling, DDH-12
Fig. III-10	Sample Procedures
	(1) High grade part
	(2) Low grade part
Fig. III-11	Geological section for DDH-4
Fig. III-12	Geological section for DDH-5
Fig. III-13	Geological section for DDH-6
Fig. III-14	Geological section for DDH-7
Fig. III-15	Geological section for DDH-8
Fig. III-16	Geological section for DDH-9
Fig. III-17	Geological section for DDH-10
Fig. III-18	Geological section for DDH-11
Fig. III-19	Geological section for DDH-12
Fig. III-20	Summary of X-ray diffraction test
Table III-1	Measurement results of specific gravity

LIST OF APPENDICES

- A. III-1 List of The used equipment for drilling
- A. III-2 Supplies and consumed parts for drilling
- A. III-3 Preparation and removal
- A. III-4 Operational results of drill hole, DDH-4
- A. III-5 Operational results of drill hole, DDH-5
- A. III-6 Operational results of drill hole, DDH-6
- A. III-7 Operational results of drill hole, DDH-7
- A. III-8 Operational results of drill hole, DDH-8
- A. III-9 Operational results of drill hole, DDH-9
- A. III-10 Operational results of drill hole, DDH-10
- A. III-11 Operational results of drill hole, DDH-11
- A. III-12 Operational results of drill hole, DDH-12
- A. III-13 Summaried operational data of each drill hole
- A. III-14 Working time of each drill hole
- A. III-15 Drilling meterage of diamond bits
- A. III-16 Specifications of diamond bits
- A. III-17 Assay results of the drilled core
- A. III-18 Microscopic observation of the thin sections
- A. III-19 Microscopic observation of the polished sections
- A. III-20 Photomicrographs
 - 20-1 Thin section
 - 20-2 Polished section
 - 20-3 EPMA analysis
- A. III-21 Charts of X-ray diffraction test

LIST OF PLATES

Plate III-4	Geologic drill log, DDH-4
Plate III-5	Geologic drill log, DDH-5
Plate III-6	Geologic drill log, DDH-6
Plate III-7	Geologic drill log, DDH-7
Plate III-8	Geologic drill log, DDH-8
Plate III-9	Geologic drill log, DDH-9
Plate III-10	Geologic drill log, DDH-10
Plate III-11	Geologic drill log, DDH-11
Plate III-12	Geologic drill log, DDH-12

Chapter 1 Outline of Diamond Drilling

1-1 Purpose of the Survey

The following areas were selected for the survey of the third year as the result of various survey of the second year in the Oyon area; that are Cunsha Punta, Limpe, Tinyag, and Antapampa Areas.

Drilling survey was conducted in these areas to elucidate the relation between geological structure and mineralization.

1-2 Outline of Operation

An advance investigator left Japan on May 22, 1981 and arrived in Oyon on May 27. Restoration of 13 km access road and construction of new 12 km access road started on May 30 using a bulldozer (Fiat-Allis, 11-B) and were completed on Aug. 5.

Equipment and materials were shipped by sea from Yokohama in the first part of May, 1981 and received at Callao. Transportation by truck to the site started on July 16 to begin preparatory works, starting from DDH-4.

The equipment included a TGM-3C (drilling capacity: NQ 510 m, BQ 660 m), an EP-1 (drilling capacity: NQ 510 m, BQ 660 m) and an L-44 (drilling capacity: NQ 790 m, BQ 1,060 m). Nine holes totaling up to 2,090.70 meters were drilled.

The operation was performed basically in four 6-hour shifts. Each team comprised a drilling engineer and 3 workers.

The wire-line method was employed in drilling to improve the core recovery ratio and process efficiency.

Extent of the drilling operations are listed below:

Hole	Drilling length (m)	Core length (m)	Core recovery ratio (%)
DDH-4	184.70	137.60	75.6
DDH-5	211.10	171.20	82.6
DDH-6	301.60	279.65	93.3
DDH-7	230.80	204.10	88.7
DDH-8	200.30	200.30	100.0
DDH-9	200.80	185.20	92.8
DDH-10	200.40	186.10	93.3
DDH-11	250.50	245.25	98.9
DDH-12	310.50	295.50	96.7
Total	2,090.70	1,904.90	91.9

Note: Surface soil is excluded from the core recovery ratio.

The drilling was operated for 114 days from June 30 to Oct. 21.

1-3 Core Evaluation and Analysis Works

All cores taken from drilling holes were evaluated for petrography, alteration, and mineralization. The results were compiled in geologic drill logs on a scale of 1 : 200.

For the ore part, a half or a quarter of each core was prepared for analysis for copper, lead, zinc, silver, etc.

Microscopic observations were made on the thin sections and polished sections of rock parts and ore parts. Part of the samples were subjected to mineral determination with X-ray diffraction and electron probe microanalysis. Main terms of the analysis works and number of the subjected samples are shown below:

- (1) Microscopic observation of thin sections 20
- (2) Microscopic observation of polished sections 30

(3)	Analysis of ore parts (Ag, Cu, Pb, Zn, Fe, S)	324
(4)	X-ray diffraction	30
(5)	Electron probe microanalysis	4
(6)	Specific gravity	21

Chapter 2 Diamond Drilling Works

2-1 Access Road for Transporting Equipment and Materials

An advance investigator left Japan on May 22, and arrived in Oyon to explore the sites of drilling survey. Based on the results of the exploration, a plan was made to restore and construct the access roads for transporting equipment and materials and to perform the transportation.

Procurement of workers were also carried out. Permission was obtained from Oyon city, police, and community association for leasing land, trespassing pastures, and constructing access roads.

A bulldozer (Fiat-Allis, 11-B) and about 25 local workers were used in the restoration of a 13 km existing road and construction of a new 12 km 3.5 m wide access road. This work involved cutting with the bulldozer and blasting of exposed rock bed.

The access roads are located in highland ranging from 4,030 to 4,980 meters altitude. One side of the 4,980 meters pass is covered with extensive talus sediment. This situation caused frequent troubles in maintaining the road and passing the vehicles through landslide and falling rocks.

The section around the pass was continuously manned with 10 - 20 maintenance workers to establish smooth operation of vehicles.

2-2 Location of Drill Holes

Iscay Cruz is about 28 km from Oyon via Pampahuay. This route takes about 2 and a half hours one way.

Location (longitudinal distance, latitudinal distance) and elevation of the drilling holes are listed below:

Hole	Longitudinal distance	Latitudinal distance	Elevation (m)
DDH-4	310.40 E	808.87 N	4,758
DDH-5	310.46 E	808.61 N	4,742
DDH-6	310.54 E	808.41 N	4,696
DDH-7	311.45 E	806.87 N	4,646
DDH-8	311.78 E	805.86 N	4,810
DDH-9	311.93 E	805.54 N	4,774
DDH-10	312.20 E	805.31 N	4,701
DDH-11	312.88 E	804.25 N	4,606
DDH-12	312.91 E	804.12 N	4,600

2-3 Preparatory Works

2-3-1 Transportation of Equipment and Materials

Equipment and materials were shipped from warehouse at Callao on July 16, 1981 after clearance and arrived at Pampahuay on July 16 via Churin and Oyon. The transportation used an 11-ton truck and an 8-ton truck. Further transportation from Pampahuay to the sites of DDH-7 and DDH-12 in the Iscay Cruz area employed three 1-ton pick-up trucks.

2-3-2 Preparation

Preparation was started from DDH-4. A 50 m access road was constructed with the bulldozer and the preparation of drilling site was done by human effort.

At DDH-6, DDH-7, DDH-8, DDH-9, and DDH-10, construction of a 60 m access road and preparation of drilling site were executed with the bulldozer.

At DDH-11 and DDH-12 sites, construction of a 400 m access road and the preparation of the drilling site were executed by human power.

2-3-3 Water Supply for Drilling.

DDH-4, DDH-5, and DDH-6 were supplied from two lakes to the north and to the south of Cumbre de Limpe with about 400 m of plumbing and pumps.

DDH-7 was supplied from a lake near Cumbre de Cunsha Punta with about 900 m of plumbing with gravity flow.

DDH-8 and DDH-9 were supplied from Lag. Chinchaycocha with about 800 m of plumbing and a pump.

DDH-10 was supplied from Lag. Chinchaycocha with about 400 m plumbing with gravity flow.

DDH-11 and DDH-12 were supplied from Lag. Jatuncocha with about 500 m plumbing with gravity flow.

2-4 Drilling Works

Drilling in surface soil was done with a 116-mm metal crown.

After reaching rock, drilling was continued with HQ wire-line method with successive insertion of casing pipes. The last step was executed with BQ wire-line method.

The following are the progress records of the drilling at each hole:

2-4-1 DDH-4

Drilling length: 184.70 m

Core length : 137.60 m

Core recovery : 75.6 % (excluding surface soil)

Commencement : June 30, 1981

Completion : Aug. 7, 1981

0 m - 2.60 m

Talus was drilled for 2.60 m with a 116-mm metal crown and bentonite mud water. Rock quality stabilized and HW casing pipe was installed at the 2.60 m depth.

2.60 m - 37.00 m

Layers of sandstone, marl, and shale were drilled with HQ-WL diamond bit and bentonite mud water. Rock quality stabilized and NW casing pipe was installed at the 37.00 m depth.

37.00 m - 39.50 m

Shale layer was drilled with an NQ-WL diamond bit and bentonite mud water. Water loss became intense and could not be prevented. The operation was returned to HQ-WL method.

39.00 m - 61.10 m

The hole was enlarged with an HQ-WL diamond bit from 37.00 m to 39.50 m deep. Thereafter the drilling was continued with HQ-WL diamond bit to 61.10 m deep. Situation in the hole became inferior since 55.00 m because of sheared shale and considerable water loss. So NW casing pipe was installed at the 61.10 m depth.

61.10 m - 152.20 m

Layers of marl, shale, and sulfide ore were drilled with NQ-WL diamond bit and bentonite mud water to 152.20 m deep.

The section between 79.00 m and 152.20 m was a fracture zone of shale scattered with clay and that of sulfide ore, and the situation in the hole became inferior. So BW casing pipe was installed at the 152.20 m depth.

Three layers of mineralization comprising lead, zinc, copper, and pyrite were detected and confirmed between 61.30 - 76.10 m, 84.90 - 89.60 m, and 94.00 - 104.70 m.

152.20 m - 184.70 m

Fracture zone of shale scattered with clay and that of sulfide ore were drilled with a BQ-WL diamond bit and bentonite mud water using cementing. The purpose was achieved and drilling was completed.

2-4-2 DDH-5

Drilling length: 211.10 m

Core length : 171.20 m

Core recovery : 82.6 % (excluding surface soil)

Commencement : Aug. 16, 1981

Completion : Sep. 1, 1981

0 m - 4.00 m

Talus was drilled for 4.00 m with a 116-mm metal crown and bentonite mud water. Rock quality stabilized after 3.80 m and an HW casing pipe was installed at the 4.00 m depth.

4.00 m - 14.30 m

Relatively stable layers of limestone and shale were drilled to 14.30 m deep with a HQ-WL diamond bit and bentonite mud water. Rock quality stabilized and NW casing pipe was installed at the 14.30 m depth.

14.30 m - 154.00 m

Relatively stable layers of limestone, sandstone, shale, marl, and sulfide ore were drilled to 154.00 m deep with an NQ-WL diamond bit and bentonite mud water. Rock quality stabilized and a BW casing pipe was installed at the 154.00 m depth.

Mineralization of lead, zinc, copper, and pyrite was detected and confirmed between 86.70 m - 108.00 m.

154.00 m - 211.10 m

Fracture zone scattered with clay, and layers of shale, marl, and ore were drilled to 211.10 m deep with a BQ-WL diamond bit and bentonite mud water. The purpose was achieved and drilling was completed.

This portion generally had numerous cracks that caused frequent blockage of the core. Mud water management for the drilling was performed with great care.

High-grade mineralization of lead, zinc, and pyrite was detected and confirmed between 174.80 m - 204.00 m.

2-4-3 DDH-6

Drilling length: 301.60 m

Core length : 279.65 m

Core recovery : 93.3 % (excluding surface soil)

Commencement : Sep. 7, 1981

Completion : Sep. 24, 1981

0 m - 3.00 m

Drilling to 3.00 m deep was done with a 116-mm metal crown and bentonite mud water. Rock quality stabilized after 2.00 m and a HW casing pipe was installed at the 3.00 m depth.

3.00 m - 34.40 m

Relatively stable layer of shale was drilled to 34.40 m deep with HQ-WL diamond bit and bentonite mud water. Rock quality stabilized and NW casing pipe was installed at the 34.40 m depth.

34.40 m - 186.50 m

Relatively stable layers of shale, limestone, sandstone, marl, and ore were drilled to 186.50 m deep with an NQ-WL diamond bit and bentonite mud water.

Rock quality stabilized and BW casing pipe was installed at the 186.50 m depth.

High grade zinc ore was detected and confirmed at 184.20 m and deeper.
186.50 m - 301.60 m

Relatively stable layers of limestone, marl, shale, and sulfide were drilled to 301.60 m deep with a BQ-WL diamond bit and bentonite mud water. The purpose was achieved and drilling was completed.

Five layers of high-grade zinc ore, sulfide ore, and dissemination

zone were detected and confirmed between 184.20 - 202.90 m, 207.00 - 215.30 m, 247.40 - 261.00 m, 267.30 - 293.20 m, and 297.60 - 301.60 m.

2-4-4 DDH-7

Drilling length: 230.80 m

Core length : 204.10 m

Core recovery : 88.7 % (excluding surface soil)

Commencement : Aug. 3, 1981

Completion : Sep. 4, 1981

0 m - 3.10 m

The drilling up to 3.10 m was done with a 116-mm metal crown and bentonite mud water. Rock quality stabilized and an HW casing pipe was installed at the 3.10 m depth.

3.10 m - 41.40 m

The Chimu formation with plenty of cracks and scattered clay and layers of sandstone, sulfide ore, and skarn was drilled to 41.40 m deep with an HQ-WL diamond bit and bentonite mud water. Rock quality stabilized at 40.40 m and an NW casing pipe was installed at the 41.40 m depth.

41.40 m - 135.80 m

Layers of skarn and sulfide ore were drilled to 135.80 m deep with an NQ-WL diamond bit and bentonite mud water. Rock quality stabilized and a BW casing pipe was installed at the 135.80 m depth.

Four layers of zinc ore were detected and confirmed between 60.40 - 63.00 m, 81.00 - 81.60 m, 106.40 - 109.00 m, and 116.00 - 135.80 m.

135.80 m - 230.80 m

Layers of shale and marl with plenty of cracks and scattered clay and layers of sulfide ore were drilled to 230.80 m deep with a BQ-WL diamond bit and bentonite mud water. The purpose was achieved and the drilling completed.

Four layers of dissemination zones comprising zinc and sulfide ore were detected and confirmed between 135.80 - 141.00 m, 185.00 - 187.00 m, 194.20 - 198.30 m, and 204.60 - 208.20 m.

2-4-5 DDH-8

Drilling length: 200.30 m
Core length : 200.30 m
Core recovery : 100 %
Commencement : Sep. 12, 1981
Completion : Sep. 21, 1981

0 m - 1.60 m

Drilling to 1.60 m deep was executed with a 116-mm metal crown and bentonite mud water.

Rock quality stabilized and an HW casing pipe was installed at the 1.60 m depth.

1.60 m - 56.00 m

Relatively stable layers of marl and shale were drilled to 56.00 m deep with an HQ-WL diamond bit and bentonite mud water.

Rock quality stabilized and an NW casing pipe was installed at the 56.00 m depth.

56.00 m - 200.30 m

Relatively stable layers of shale, marl, and sandstone were drilled to 200.30 m deep with an NQ-WL diamond bit and bentonite mud water.

The purpose was achieved and drilling was completed.

2-4-6 DDH-9

Drilling length: 200.80 m
Core length : 185.20 m
Core recovery : 92.8 %
Commencement : Sep. 29, 1981
Completion : Oct. 10, 1981

0 m - 1.50 m

Drilling to 1.50 m deep was done with a 116-mm metal crown and bentonite mud water. Rock quality stabilized and an HW casing pipe was installed at the 1.50 m depth.

1.50 m - 60.00 m

Relatively stable layers of shale and sandstone were drilled to 60.00 m deep. Rock quality stabilized and an NW casing pipe was installed at the 60.00 m depth.

60.00 m - 149.60 m

Relatively stable layers of sandstone, shale, and marl were drilled to 149.60 m deep. Rock quality stabilized and a BW casing pipe was installed at the 149.60 m depth.

149.60 m - 200.80 m

Relatively stable layers of shale and marl were drilled to 200.80 m deep with a BQ-WL diamond bit. The purpose was achieved and drilling was completed.

2-4-7 DDH-10

Drilling length: 200.40 m
Core length : 186.10 m
Core recovery : 93.3 %
Commencement : Oct. 2, 1981
Completion : Oct. 12, 1981

0 m - 2.50 m

Drilling to 2.50 m deep was done with a 116-mm metal crown and bentonite mud water. Rock quality stabilized at 2.40 m and an HW casing pipe was installed at the 2.50 m depth.

2.50 m - 81.30 m

Layers of shale, sandstone, and sulfide ore with scattered clay was

drilled to 81.30 m deep with an HQ-WL diamond bit and bentonite mud water. Rock quality stabilized at 75.00 m and an NW casing pipe was installed at the 81.30 m depth.

A dissemination zone containing zinc and sulfide ore was detected and confirmed between 58.20 m - 70.00 m.

81.30 m - 162.30 m

Layers of shale with relatively abundant cracks were drilled to 162.30 m deep with an NQ-WL diamond bit and bentonite mud water. Rock quality stabilized relatively and a BW casing pipe was installed at the 162.30 m depth.

162.30 m - 200.40 m

This relatively stable layer of shale was drilled to 200.40 m deep with a BQ-WL diamond bit and bentonite mud water. The purpose was achieved and drilling was completed.

2-4-8 DDH-11

Drilling length: 250.50 m

Core length : 245.25 m

Core recovery : 98.9 %

Commencement : Oct. 6, 1981

Completion : Oct. 20, 1981

0 m - 2.50 m

Drilling to 2.50 m deep was performed with a 4-3/4" tricone rock bit and bentonite mud water. Rock quality stabilized and an HW casing pipe was installed at the 2.50 m depth.

2.50 m - 102.30 m

Layers mainly comprising shale, limestone, and dolostone with scattered clay were drilled to 102.30 m with an HQ-WL diamond bit and bentonite mud water. Formations were generally soft and drilling became

difficult. So an NW casing pipe was installed at the 102.30 m depth.

102.30 m - 250.50 m

Layers of dolostone and shale with plenty of cracks and scattered clay were drilled to 250.50 m deep with an NQ-WL diamond bit and bentonite mud water. The purpose was achieved and drilling was completed.

Sheared shale with clay continued from 103.00 m to 111.60 m to make the situation in the hole especially inferior.

2-4-9 DDH-12

Drilling length: 310.50 m

Core length : 295.50 m

Core recovery : 96.7 %

Commencement : Sep. 9, 1981

Completion : Oct. 1, 1981

0 m - 3.05 m

Drilling to 3.05 m deep was performed with a 4-3/4" tricone rock bit and bentonite mud water. Rock quality stabilized at 3.00 m and an HW casing pipe was installed at the 3.05 m depth.

3.05 m - 111.35 m

Layers of marl, limestone, and dolostone with plenty of cracks and scattered clay were drilled to 111.35 m deep with an HQ diamond bit and bentonite mud water.

Sheared shale with continued from 68.60 m to 82.00 m to make the condition in the hole inferior. An NW casing pipe was installed at the 111.35 m depth.

111.35 m - 223.35 m

Layers of dolostone, marl, and sulfide ore containing clay were drilled to 223.35 m with an NQ-WL diamond bit and bentonite mud water.

Sheared sulfide ore continued from 157.60 m - 223.35 m and drilling

became difficult. A BW casing pipe was installed at the 223.35 m depth.

Five layers of dissemination zones containing zinc and sulfide ore were detected and confirmed between 122.80 - 131.00 m, 137.40 - 144.60 m, 157.60 - 183.00 m, 193.10 - 207.70 m, and 215.60 - 223.35 m.
223.35 m - 310.50 m

Layers of marl, shale, and sandstone with clay were drilled to 310.50 m deep with an BQ-WL diamond bit and bentonite mud water. The purpose was achieved and drilling was completed.

Four layers of dissemination zones containing sulfide ore and copper ore were detected and confirmed between 223.35 - 232.60 m, 237.50 - 249.00 m, 262.20 - 274.00 m, and 281.20 - 285.40 m.

2-5 Mobilization and Demobilization

2-5-1 Mobilization

DDH-5, DDH-6, DDH-7, DDH-8, DDH-9, DDH-10, DDH-11, and DDH-12 were located to the south of DDH-4 within about 12 km. The time required for mobilization and preparatory work before the drilling of each hole was 2 to 10 days.

2-5-2 Demobilization

The demobilization from DDH-9, DDH-10, and DDH-11 was obstructed by inclement weather. A team of 15 to 20 workers transported the equipment and materials to the camp (15 km) and Pampahuay (30 km) while repairing the damaged access way, and completed the rearrangement and housing. Mineral portions of the drilling cores were stored in the warehouse of INGEMMET in Lima. Other cores were kept at the camp.

2-6 Progress Records

2-6-1 Efficiency of Works

As shown in A. III-13, the total drilling length of 2,090.70 meters was completed at 3.36 m/shift for total drilling work and at 4.04 m/shift for actual drilling work.

Drilling speed and bit revolution were as shown below:

	Drilling speed	Bit revolution
Hard rock	1.0-2.0 cm/min	500-600 rpm
Medium rock	2.0-2.5 cm/min	400-500 rpm
Soft rock	2.5-3.0 cm/min	300-400 rpm

In general, fracture zones with clay and plenty of cracks lowered the drilling rate.

2-6-2 Core Recovery Ratio

As shown in A. III-13, 1,904.90 meters of core were obtained from 2,072.50 meters of total drilling length excluding surface soil comprising sand and gravel. The average core recovery ratio was 91.9 %.

Fig III-1

PROGRESS RECORD OF DIAMOND DRILLING DDH-4

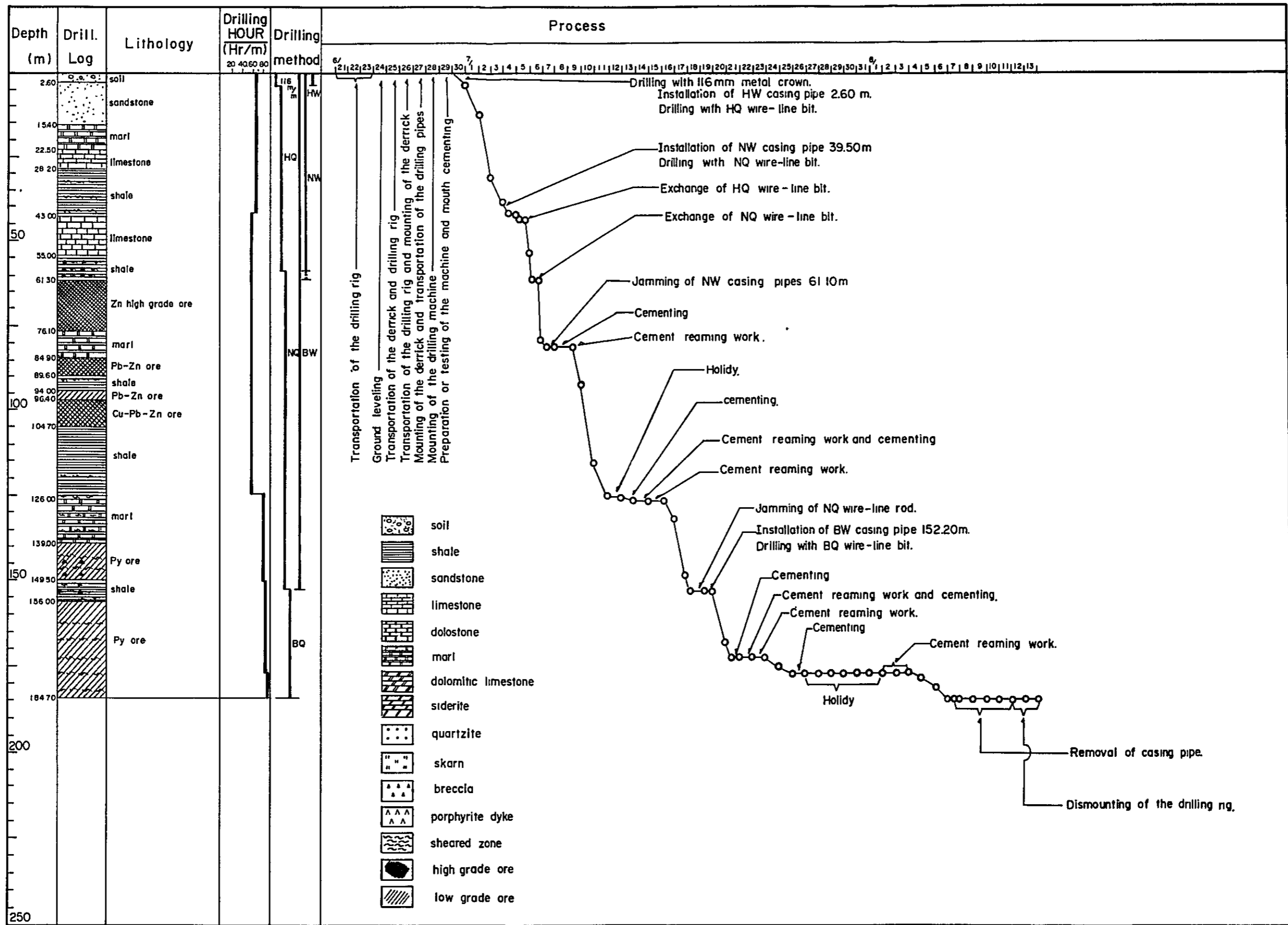


Fig. III - 2

PROGRESS RECORD OF DIAMOND DRILLING DDH-5

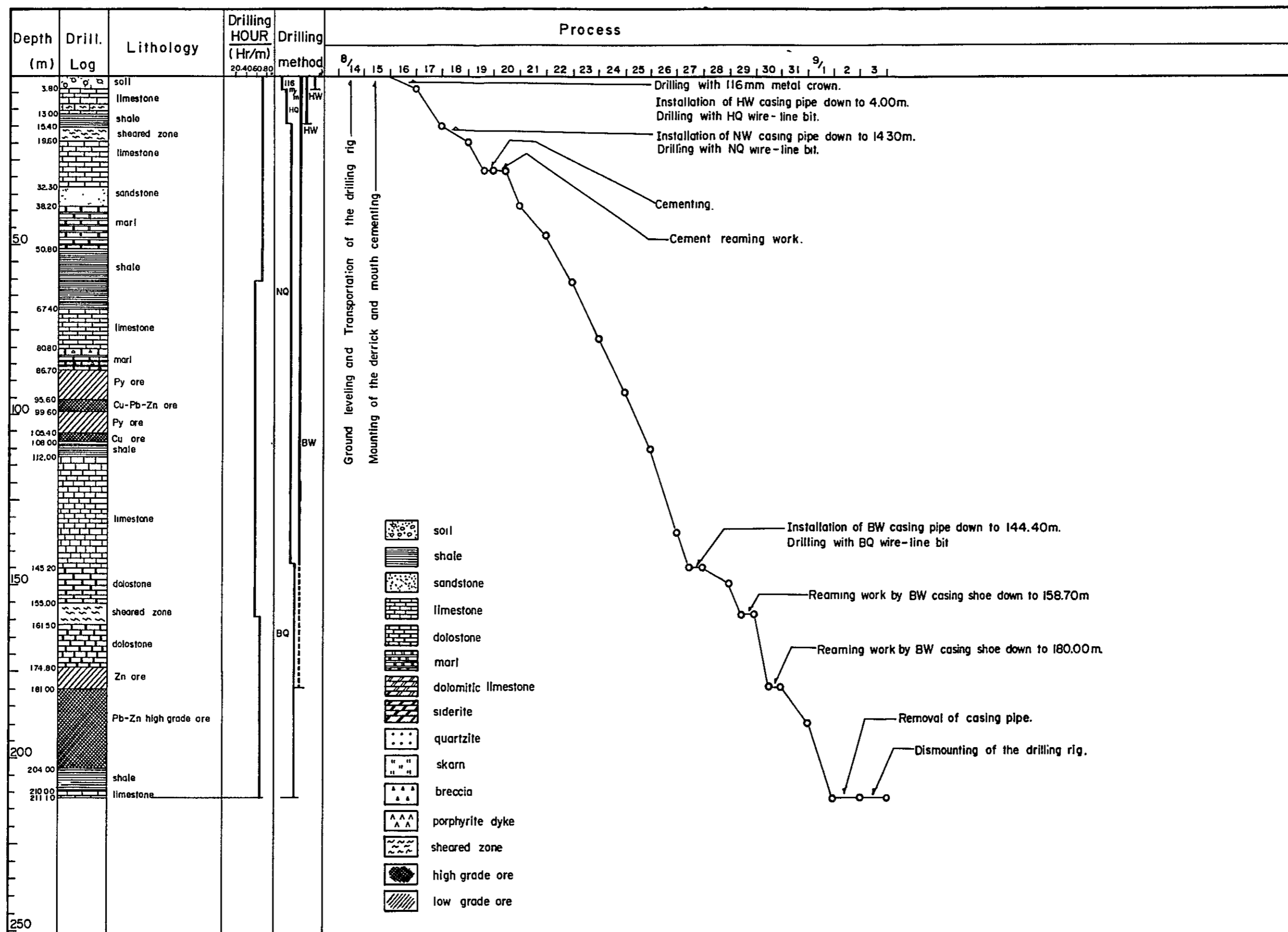


Fig. III-3

PROGRESS RECORD OF DIAMOND DRILLING DDH-6

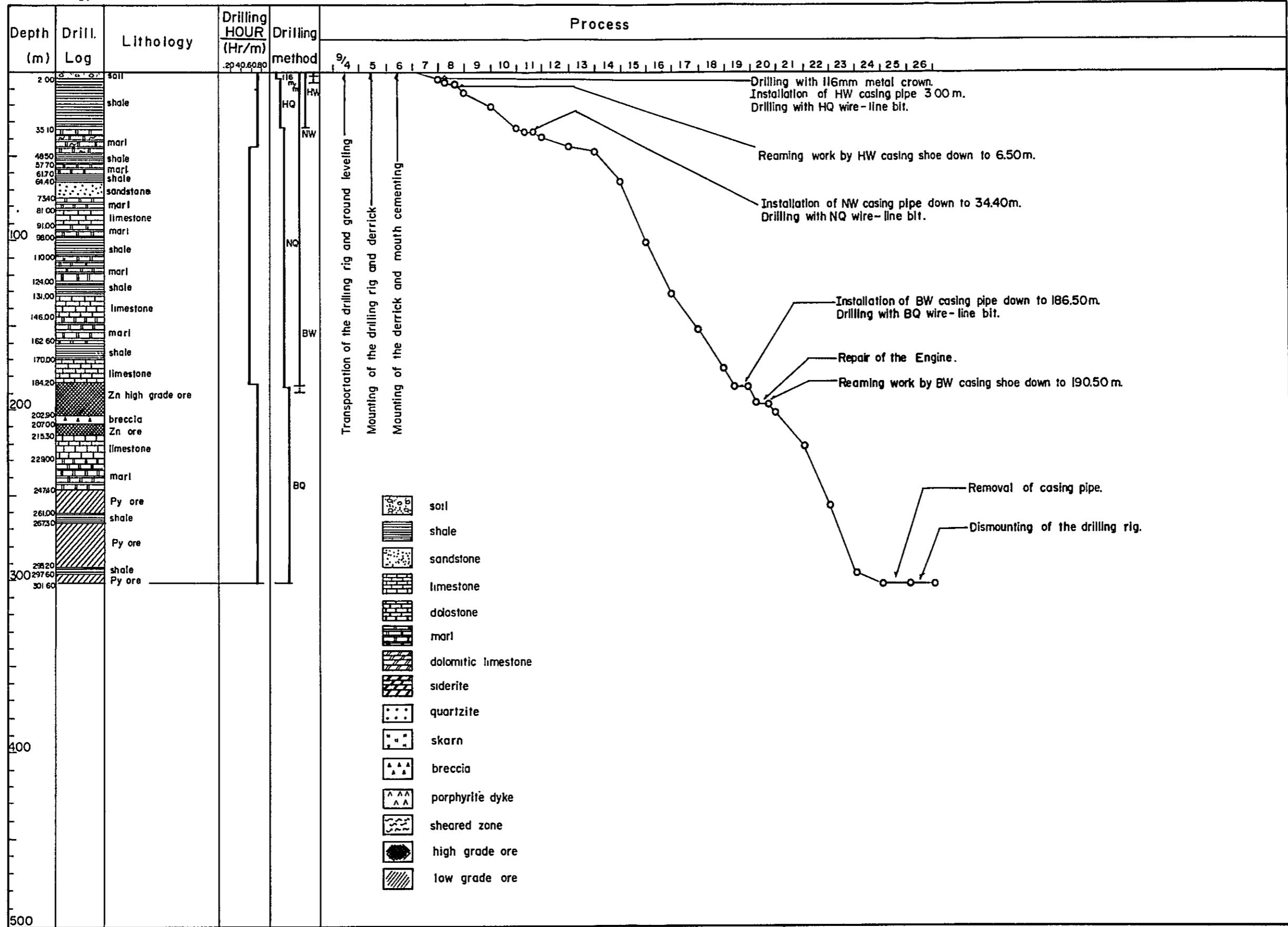


Fig. III - 4

PROGRESS RECORD OF DIAMOND DRILLING DDH - 7

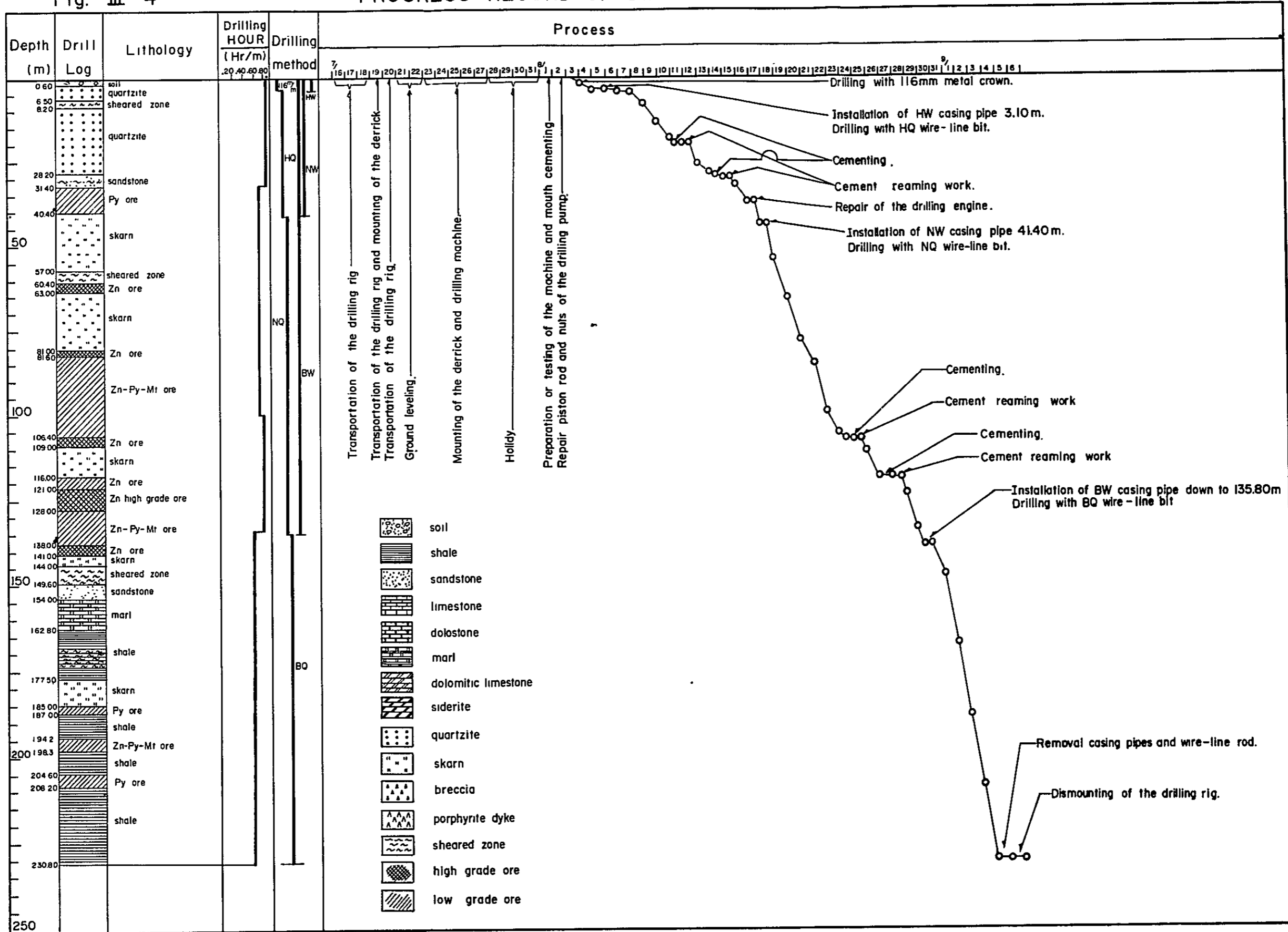


Fig. III - 5

PROGRESS RECORD OF DIAMOND DRILLING DDH-8

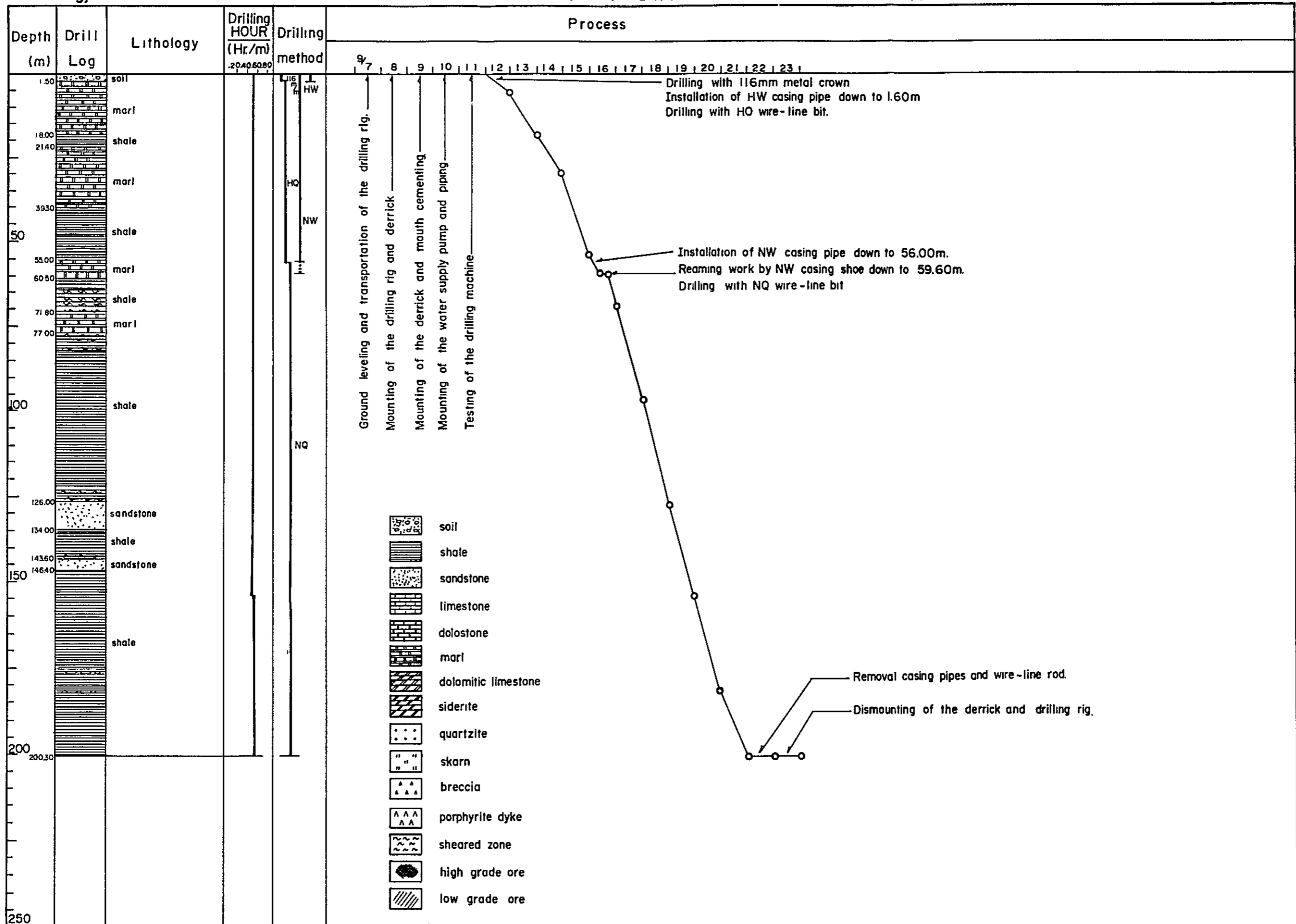


Fig. III-6

PROGRESS RECORD OF DIAMOND DRILLING DDH-9

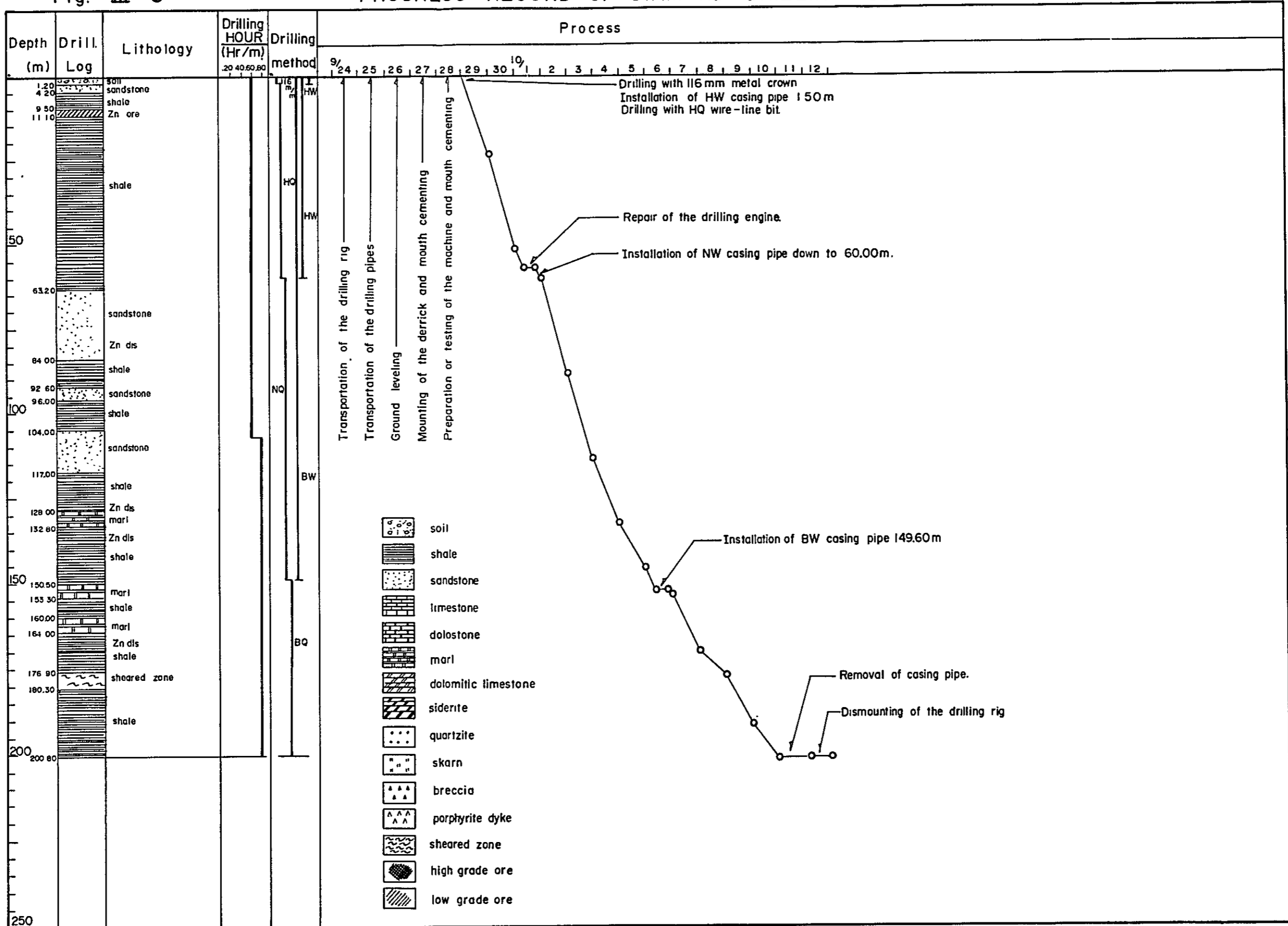


Fig. III - 7

PROGRESS RECORD OF DIAMOND DRILLING DDH-10

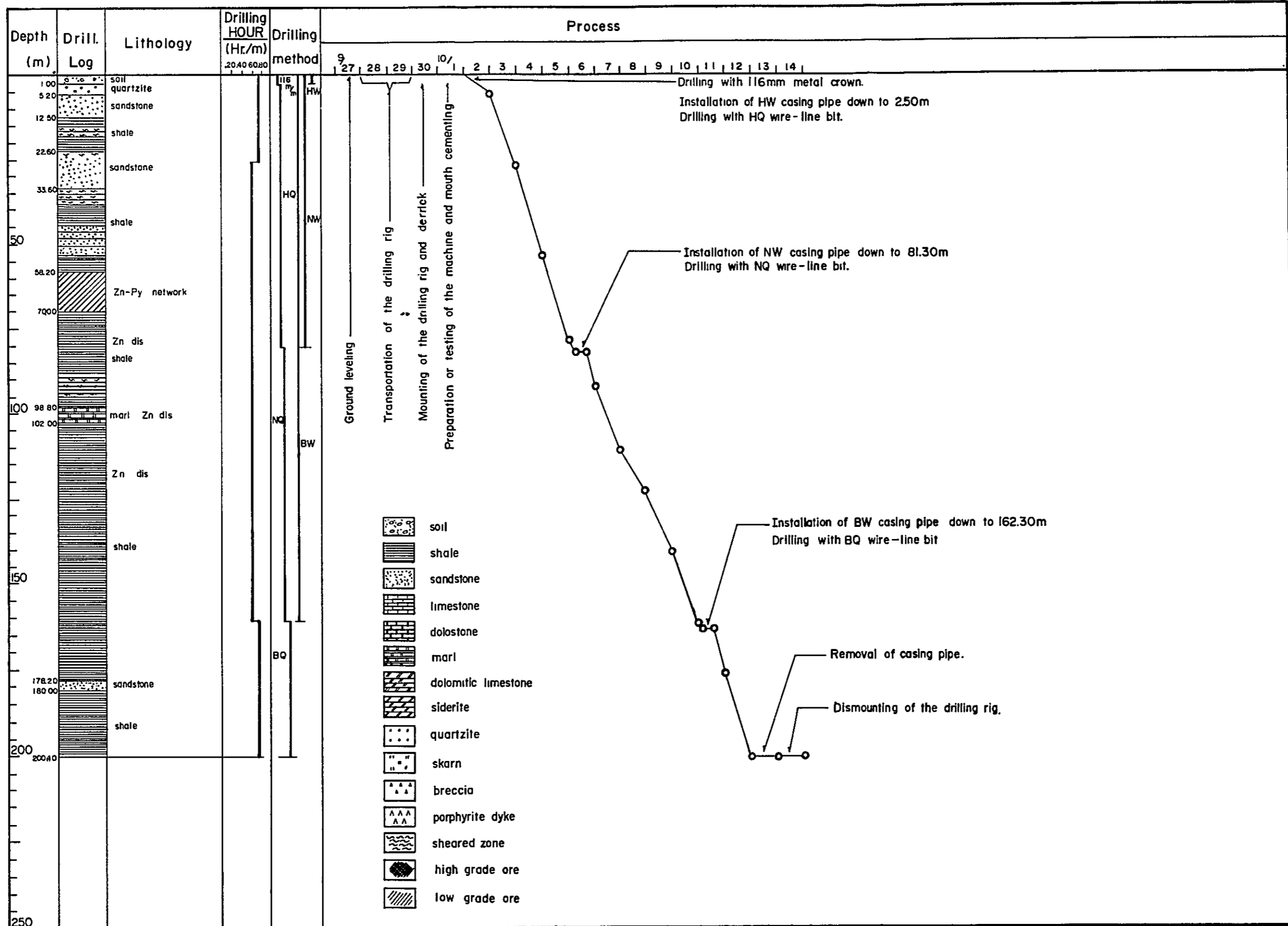
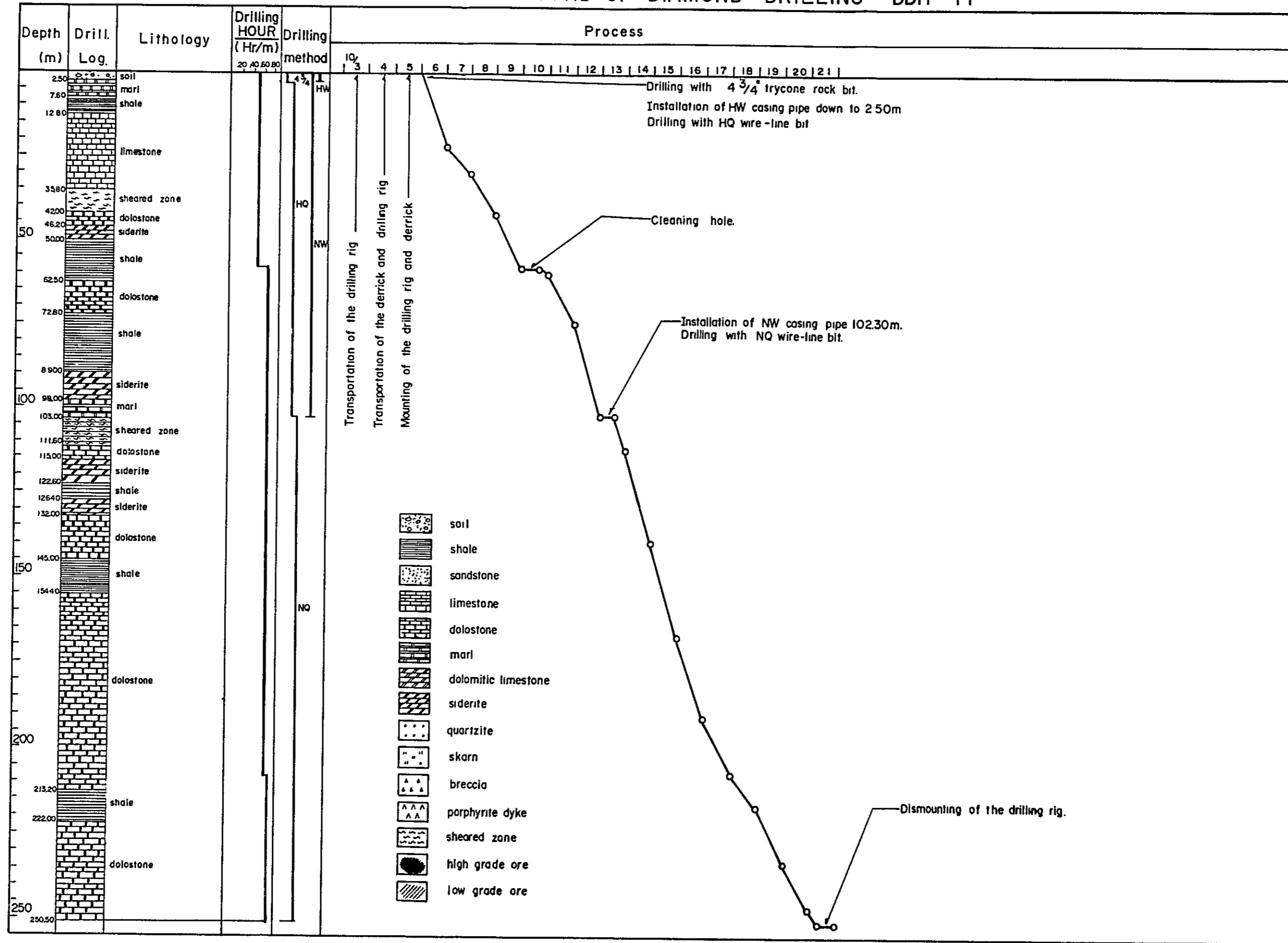


Fig. III-8

PROGRESS RECORD OF DIAMOND DRILLING DDH-11



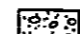


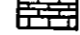
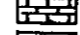
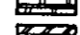
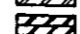

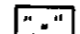
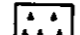

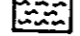



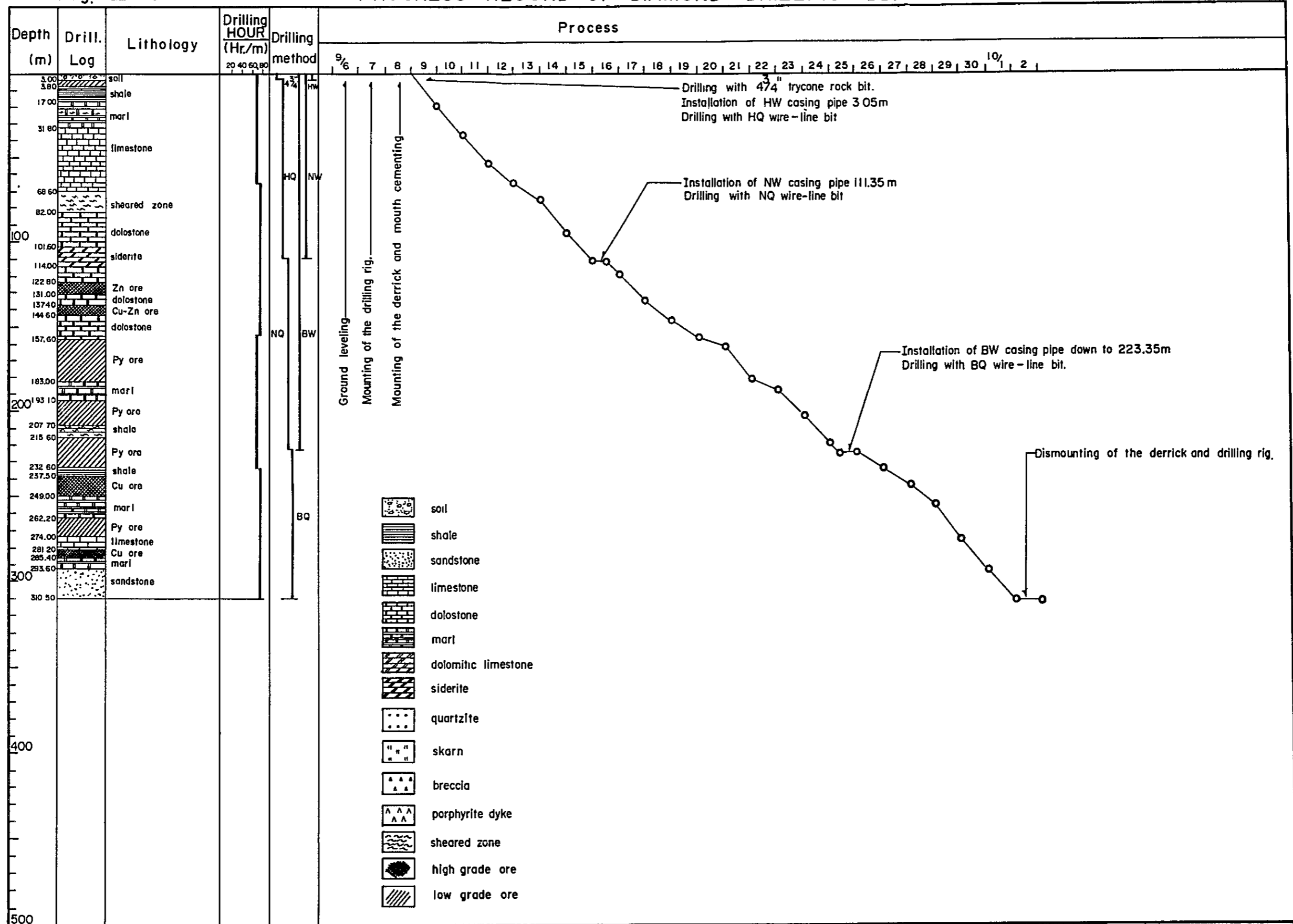
-  soil
-  shale
-  sandstone
-  limestone
-  dolostone
-  marl
-  dolomitic limestone
-  siderite
-  quartzite
-  skarn
-  breccia
-  porphyrite dyke
-  sheared zone
-  high grade ore
-  low grade ore

Fig. III-9

PROGRESS RECORD OF DIAMOND DRILLING DDH-12



Chapter 3 Geology and Mineralization of the Drill Holes

3-1 DDH-4

(1) Purpose: This drilling was made to clarify the lower part of hematite-dolomite gossan and remarkable FE anomaly zone observed by geophysical prospecting.

(2) Location: The drilling site is about 100 m north of Cumbre de Limpe and about 250 m south of DDH-3. The altitude is 4,757.5 m. The hole was drilled to 70° with inclination of -60° and was completed down to 184.7 m.

(3) Geology: The first recovered rock was seen at 2.2 m. Down to 43.0 m there presents the Carhuaz formation which consists of calcareous sandstone, shale and marlstone. Downward from 43.0 m it follows the Santa formation which consists of limestone, marlstone and shale. Calcareous sandstone is fine-grained, compact and light-grey, and is useful as a key-bed showing the lower horizon of the Carhuaz formation. The Santa formation suffers intensive mineralization and in it two mineralized layers are found between 61.3 m and 104.7 m, and between 139.0 m and the bottom of the hole. The fracture zone between 118.8 m and 135.6 m, and brecciated zone between 135.6 m and 156.0 m are found. Pyrite orebody continued from 139.0 m is very weak and easily crushed. The obtained core is powdery (c.f. PL. III-4).

(4) Mineralization and ore grade: Assay results on the series of samples at the mineralized parts are as follows:

Depth (m)	Interval (m)	No. of Samples	Ag (g/t)	Cu (%)	Pb (%)	Zn (%)	Fe (%)	S (%)
61.3 - 76.1	14.8	15	13	0.07	0.04	14.49	31.61	40.18
84.9 - 104.7	19.8	16	10	0.10	0.30	7.78	33.71	41.87

As shown in above-mentioned assay values and polished section (CB-04-064), the mineralized parts are dissemination of spalerite in pyrite mass, in which brecciation is strong and druses are formed.

Sphalerite occurs as banding structure or spotted structure in the groundmass of pyrite. Massive pyrite from 139.0 m carries 0.2 % Cu, and 0.01 % Pb and Zn in average (see Fig. III-11).

(5) Interpretation: X-ray diffraction and microscopic observation suggest that silicification and dolomitization are dominated in the marginal part of Zn-bearing pyrite body, while silicification is dominated in pyrite body. Although the drilling was suspended in the Santa formation, it reaches the border zone to the Chimu formation, judging from the correlation to the surface geology and data of other drilling holes. At this location the Santa formation is vertical and about 80 m in thickness.

3-2 DDH-5

(1) Purpose: As same as DDH-4, this hole was planned to explore the lower part of hematite-dolomite gossan and the FE anomalous zone.

(2) Location: The drilling site is 160 m south of Cumbre de Limpe and 260 m south of DDH-4 at an elevation of 4,742.2 m. The direction is 70° and the inclination is -45°. The total length is 211.1 m.

(3) Geology: At 3.5 m depth the first rock was recovered. Down to 67.4 m the Carhuaz formation is present and successively turns up to the Santa formation. The Carhuaz formation is an alternation of shale, marlstone, limestone and calcareous sandstone. The Santa formation consists mainly of limestone accompanied by shale and marlstone. As same as DDH-4, two mineralized layers are found from 86.7 m to 108.0 m and from 174.8 m to 204.0 m. Between 151.2 m and 174.8 m it appears brecciated zone. The breccia consists mainly of marlstone, limestone and shale, and its matrix is composed of tuffaceous material. This part is soft and weak due to strong alteration and leaching (c.f. PL. III-5).

(4) Mineralization and ore grade: Assays of main ore parts are as follows (see Fig. III-12):

Depth (m)	Interval (m)	No. of Samples	Ag (g/t)	Cu (%)	Pb (%)	Zn (%)
95.6 - 99.6	4.0	3	32	1.64	4.38	20.09
99.6 - 108.0	8.4	7	21	0.31	0.04	3.13
181.0 - 204.0	23.0	23	163	0.14	2.92	27.15

Total grade added together Pb and Zn attains 30 % in average of 23 m length, and occasionally it exceeds 45 % (Fig. III-12).

(5) Interpretation: Based on measurement and analysis of bedding plane in the core, the Santa formation in this hole shows a dip of 75° E forming an overturned structure. The thickness is assumed to be 80 m. The high grade ore found in the lower wall seems to correspond to the massive pyrite orebody of DDH-4 to the north. Anatase was detected in the brecciated zone by X-ray diffraction.

3-3 DDH-6

(1) Purpose: DDH-6 was made in order to explore the lower part of dolomitized gossan and pyrite-dissemination on the surface.

(2) Location: The drilling site is 380 m south of Cumbre de Limpe and 220 m south of DDH-5 station. The elevation is 4,696.1 m.

The site is at the southern end of FE anomaly zone observed along the line A. The drilling direction is 70° with inclination of -55°, and total depth is 301.6 m.

(3) Geology: The first rock was recovered at 4.0 m depth. Down to 159.0 m it comes out the Carhuaz formation, and then it turns the Santa formation to the bottom. The Carhuaz formation consists of shale down to 35.1 m, and then alternation of marlstone, shale and limestone down to the boundary with the Santa formation. Between 64.4 m and 73.3 m is calcareous sandstone.

The Santa formation from 159.0 m to 247.4 m is an alternation of limestone, shale and marlstone. Between 184.2 m and 215.3 m sphalerite pyrite ores are found. Around 188 m it becomes rich in pyrrhotite and around 205 m it occurs brecciated zone. From 247.4 m downward appears massive pyrite body partially accompanied with copper (c.f., PL. III-6).

(4) Mineralization and ore grade: Assays of the main ore are as follows:

Depth (m)	Interval (m)	No. of Samples	Ag (g/t)	Cu (%)	Pb (%)	*Zn (%)
194.4 - 200.4	6.0	6	29	0.33	0.03	39.36
204.0 - 207.0	3.0	2	12	0.26	0.03	9.40
209.0 - 215.3	6.3	6	24	0.08	0.59	10.07
248.0 - 262.0	14.0	7	13	1.67	0.03	0.10

(5) Interpretation: Based on measurement and analysis of bedding plane of the core, the Carhuaz formation shows a dip of 80° - 85° E down to the depth of 80 m, then the dip becomes gentle, 70° - 75° E around 140 m and 55° - 65° E, nearly parallel to the drilling direction around 160 m - 170 m. In the Santa formation the dip comes back to 75° - 85° E. This fact indicates that the Santa formation has been transformed itself to the east between 4,550 m and 4,600 m. This fact is an important information for the planning of deeper drilling in future (see Fig. III-13).

X-ray diffraction reveals that marcasite is associated with pyrite (BC-06-191 & 288). In the high grade Zn ore silicification is most important alteration. In addition to silicification, kaolitization is characteristic in the massive pyrite bodies and chloritization is also distinct at the marginal parts. Tetrahedrite was detected by electron probe microanalysis (BC-06-267).

3-4 DDH-7

(1) Purpose: DDH-7 was drilled to find lower extension of skarn outcrop

exposed to the south of Lags. Tinyag.

(2) Location: The drilling site is about 300 m south of Lags. Tinyag and about 600 m northeast of the Chupa ore deposit. The elevation is 4,645.5 m. The drilling direction is 250° with inclination of -80°. The drilling was started on the Chimu formation and completed down to 230.8 m.

(3) Geology: At 0.6 m it reached quartzite of the Chimu formation. The Santa formation continues from 30.0 m to 144.0 m and then the Carhuaz formation appears. The Santa formation suffers intensive mineralization to be replaced completely by skarn concentrating Zn and Cu. Skarn minerals consist of tremolite, garnet, chlorite, epidote and quartz, and ore minerals are sphalerite, pyrrhotite, pyrite and chalcopyrite (see Fig. III-20).

Within the Santa formation, pyrite body is present between 31.4 m and 40.4 m, and down to 81.0 m occurs low grade skarn disseminated with pyrrhotite and pyrite and partly sphalerite. High grade skarn of abundant sphalerite and chalcopyrite accompanied with pyrrhotite and pyrite is present between 81.0 m and 135.8 m. In the deeper place grade of ore becomes lower, consisting mainly of pyrite. From 144.0 m downward the Carhuaz formation of alternation of shale, marlstone and sandstone, comes out, which are disseminated extensively with pyrite and intercalated with skarn and massive pyrite beds in many places (c.f. PL. III-7).

(4) Mineralization and ore grade: The Santa formation is completely replaced by skarn minerals for 114 m length about 80 m in real thickness.

Assays of the part of ore embedded in skarn mass are as follows.

(see Fig. III-14):

Depth (m)	Interval (m)	No. of Samples	Ag (g/t)	Cu (%)	Pb (%)	Zn (%)
56.0 - 63.0	7.0	5	5	0.21	0.01	19.71
81.0 - 99.0	18.0	18	4	0.11	0.05	5.34
106.0 - 110.0	4.0	2	3	0.12	tr	6.35
116.0 - 135.0	19.0	15	9	3.18	tr	19.53

(5) Interpretation: According to X-ray diffraction, the skarn is characterized by a large amount of hydrothermal alteration minerals such as sericite (BC-07-121), talc (BC-07-058), chlorite (BC-07-075) and others. Phlogopite, dolomite and siderite are also identified by X-ray diffraction (see Fig. III-20).

3-5 DDH-8

(1) Purpose: The drilling of DDH-8 was carried out to clarify the details of the Santa formation expected occurring on the west side of the Chimu quartzite which is conspicuously brecciated and disseminated with pyrite and limonite.

(2) Location: The drilling site is 300 m south of Cumbre de Cunsha Punta with elevation of 4,810.2 m. The site is located at the northern end of FE anomaly zone measured by the line A and also at the western end of EM anomaly observed along the line L. The drilling direction is 70° with inclination of -60° and total depth is 200.3 m.

(3) Geology: From 1.5 m down to the bottom goes on the Carhuaz formation consisting mainly of shale, marlstone and sandstone.

Fault fracture zones are confirmed at the depths of about 28 m, 35 m and 143 m (c.f. PL. III-8).

(4) Interpretation: Around the drilling site relationships among Santa, Chimu and Carhuaz formations were not confirmed, because the Santa formation is completely covered by thick recent sediments. However, as a result of the drilling, it is inferred that the Santa formation has been displaced to the east under the Chimu quartzite by thrust fault (see Fig. III-15).

3-6 DDH-9

(1) Purpose: The drilling DDH-9 was carried out in order to clarify the details of the lower part of Pb-Zn-Fe bearing mineralized zone in the limestone

of the Santa formation exposed on the surface.

(2) Location: The site is about 500 m south of Cumbre de Cunsha Punta with elevation of 4,778.3 m. The site is located at the center of FE anomaly zone observed along the line A and also at the eastern margin of FE anomaly confirmed by the line D. At this site the Chimu and Santa formations strike N 25° W and dip 75° - 85° E. The drilling site is located at 12 m to the west of the Santa formation. The drilling direction is 70° with inclination of -70°. Total depth is 200.8 m.

(3) Geology: The Carhuaz formation consisting mainly of shale intercalating sandstone and marlstone continues from 1.2 m to the bottom. The Carhuaz formation is disseminated with sphalerite and pyrite in many places. Fault fracture zone with a gentle dip was found between 56.3 m and 58.0 m. Nearby 12 m, 57 m and 178 m fault fracture zones are encountered (c.f. PL III-9).

(4) Mineralization and ore grade: Assays of the mineralized part are as follows (see Fig. III-16).

Depth (m)	Interval (m)	Zn (%)	Type of Mineralization
9.5 - 11.1	1.6	3.9	Sphalerite disseminated skarn
78.6 - 80.0	1.4	1.0	Sphalerite dissemination along joints in sandstone
127.9 - 128.4	0.5	1.3	Sphalerite-pyrite network in marlstone
135.2 - 136.1	0.9	1.0	Sphalerite dissemination in marlstone
138.2 - 138.8	0.6	1.3	Sphalerite network in marlstone
166.2 - 167.4	1.2	1.1	Sphalerite-pyrite dissemination in shale

(5) Interpretation: By the geological survey in this year, fault group, composed of NS strike dipping 75° E and N25° W strike dipping 70° E, was confirmed in the boundary zone between the Santa and Carhuaz formation. The fault system is as echelon form and displacements by each fault were supposed to be not large. However, the drilling result indicates that

conspicuous faults are developed at the depths about 57 m and 178 m, and as the result the Santa formation has been displaced by these faults to the east for fairly long distance under the Chimu formation. Still more, as the Carhuaz formation is intensively mineralized, a large potentiality of ore reserves is expected in the Santa formation dislocated under the Chimu formation to the east.

3-7 DDH-10

(1) Purpose: The drilling DDH-10 was carried out in order to explore the lower part of the Santa gossan exposed on the surface.

(2) Location: The site is about 900 m southeast of Cumbre de Cunsha Punta with elevation of 4,700.9 m. This site is located at the southern margin of FE anomalous zone observed along the line A. This hole was drilled on the quartzite of Chimu formation to the direction of 285° with inclination of -60°. Total depth is 200.4 m.

(3) Geology: The Chimu formation consisting of quartzite, sandstone and shale succeeds. From 33.6 m to 38.4 m a remarkable fault fracture zone is developed and below the fault it turns to the Carhuaz formation. The fault is considered to be a gentle thrust fault judging from the inner structure.

The Carhuaz formation is mainly composed of shale intercalating sandstone and marlstone, and in part intensively mineralized and disseminated with sphalerite and pyrite (c.f. PL. III-10).

(4) Mineralization and ore grade: Assays of the main mineralized parts are as follows (see Fig. III-17).

Depth (m)	Intervals (m)	No. of Samples	Ag (g/t)	Cu (%)	Pb (%)	Zn (%)
59.2 - 64.2	5.0	3	11	0.04	0.06	3.11
65.9 - 70.0	4.1	4	13	0.08	0.05	5.38
76.2 - 81.2	5.0	5	11	0.06	0.48	1.20
98.8 - 101.8	3.0	3	12	0.03	0.33	0.87
110.4 - 116.4	6.0	6	11	0.01	0.10	0.57

(5) Interpretation: The Santa formation is displaced to the east in the southern area. The cause of structural transformation was not clear. As the result of this drilling, it was clarified that the transformation had been brought forth by the thrust fault thrusting up to the west. The displacement by the thrust fault can be estimated about 400 m in maximum. The Santa formation, that was cut and displaced by the fault, is expected to appear under the Chimu formation to the east. The apparent thickness of the Carhuaz formation is 400 m to 600 m in the northern Tinyag area and southern Antapampa area. However, it decreases about 200 m in this area. The discrepancy is considered to be caused by the thrust fault (c.f. Fig. I-6).

3-8 DDH-11

(1) Purpose: The drilling of DDH-11 was carried out to clarify the features of the lower part of black gossan and concealed FE anomaly zone in Antapampa area.

(2) Location: The drilling site is about 700 m north-northwest at Antapampa villige. The altitude is 4,605.6 m. This hole was drilled vertically -90° down to 250.5 m.

(3) Geology: From 2.5 m rock core was recovered and down to the bottom the Santa formation continues. Down to 41.0 m the Santa formation is an alternation of limestone, shale and marlstone, down to 111.6 m dolostone, siderite and shale, and to 197.0 m dolostone and siderite. From 197.0 m to the bottom it is limestone intercalating marlstone and shale (c.f. PL. III-11).

Dolostone with dark grey is penetrated with white siderite veinlets (BC-11-137). Dark grey siderite is considerably brecciated forming druses. Veinlets and druses are precipitated by white siderite (BC-11-067, Fig. III-20).

(4) Mineralization and ore grade: Dolomite and siderite are fresh with the naked eye, and contains rarely pyrite as ore minerals.

Assays by means of random sampling are as follows (see Fig. III-18).

	Samples	Total Length (m)	Ag (g/t)	Cu (%)	Pb (%)	Zn (%)
Dolostone	4	4	16	0.02	0.28	2.73
Siderite	4	4	16	0.01	0.15	2.78

Assays of pyrite disseminated parts are as follows.

Depth (m)	Intervals (m)	Ag (g/t)	Cu (%)	Pb (%)	Zn (%)
Dolostone 163.0 - 164.0	1	21	0.05	1.1	5.4
Shale 215.0 - 216.0	1	14	0.04	0.2	7.7

(5) Interpretation: According to X-ray diffraction, reflective peaks of siderite are shifted to the low angle side in comparison with usual siderite. This is characteristics of maganiferous siderite. Black gossan on the surface is considered to be an oxidation product of manganiferous siderite occurring subterranean. Moreover, minor sphalerite and galena contained in siderite were identified by X-ray diffraction. Tetrahedrite was detected by electron probe microanalysis (BC-11-238).

3-9 DDH-12

(1) Purpose: The drilling DDH-12 was carried out in order to clarify the lower part of black gossan exposed on the surface and underlying FE anomalous zone.

(2) Location: The drilling site is about 200 m to the south of DDH-11 with elevation of 4,599.9 m. It was drilled to 70° direction with inclination of -85°. Total depth is 310.5 m.

(3) Geology: The first rock was recovered at 3.0 m, and down to 302.6 m the Santa formation continues. The Santa formation is strongly altered such as dolomitization, sideritization, silicification and skarnization, and

concentrates partly pyrite, specularite, chalcopyrite and sphalerite.

Down to 77.6 m is an alternation of limestone, shale and marlstone, and to 157.6 m siderite and dolomite partially concentrating specularite. Down to 237.5 m the formation is strongly silicified and enriched in pyrite. From 237.5 m down to 249.5 m it carries specularite associated with pyrite, and down to 293.0 m it turns alteration of marlstone, skarn and pyrite mass. At the depth of 302.6 m appears Chimu formation composed of siliceous sandstone (c.f. PL. III-12).

(4) Mineralization and ore grade: Assays of the main mineralized part are as follows (see Fig. III-19).

Depth (m)	Intervals (m)	No. of Samples	Ag (g/t)	Cu (%)	Pb (%)	Zn (%)
122.8 - 128.1	5.3	2	12	0.12	0.10	4.89
137.4 - 141.6	4.2	2	16	0.52	0.15	3.35
142.4 - 144.6	2.4	1	34	1.89	tr.	0.20
237.5 - 247.2	9.7	5	94	3.08	0.01	0.33
281.2 - 285.4	4.2	2	35	2.73	tr.	0.40

(5) Interpretation: It was confirmed by X-ray diffraction that bornite as well as chalcopyrite occurs in the high grade part. Zonal arrangement in the mineralized zones is found from the upper to the lower. Copper and zinc are not concentrated in pyrite ore, but in hematite ore. The following zoning was clarified:

(Upper part) unmineralized limestone - dolomite·siderite - Zn·Cu·hematite
(specularite) -pyrite-Cu·hematite·pyrite-Cu·skarn (lower part)

3-10 Summary of Drilling Exploration

1) Sampling Method

The sampling method is shown in Fig. II-10. As a rule, a quarter of core was taken with an interval of 1 m using diamond cutter for the high

grade part, and a half of core with an interval of 2 m using core splitter for the low grade part. For eight holes, DDH-1, 3, 4, 8, 9, 10, 11 and 12, assay samples were prepared at Churin office, and for four holes, DDH-2, 5, 6 and 7, crushed samples were sent to laboratories and sample preparation was done in the laboratories.

2) Data Analysis

Assay results, microscopic observations, data of electron probe micro-analysis, and others are shown in the appendices. Results of X-ray diffraction are summarized in Fig. III-20.

Measurement results of apparent specific gravity of ores are shown in Table III-10, which indicates 4.07 in average for 12 pyritic ores and 3.51 for 5 skarn ores. Proceeding in measurements samples were dried in the air for 24 hours under 60°C temperature and then they were coated with paraffin.

3) Average Grades and Perspective Reserves

(1) Limpe Area

In Limpe area, four drillings were performed for the extent of 730 m and all hit high grade ores.

Main orebodies confirmed are as follows:

	Depth (m)	Interval (m)	No. of Samples	Ag (g/t)	Cu (%)	Pb (%)	Zn (%)	Real Wid. (m)
DDH-3	104.6 - 108.6	4.0	4	89	0.03	6.74	14.17	2.57
DDH-4	61.3 - 76.1	14.8	15	13	0.07	0.04	14.49	7.40
"	84.9 - 104.7	19.8	16	10	0.10	0.30	7.78	9.90
DDH-5	95.6 - 99.6	4.0	3	32	1.64	4.38	20.09	2.07
"	181.0 - 204.0	23.0	23	163	0.14	2.92	27.15	11.91
DDH-6	194.4 - 200.4	6.0	6	29	0.33	0.03	39.36	3.01
"	209.0 - 215.3	6.3	6	24	0.08	0.59	10.07	3.16
Weighted average based on individual holes			73	64	0.20	1.57	18.35	10.0

Ore grades in weighted average are 64 (g/t) in Ag, 0.20 (%) in Cu, 1.57 (%) in Pb and 18.35 (%) in Zn. Total length of ores for 4 holes is 77.9 m and average length for each hole is 19.5 m. Real widths of each layer can be calculated from the inclination of drilling and angle of bedding plane. The real width of ores is presumed to be 10.0 m in average for each hole.

On the assumption that the mineralized zone extends 800 m and specific gravity is 3.5, ore reserves of 28,000 t can be expected for each height of 1 m, as following equation; $800 \text{ m} \times 10.0 \text{ m} \times 3.5 = 28,000 \text{ t}$.

(2) Tinyag Area

In Tinyag area, main ores confirmed by the drilling of DDH-7 are as follows:

	Depth (m)	Intervals (m)	No. of Samples	Ag (g/t)	Cu (%)	Grade Pb (%)	Zn (%)	Real Wid. (m)
DDH-7	56.0 - 63.0	7.0	5	5	0.21	0.01	19.71	4.43
"	116.0 - 135.0	19.0	15	9	3.18	tr.	19.53	12.03
Weighted average		26.0	20	8	2.38	tr.	19.58	16.5

Total length of ores is 26.0 m and real width of ores is 16.5 m. Average grades of ores are 8 (g/t) in Ag, 2.38 (%) in Cu and 19.58 (%) in Zn.

I. High Grade Ore (1 m interval)

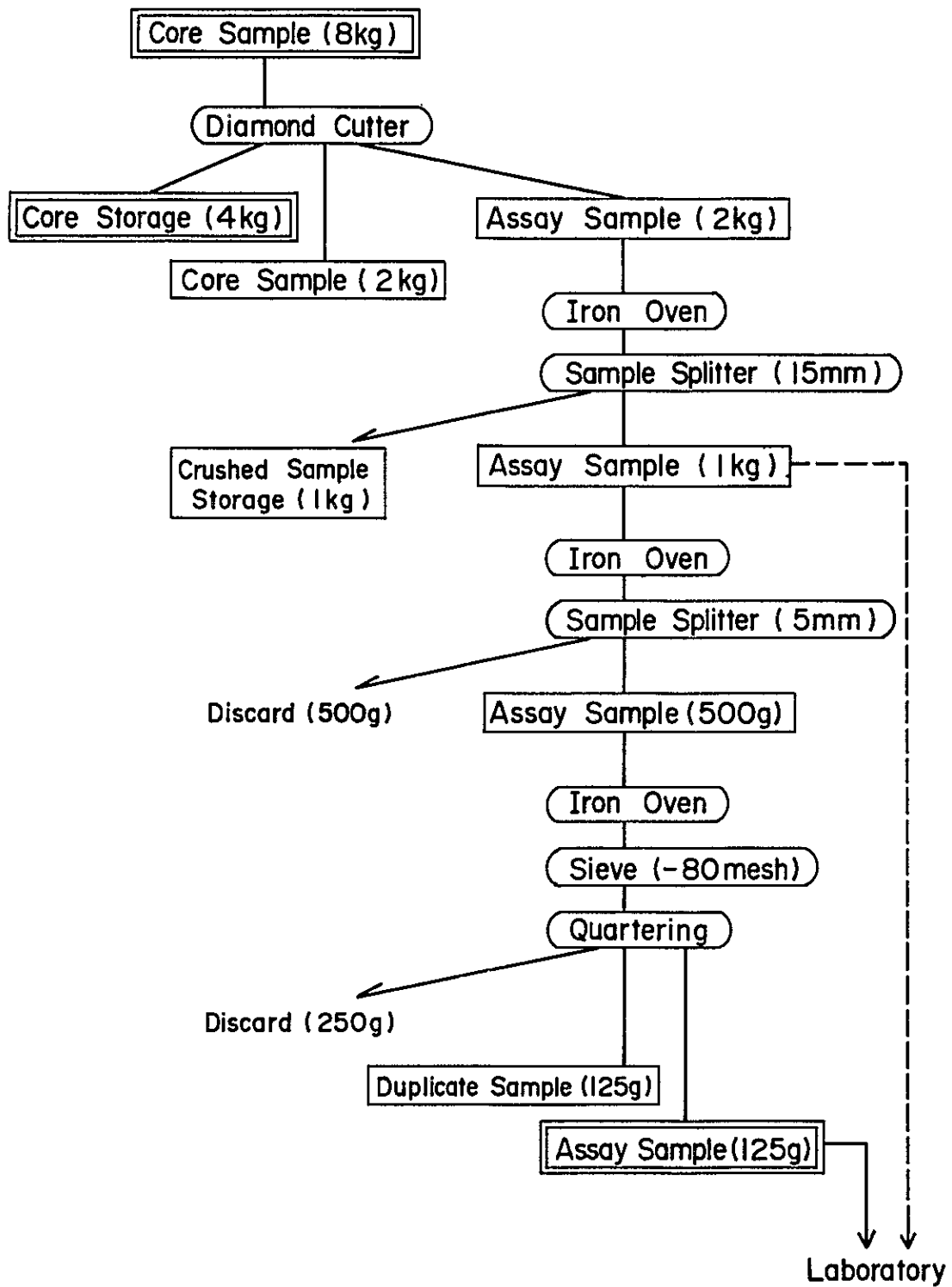


Fig. III - 10. Sample Procedures (I)

2. Low Grade Part (2.m interval)

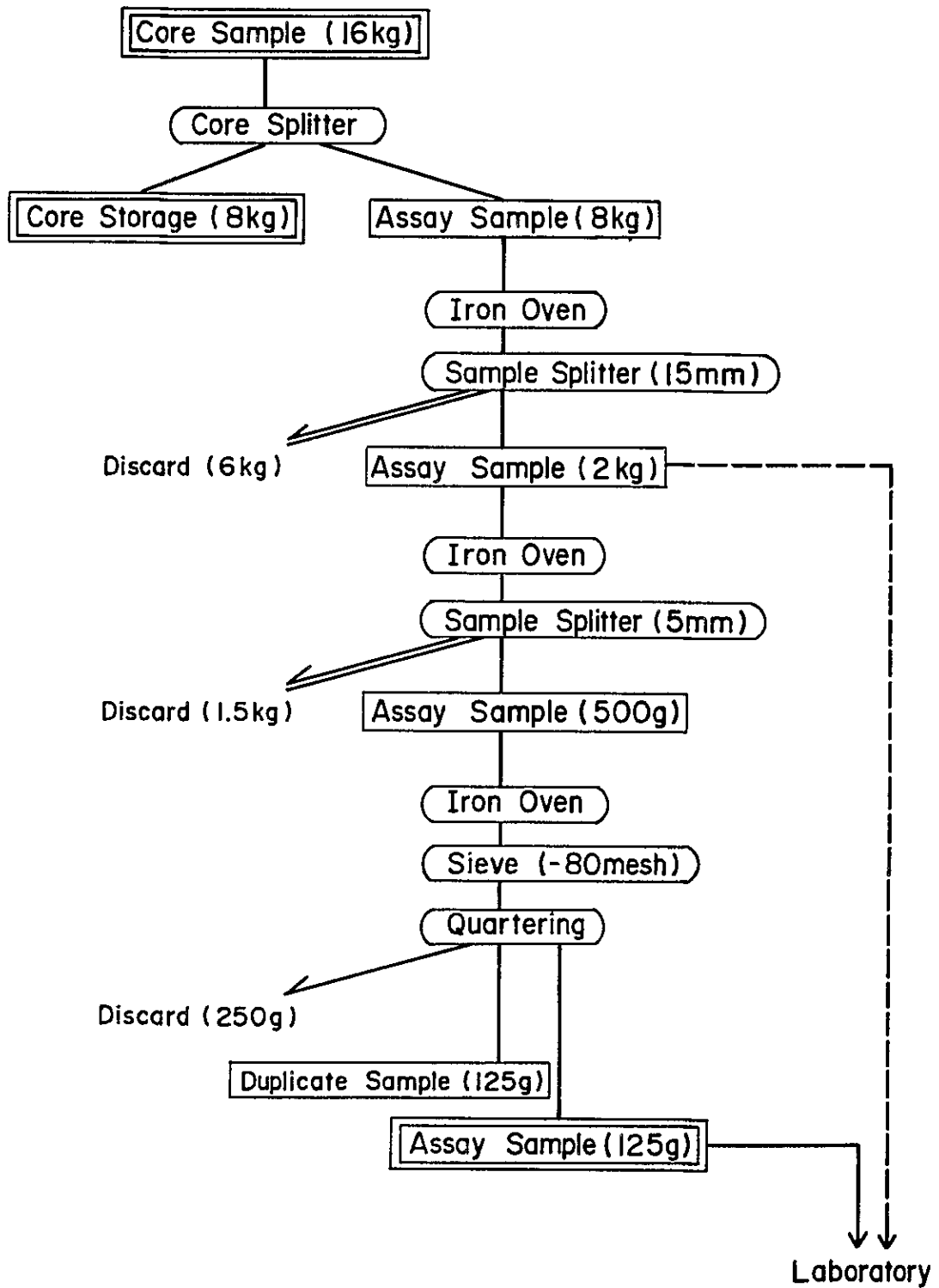
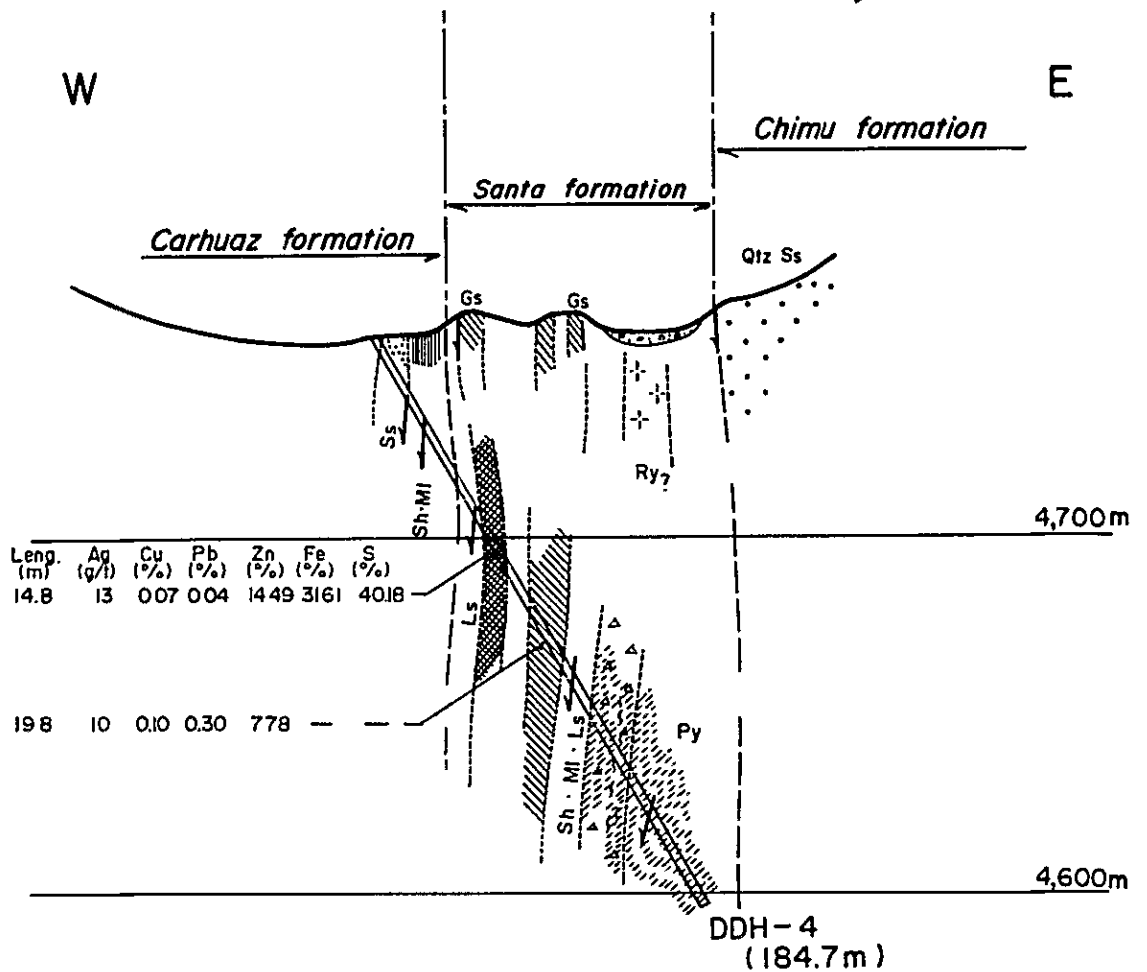


Fig. III - 10. Sample Procedures (2)



Abbreviation

- | | |
|---------------------|-----------------|
| Sh ----- Shale | High grade ore |
| Ss ----- Sandstone | Low grade ore |
| MI ----- Marl | Pyrite |
| Ls ----- Limestone | Gs ----- Gossan |
| Do ----- Dolostone | Sheared zone |
| Qtz ----- Quartzite | Brecciated zone |
| Ry ----- Rhyolite | Bedding |

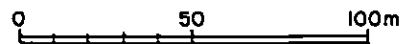


Fig. III - 11 Geological Section for DDH-4
(S70°W - N70°E)

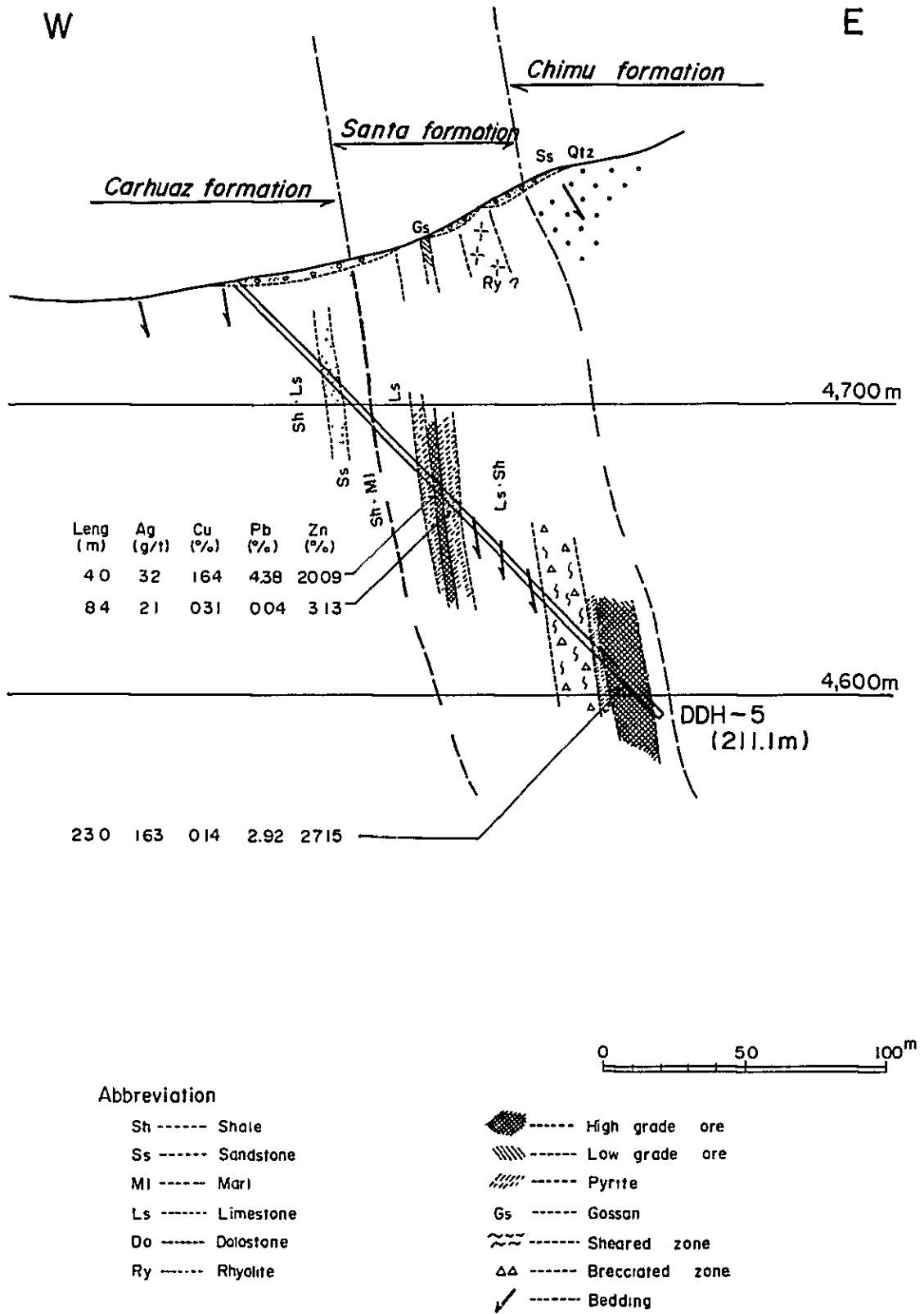


Fig. III-12 Geological Section for DDH-5 (S70°W - N70°E)

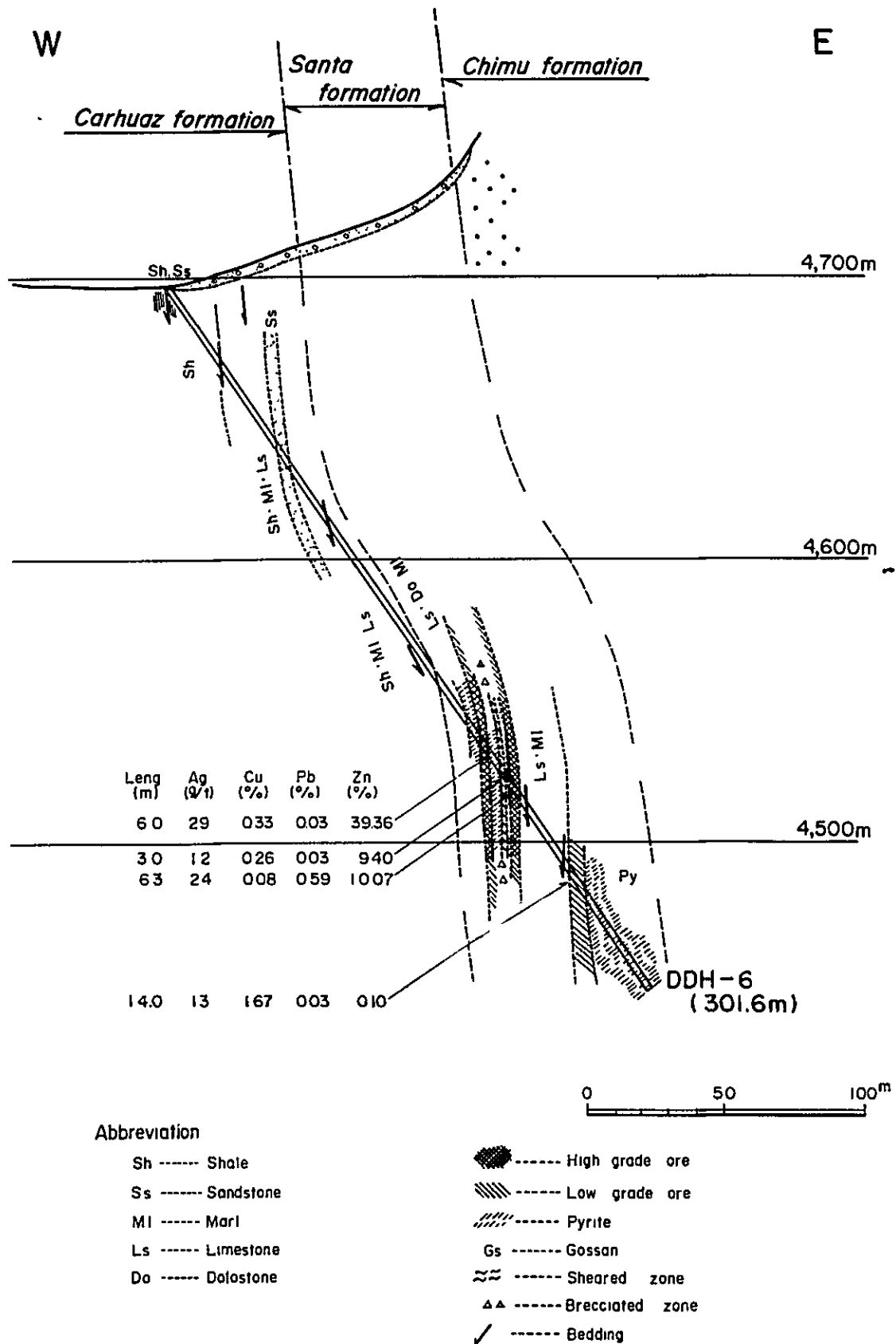


Fig. III - 13. Geological Section for DDH - 6 (S70°W - N70°E)

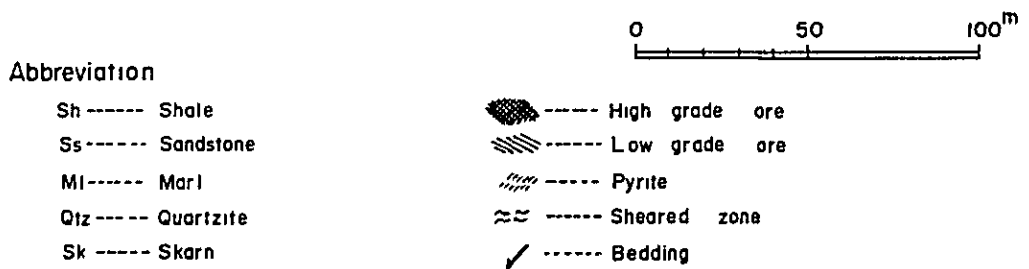
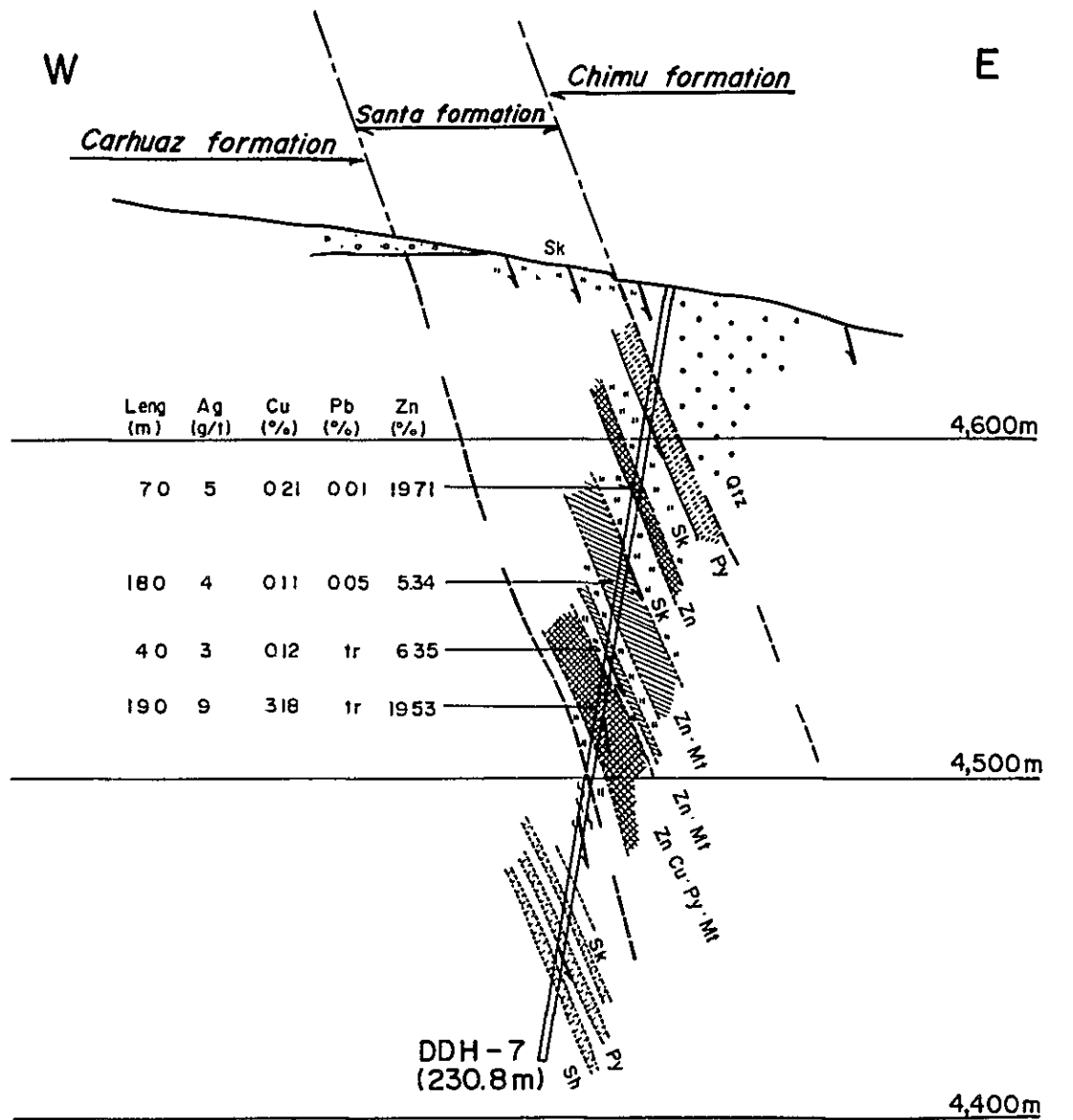


Fig. III - 14 Geological Section for DDH-7 (S70°W-N70°E)

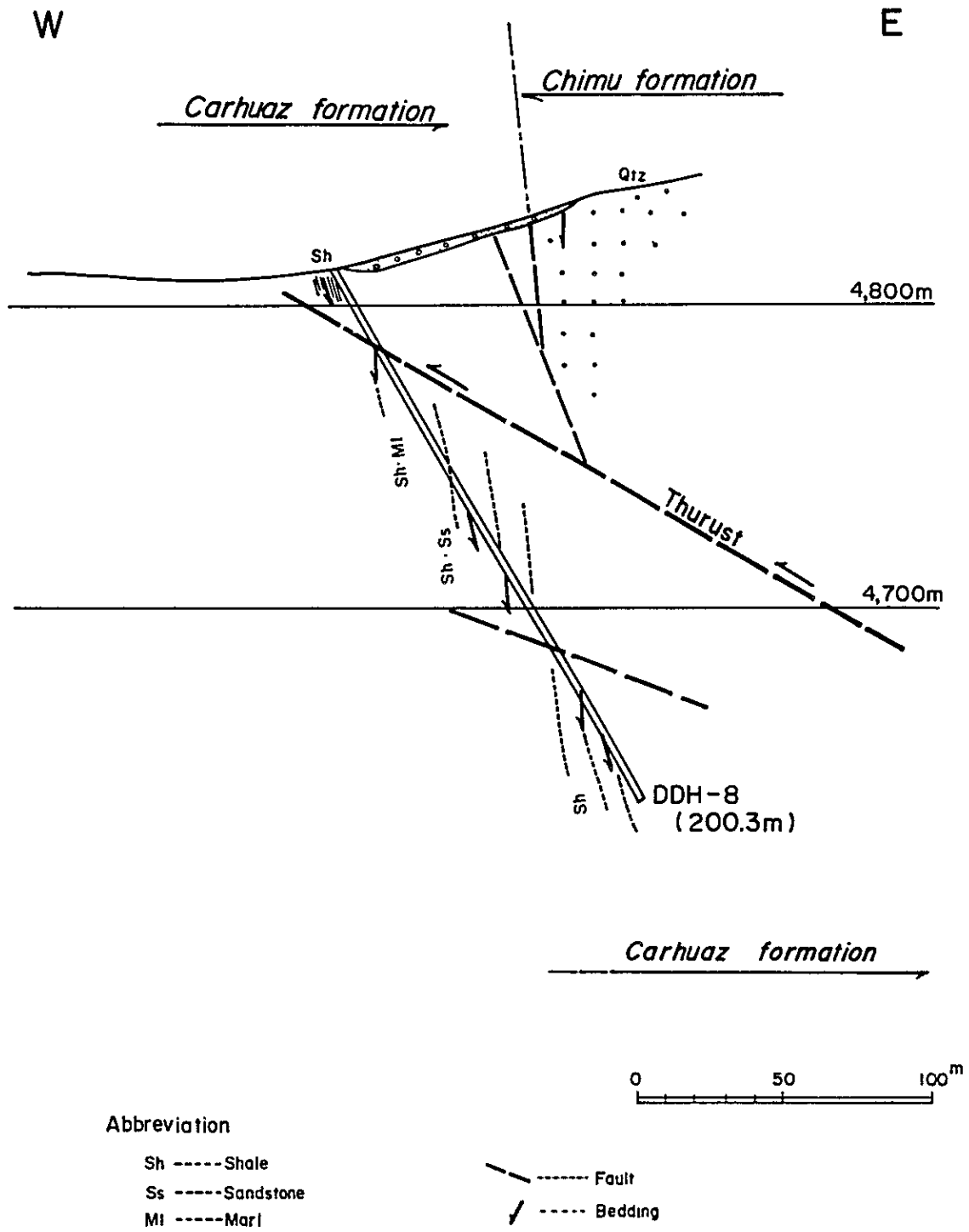


Fig. III - 15 Geological Section for DDH-8
(S70°W - N70°E)

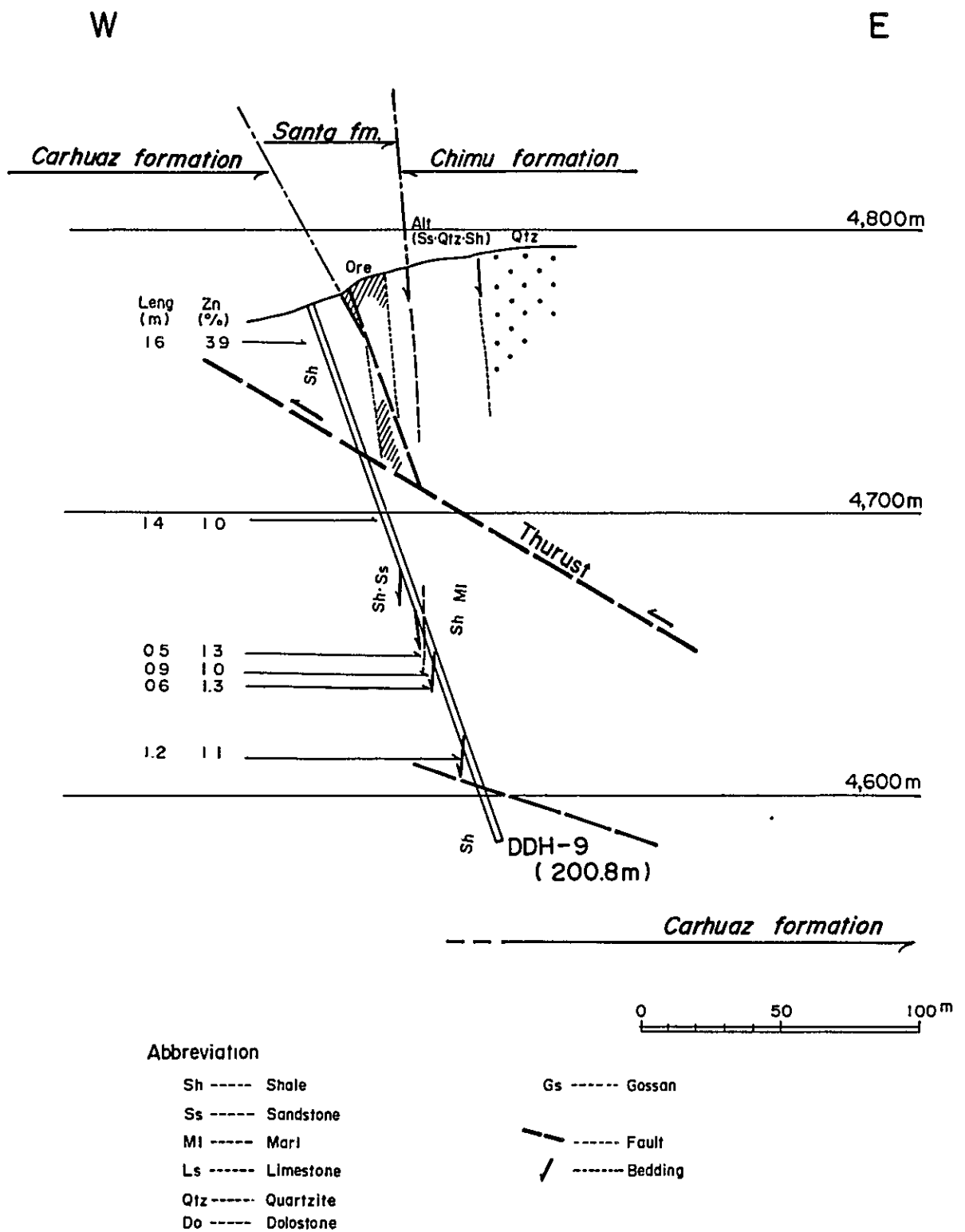


Fig. III - 16 Geological Section for DDH - 9 (S70°W-N70°E)

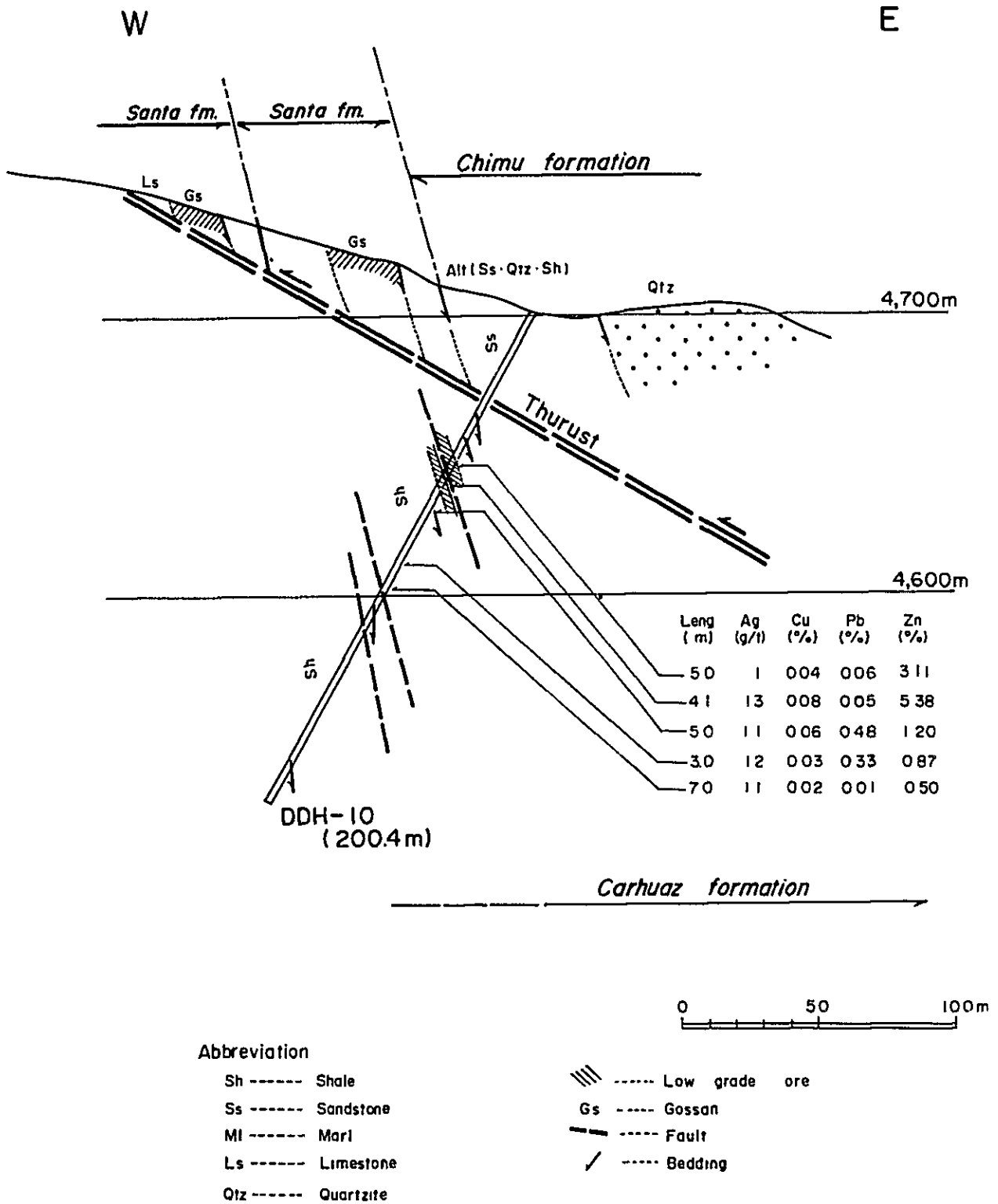


Fig III -17 Geological Section for DDH - 10 (S 75°E - N 75°W)

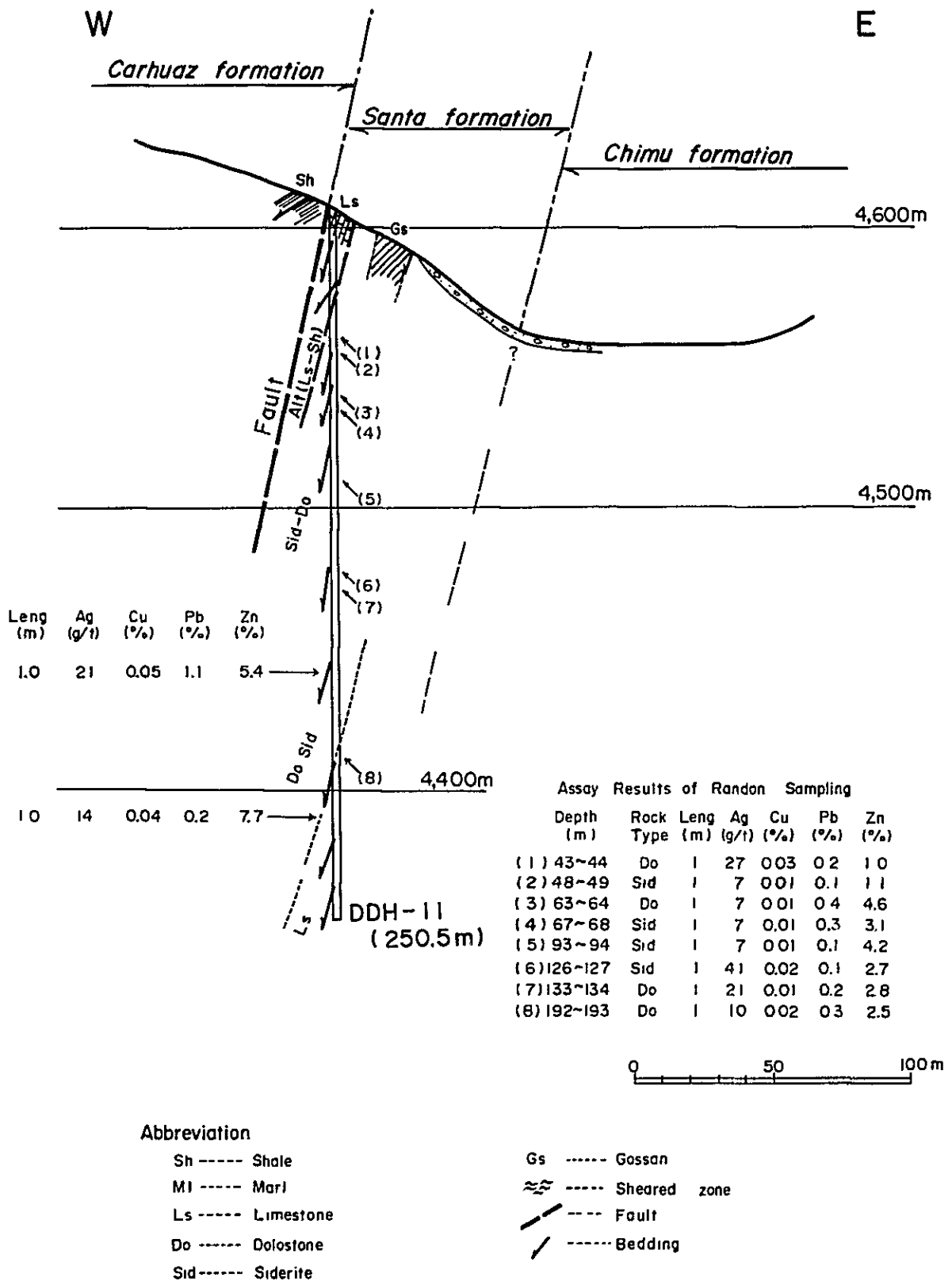


Fig. III-18 Geological Section for DDH-11

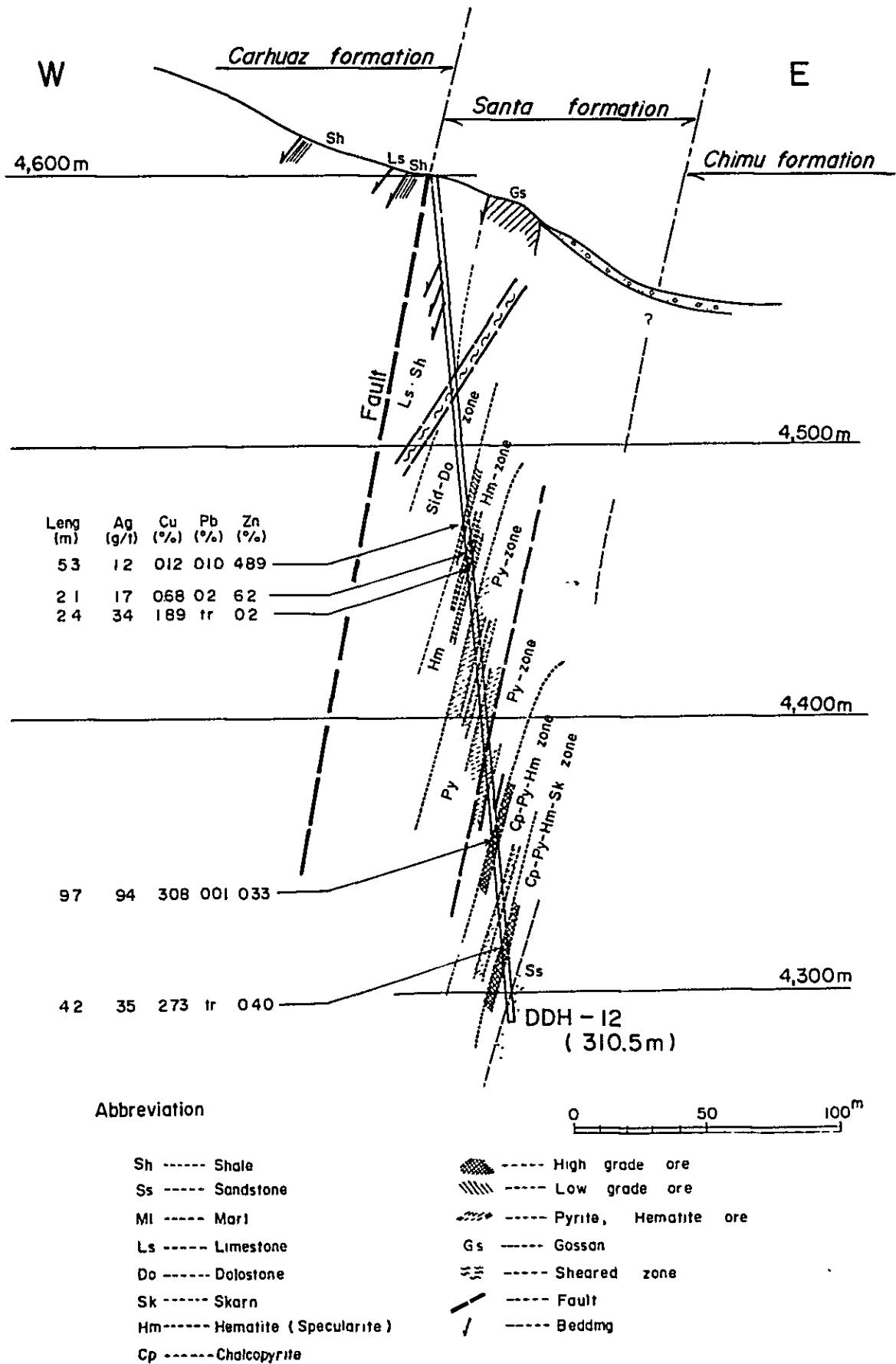


Fig. III - 19 Geological Section for DDH - 12 (S70°W - N70°E)

Table III-1 Measurement Results of Specific Gravity

<u>Sample No.</u>	<u>Type of Ore</u>	<u>Wa(g)</u>	<u>Wp(g)</u>	<u>Ww(g)</u>	<u>D</u>
BC-03-107	G1-Sp-Py ore	70.40	71.70	53.25	4.13
BC-04-064	Sp-Py ore	182.15	185.45	138.90	4.24
068	Sp-Py ore	115.90	117.50	88.15	4.19
076	Sp-Py ore	141.50	143.50	107.30	4.16
087	Sp-Py ore	124.95	126.90	96.00	4.34
104	Sp-Py ore	79.30	80.60	59.80	4.08
BC-05-099	G1-Sp-Py ore	65.45	66.50	48.60	3.90
183	Sp-Py ore	62.40	63.70	47.40	4.19
190	Sp-Py ore	61.05	62.30	45.30	3.90
192	Sp-Py ore	64.25	65.45	47.00	3.74
195	Sp-Py ore	75.50	77.00	56.35	3.97
199	G1-Sp-Py ore	71.05	72.90	52.90	3.95
<u>Av. of Massive Pyrite Ore</u>					<u>4.07</u>
BC-07-085(A)	Sk ore	152.35	154.30	107.90	3.43
085(B)	Sk ore	108.50	110.30	73.35	3.10
123	Sp Sk ore	104.50	105.85	78.65	4.05
126	Sp Sk ore	104.60	106.40	70.50	3.08
127	Sp-Mt Sk ore	80.30	81.50	59.70	3.91
<u>Av. of Skarn Ore</u>					<u>3.51</u>
BC-03-111	Py-Po	100.60	103.65	77.20	4.35
BC-06-257	Py	104.30	106.40	69.85	3.04
BC-07-109	Skarn	127.85	130.10	80.65	2.71
BC-07-218	Py Vein	137.00	139.05	101.07	3.83

D : Apparent specific gravity

Wa: Weight of dried sample in the air

Wp: Weight of paraffin coated sample in the air

Ww: Weight of paraffin coated sample in the water

Dp: Specific gravity of paraffin (=0.9)

Dw: Specific gravity of water (=0.997)

$$D = \frac{W_a \times D_w}{W_p - W_w - (W_p - W_a) / D_p}$$

APPENDICES
PART I
GEOLOGICAL DATA

A. I-1 List of Rock and Ore Samples

Index of Geological Units

Jm Jumasha formation
Pt Pariatambo formation
Cl Chulec formation
Ph Pariahuanca formation
Fr Farrat formation
Cz Carhuaz formation
St Santa formation
Ig Igneous rock
Cp Calipuy volcanics

Index of Analysis

T Thin section
P Polished section
X X-ray diffraction test
E EPMA (electron probe micro-
analysis)
O Assay of ore
R Complete analysis of rock
D Isotopic age determination
M Analysis of rock forming
elements

Abbreviation

Cu Cu-Minerals
Pb Pb-Minerals
Zn Zn-Minerals
Py Pyrite
Spc Specularite

Po Pyrrhotite
Mt Magnetite
Hm Hematite
Mn Mn-Minerals

List of Rock and Ore Samples

(1)

No.	Sample No.	Location	Geological Unit	Rock Name	T	P	X	E	O	R	D	M
1	NO-601	G4	Jm	Gossan					○			
2	NO-602	G4	Ph	Gossan (Py)					○			
3	NO-603	G4	Ph	Gossan (network)					○			
4	NO-604	G4	Fr	Gossan					○			
5	NO-605	G4	Ph	Altered limestone					○			
6	NO-606	G4	Ph	Skarn					○			○
7	NO-613	G4	Cp	Andesitic tuff	○							
8	NO-614	G4	Cl	Gossan (network)					○			
9	NO-616	G4	Jm	Limestone								○
10	NO-617	G4	Ph	Limestone								○
11	NO-620	G4	Pt	Limestone								○
12	NO-621	G4	Ph	Limestone								○
13	NO-624	G4	Cp	Welded tuff	○							
14	NO-625	G4	Cp	Andesite	○					○	○	
15	NO-629	G4	Cp	Altered rock			○					
16	NO-630	G4	Ig	Dacite porphyry	○							
17	NO-633	G4	Ig	Granodiorite	○					○	○	
18	NO-641	G4	St	Ore (Zn, Py)					○			
19	NO-642	G4	St	Ore (Zn, Py)					○			
20	NO-643	G4	St	Ore (Pb, Zn, Py)	○	○			○			
21	NO-644	G4	St	Ore (Cu, Zn)					○			
22	NO-647	G4	Cp	Welded tuff	○					○		
23	NO-652	G4	Ig	Granite porphyry	○					○	○	
24	NO-654	G4	Cl	Limestone								○
25	NO-655	G4	Pt	Limestone								○
26	NO-656	G4	St	Siderite ore (Py)			○					
27	NO-657	G4	St	Ore (Py, Mt)			○					
28	NO-658	G4	St	Muscovite skarn			○					
29	NO-661	IC-5	St	Altered rock			○					
30	NO-662	CQ	St	Green skarn			○					
31	NO-663	CQ	St	Ore (Pb, Zn)					○			
32	SO-501	G4	Cz	Siderite gossan					○			
33	SO-502	G4	Cz	Gossan					○			
34	SO-503	G4	Cz	Gossan					○			
35	SO-504	G4	Cz	Ore (Mn)			○		○			

(2)

No.	Sample No.	Location	Geological Unit	Rock Name	T	P	X	E	O	R	D	M
36	SO-505	G4	Cz	Gossan (Cu, Zn)					○			
37	SO-506	G4	Ph	Ore (Zn)					○			
38	SO-508	G4	Ph	Ore (Py, Zn, Pb)					○			
39	SO-511	G4	Ph	Ore (Cu, Py)			○					
40	SO-514	G4	Ig	Dacite	○							
41	SO-518	G4	Ig	Dacite	○							
42	SO-523	G4	Ig	Granodiorite porphyry	○							
43	SO-529	G4	Ig	Altered rock	○							
44	SO-530	G4	St	Skarn (Mt)					○			
45	SO-531	G4	St	Skarn (Py, Zn)					○			
46	SO-532	G4	St	Gossan (Py, Zn)					○			
47	SO-533	G4	St	Ore (Py, Zn)					○			
48	SO-534	G4	St	Ore (Zn, Py)					○			
49	SO-535	G4	St	Ore (Py, Zn)					○			
50	SO-536	G4	St	Ore (Py, Zn)					○			
51	SO-537	G4	St	Ore (Cu, Po)					○			
52	TO-505	G4	St	Ore (Py)					○			
53	TO-506	G4	St	Ore (Pb, Zn)		○						
54	TO-507	G4	St	Ore					○			
55	TO-508	G4	St	Gossan (Py)					○			
56	TO-509	G4	St	Garnet skarn			○		○			
57	TO-510	G4	St	Ore					○			
58	TO-511	G4	St	Ore					○			
59	TO-512	G4	St	Ore					○			
60	TO-513	G4	Ig	Dacite		○						
61	TO-514	G4	Ph	Ore (Py, Zn)					○			
62	TO-515	G4	Ph	Epidote skarn (Py, Zn)					○			
63	TO-517	G4	St	Gossan (Cu, Py)					○			
64	IC-701	IC-3	St	Gossan			○					
65	IC-702	IC-3	St	Gossan					○			
66	IC-703	IC-3	St	Gossan					○			
67	IC-705	IC-3	St	Ore (Cu, Zn, Hm)		○			○			
68	IC-706	IC-3	Ig	Altered rock	○		○					

(3)

No.	Sample No.	Location	Geological Unit	Rock Name	T	P	X	E	O	R	D	M
69	IC-801	IC-3	St	Ore (Zn)					○			
70	IC-802	IC-3	St	Ore (Zn, Py)		○	○					
71	IC-804	IC-3	St	Ore					○			
72	IC-805	IC-3	St	Ore (Zn)					○			
73	IC-806	IC-3	St	Ore (Zn)		○	○		○			
74	IC-807	IC-3	St	Ore					○			
75	IC-808	IC-3	St	Gossan (Spc)					○			
76	IC-901	IC-5	Ig	Altered rhyolite	○							
77	IC-902	IC-5	Ig	Brecciated rock	○							
78	CQ-301	CQ	Ph	Green skarn (Py)			○		○			
79	CQ-302	CQ	Ph	Green skarn					○			
80	CQ-303	CQ	Ph	Green skarn					○			
81	CQ-304	CQ	Ph	Green skarn					○			
82	CQ-305	CQ	Ph	Ore (Zn, Pb)					○			
83	CQ-306	CQ	Ph	Ore (Zn, Pb, Py)		○			○			
84	CQ-307	CQ	Ph	Green skarn					○			
85	CQ-308	CQ	Ph	Green skarn					○			
86	CQ-309	CQ	Ph	Green skarn					○			
87	CQ-310	CQ	Ph	Ore (Zn)					○			
88	CQ-311	CQ	Ph	Green skarn					○			
89	CQ-312	CQ	Ph	Skarn (Pb, Zn)					○			
90	CQ-313	CQ	Ph	Skarn					○			
91	CQ-314	CQ	Ph	Skarn					○			
92	CQ-315	CQ	Ph	Skarn					○			
93	CQ-316	CQ	Ph	Skarn					○			
94	CQ-317	CQ	Ph	Skarn (Zn, Pb)					○			
95	CQ-318	CQ	Ph	Skarn					○			
96	CQ-319	CQ	Ph	Garnet skarn					○			
97	CQ-320	CQ	Ph	Garnet skarn					○			
98	CQ-321	CQ	Ph	Garnet skarn					○			
99	CQ-322	CQ	Ph	Garnet skarn					○			
100	CQ-323	CQ	Ph	Garnet skarn (Py)					○			
101	CQ-324	CQ	Ph	Garnet skarn (Mt)					○			
102	CQ-325	CQ	Ph	Garnet skarn (Mt)					○			
103	CQ-326	CQ	Ph	Garnet skarn (Mt)					○			

(4)

No.	Sample No.	Location	Geological Unit	Rock Name	T	P	X	E	O	R	D	M
104	CQ-327	CQ	Ph	Gossan (Py)					○			
105	CQ-328	CQ	Ph	Garnet skarn (Mt)					○			
106	CQ-329	CQ	Ph	Garnet skarn (Mt)					○			
107	CQ-330	CQ	Ph	Garnet skarn (Mt)					○			
108	CQ-331	CQ	Ph	Skarn (Mt)					○			
109	CQ-332	CQ	Ph	Garnet skarn	○				○			
110	CQ-333	CQ	Ph	Garnet skarn (Mt)					○			
111	CQ-334	CQ	Ph	Garnet skarn (Py)					○			
112	CQ-335	CQ	Ph	Garnet skarn (Py)					○			
113	CQ-336	CQ	Ph	Garnet skarn(Cu,Py)					○			
114	CQ-337	CQ	Ph	Ore (Cu, Py)					○			
115	CQ-338	CQ	Ph	Ore (Cu, Py)					○			
116	CQ-339	CQ	Ph	Garnet skarn					○			
117	CQ-340	CQ	Ph	Ore (Cu, Py)					○			
118	CQ-341	CQ	Ph	Ore (Cu, Py)					○			
119	CQ-342	CQ	Ph	Garnet skarn(Mt,Py)					○			
120	CQ-343	CQ	Ph	Ore (Py, Mt)					○			
121	CQ-344	CQ	Ph	Garnet skarn					○			
122	CQ-345	CQ	Ph	Ore (Py)					○			
123	CQ-346	CQ	Cl	Ore (Cu, Py)					○			
124	CQ-347	CQ	Cl	Skarn (Py)					○			
125	CQ-348	CQ	Ph	Ore (Py, Zn)					○			
126	CQ-349	CQ	Ph	Ore (Py, Zn)					○			
127	CQ-350	CQ	Ph	Green skarn					○			
128	CQ-351	CQ	Ph	Green skarn					○			
129	CQ-352	CQ	Ph	Green skarn					○			
130	CQ-353	CQ	Ph	Pyroxene skarn	○				○			
131	CQ-354	CQ	Ph	Green skarn(Py,Mt)					○			
132	CQ-355	CQ	Ph	Green skarn (Py)					○			
133	CQ-356	CQ	Ph	Ore (Pb,Zn,Py)		○	○		○			
134	CQ-357	CQ	Ph	Green skarn					○			
135	CQ-358	CQ	Ph	Green skarn					○			
136	CQ-359	CQ	Ph	Green skarn					○			
137	CQ-360	CQ	Ph	Ore (Py, Zn)					○			
138	CQ-361	CQ	Ph	Green skarn					○			

(5)

No.	Sample No.	Location	Geological Unit	Rock Name	T	P	X	E	O	R	D	M
139	CQ-362	CQ	Ph	Green skarn					○			
140	CQ-363	CQ	Ph	Ore (Py, Zn)					○			
141	CQ-364	CQ	Ph	Ore (Py, Pb, Zn)					○			
142	CQ-365	CQ	Ph	Ore (Py, Pb)					○			
143	CQ-366	CQ	Ph	Ore (Py)					○			
144	CQ-367	CQ	Ph	Ore (Py)					○			
145	CQ-368	CQ	Ph	Green skarn (Py)					○			
146	CQ-369	CQ	Ph	Green skarn(Pb,Py)					○			
147	CQ-370	CQ	Ph	Green skarn (Pb)					○			
148	CQ-371	CQ	Ph	Ore (Pb, Zn, Py)					○			
149	CQ-372	CQ	Ph	Ore (Zn, Py)		○	○		○			
150	CQ-373	CQ	Ph	Ore (Zn)					○			
151	CQ-374	CQ	Ph	Green skarn					○			
152	CQ-375	CQ	Ph	Green skarn					○			
153	CQ-376	CQ	Ph	Green skarn					○			
154	CQ-377	CQ	Ph	Green skarn					○			
155	CQ-380	CQ	Ph	Skarn					○			
156	CQ-381	CQ	Ph	Gossan					○			
157	CQ-382	CQ	Ph	Gossan					○			
158	CQ-383	CQ	Ph	Gossan					○			
159	CQ-384	CQ	Ph	Skarn					○			
160	CQ-385	CQ	Ph	Skarn					○			
161	CQ-386	CQ	Ph	Garnet skarn	○				○			
162	CQ-387	CQ	Ph	Skarn					○			
163	CQ-388	CQ	Ph	Skarn					○			
164	CQ-389	CQ	Ph	Garnet skarn (Mt)					○			
165	CQ-390	CQ	Ph	Garnet skarn (Mt)					○			
166	CQ-391	CQ	Ph	Garnet skarn (Mt)			○		○			
167	CQ-392	CQ	Ph	Garnet skarn					○			
168	CQ-393	CQ	Ph	Garnet skarn					○			
169	CQ-394	CQ	Ph	Garnet skarn					○			
170	CQ-395	CQ	Ph	Skarn					○			
171	CQ-396	CQ	Ph	Skarn					○			
172	CQ-397	CQ	Ph	Skarn					○			
173	CQ-398	CQ	Ph	Skarn					○			

(6)

No.	Sample No.	Location	Geological Unit	Rock Name	T	P	X	E	O	R	D	M
174	CQ-399	CQ	Ph	Skarn					○			
175	TP-301	G4	Ph	Ore (Zn, Cu)					○			
176	TP-302	G4	Ph	Altered rock			○		○			
177	TP-303	G4	Ph	Ore					○			
178	TP-304	G4	Ph	Skarn (Mt)	○				○			
179	TP-305	G4	Ph	Skarn (Cu, Mt)			○		○			
180	TP-306	G4	Ph	Ore (Py, Mt)					○			
181	TP-307	G4	Ph	Ore (Cu, Zn, Mt)		○	○		○			
182	TP-308	G4	Ph	Ore (Zn, Mt)					○			
183	TP-309	G4	Ph	Ore (Zn, Mt)					○			
184	TP-310	G4	Ph	Ore (Zn)					○			
185	TP-311	G4	Ph	Ore					○			
186	TO-312	G4	Ph	Ore (Zn, Po)		○			○			
187	TP-313	G4	Ph	Ore (Cu, Py)					○			
188	TP-314	G4	Ph	Ore (Cu, Zn)					○			

A. I-2 Microscopic Observation of the Thin Section

(1)

<u>Sample No.</u>	<u>Rock Type</u>	<u>Microscopic Observation</u>
IC-706	Altered rock (Ig)	This rock is so strongly altered that it is difficult to make clear the original rock. It is composed mainly of quartz and sericite. Quartz crystals, which are usually less than 0.1 mm in diameter, are scattered in a microcrystalline matrix. A small amount of opaque minerals is commonly found in this rock.
IC-901	Altered rhyolite (Ig)	It is composed essentially of quartz and sericite, showing porphyritic texture. Phenocrysts are completely replaced by quartz aggregates and sericite. They are embedded in a fine-textured groundmass with interstitial glass. Some cavities and cracks are found in the groundmass which is also sericitized and silicified.
IC-902	Brecciated rock (Ig)	It is composed essentially of rock and crystal fragments, with accessory zircon. Rock fragments are granular and/or subangular, 2.5 x 2.0 mm to 0.3 x 0.3 mm in size, and consist of quartzite and sericitized rhyolite(?). Crystal fragments are composed mainly of quartz, 1.0 mm to 0.5 mm in diameter. Strong silicification and sericitization are found in a fellopathic matrix which are enclosed by scattering small grained opaque minerals. (See photograph)
TP-304	Magnetite skarn (Ph)	A lot of magnetite in idiomorphic crystals are scattered in the aggregates of bladed or needlelike crystals. These aggregates appear to be originally amphibole, but they have been strongly altered to chlorite and carbonates. A little quartz and sphalerite is also seen as accessory minerals.
CQ-332	Garnet skarn	It is composed mainly of garnet, carbonate and quartz, with subordinate amount of chlorite. Garnet shows an idiomorphic crystal, 0.8 to 0.1 mm in diameter, showing strongly anomalous. A little of chlorite and calcite are seen as alteration products in it. Quartz and carbonate show xenomorphic and large crystals, respectively, and develop to be filled with interstices of garnet crystals. It is also seen to contain a little of opaque minerals.
CQ-353	Pyroxene skarn	It consists mainly of clinopyroxene, with accessory of opaque minerals, sphalerite and quartz. Clinopyroxene of idiomorphic and hypidiomorphic crystals shows slender columnar aggregates, up to 0.8 mm in size. A small amount of quartz, carbonate and chlorite are seen in these aggregates. Pseudomorph of garnet occurs in parts showing granular form. It is completely altered to carbonate, clinopyroxene and a little chlorite. (See photograph)
CQ-386	Garnet skarn (Ud, h)	It is composed mainly of garnet, carbonate and quartz, and a small amount of chlorite and sphalerite. Garnet in idiomorphic crystals shows optical anomaly and up to 0.8 mm in size. It is altered to calcite in the interior. Under the open nicol, the original structure of this skarn can be observed, but under the crossed nicols it is confirmed that it is completely altered to calcite and quartz. (See photograph)
SO-514	Dacite (Ig) (Cochaquillo)	It shows porphyritic texture and is composed essentially of plagioclase and quartz, with accessory epidote, apatite and zircon. The phenocrysts are of plagioclase and quartz, occasionally with scattered clinopyroxene which is completely altered to epidote. The groundmass shows a devitrified cryptofelsitic base and contains a little of quartz and clinopyroxene. A few veinlets of quartz and epidote are also seen in it. (See photograph)

<u>Sample No.</u>	<u>Rock Type</u>	<u>Microscopic Observation</u>
SO-518	Dacite (Ig) (Cochaquillo)	It shows porphyritic texture and is composed mainly of plagioclase and quartz, with accessory zircon. The phenocrysts are of plagioclase and quartz. The phenocryst of plagioclase shows idiomorphic crystal, up to 1.5 x 0.8 mm in size, and is altered to carbonate and sericite in parts. It shows albite and carlsbad twins. The constituents of the groundmass are of minute quartz, carbonate, sericite and salic minerals.
SO-523	Granodiorite porphyry (Ig) (Chagapata)	It shows porphyritic texture and is composed mainly of plagioclase, quartz, k-feldspar, biotite and hornblende, with accessory sphene, apatite and zircon. The phenocrysts are of plagioclase, k-feldspar, biotite and hornblende. Plagioclase shows clearly albite and carlsbad twins. Hornblende shows tabular form and is altered to biotite and chlorite in parts. The groundmass shows holocrystalline and consists of a lot of quartz, plagioclase and a little of k-feldspar. (See photograph)
SO-529	Altered rock (Ig) (Chagapata)	This rock is strongly altered to be seemed to be sericitized shale. The constituents are quartz, sericite, felsic minerals and interstitial chloritic and glassy material, a few of zircon. Under the microscope, it is divided into two phases by its lithology. One is composed mainly of sericite and a small amount of quartz. The other is composed of a glassy matrix with a lot of dust. These phases are intergradational.
TO-513	Dacite (Ig) (Chagapata)	It shows porphyritic texture and is composed of plagioclase, k-feldspar and quartz. Plagioclase and k-feldspar phenocrysts lie in a groundmass that is composed chiefly of quartz and feldspar, accompanied by a little chlorite. Plagioclase shows albite and carlsbad twins and suffers from argillization and chloritization. Mafic minerals are completely altered to carbonate mineral, chlorite and a little epidote.
NO-613	Andesitic tuff (Cp) (Cochaquillo)	The constituents are abundant rock fragments and a little quartz. They lie in a matrix with interstitial iron oxide. These rock fragments consist mainly of andesite, with subordinate amount of dolerite, and they are subjected to carbonatization and chloritization. The phenocrysts are of plagioclase and completely carbonatized mafic minerals. The groundmass shows flow texture and the constituents are idiomorphic laths of plagioclase, quartz and silica minerals.
NO-624	Welded tuff (Cp) (Cochaquillo)	It shows porphyritic texture and is composed mainly of plagioclase and a little quartz. The phenocrysts of plagioclase show tabular form, and suffering from strong carbonatization and weak sericitization, in parts, completely altered to carbonate aggregates. The groundmass shows weakly flow texture and is composed mainly of idiomorphic laths of plagioclase and quartz, accompanied by alteration products of carbonate minerals and a little chlorite.
NO-625	Andesite (Cp) (Cochaquillo)	It shows porphyritic texture and is composed mainly of plagioclase, with subordinate amount of hornblende and quartz. Phenocrysts of plagioclase, clinopyroxene and hornblende are embedded in a glassy groundmass that consists of plagioclase, clinopyroxene and quartz. The phenocrysts of plagioclase show albite twin and are altered to orthoclase and carbonate minerals in the interior. Mafic minerals sometimes suffer from chloritization and weak epidotization. A small amount of apatite and zircon is seen as accessory minerals. (See photograph)

<u>Sample No.</u>	<u>Rock Type</u>	<u>Microscopic Observation</u>
NO-630	Dacite porphyry (Ig) (Cochaquillo)	This rock is so strongly altered and it is difficult to presume the original rock. It is composed mainly of quartz, plagioclase, epidote, barite and rock fragments, with accessory sphene and zircon. Plagioclase shows tabular form and is altered to albite and in part completely altered to barite. Barite is seen as alteration product and shows xenomorphic aggregates or a slender prism, closely in epidote intergrowth. The matrix is composed essentially of fine-grained felsic minerals and quartz, with subordinate amount of barite.
NO-633	Granodiorite (Ig) (Cochaquillo)	It is composed mainly of plagioclase and quartz, with subordinate amount of k-feldspar and hornblende. Plagioclase shows idiomorphic or hypidiomorphic tabular forms suffered from argillization and sericitization. K-feldspar is also argillized and occurs in micrographic intergrowth with quartz. Hornblende is strongly altered and, in part, completely altered to chlorite. A small amount of epidote and sphene is seen as accessory minerals. (See photograph)
NO-643	Zn-Py ore (St) (Chagapata)	It is composed mainly of garnet, calcite and quartz, with subordinate amount of sphalerite. Garnet shows idiomorphic form, up to 1.8 mm in diameter, and clear zoning between crossed nicols. Surrounded by xenomorphic quartz and calcite, sphalerite is occasionally observed. Sphalerite is yellowish brown in color and shows xenomorphic form. A small amount of chlorite and epidote is seen as secondary minerals.
NO-647	Welded tuff (Cp) (Chagapata)	This rock shows flow structure (welding structure) and is composed mainly of plagioclase, quartz and rock fragments, with subordinate amount of hornblende and clinopyroxene. Rock fragments are andesite, rhyolite, quartzite and granitic rock. (See photograph)
NO-652	Granite Porphyry (Ig) (Chagapata)	It shows porphyritic texture and is composed mainly of plagioclase, K-feldspar, quartz and biotite. Phenocrysts of zoned plagioclase show albite and Carlsbad twins, and, in part, are altered to orthoclase. The quartz phenocrysts are up to 1.5 mm in diameter and are partly corroded. The constituents of the groundmass are very fine-grained quartz and feldspathic material, with accessory apatite and zircon. The matrix shows cryptocrystalline, in which a small amount of quartz, clay mineral and dust is observed. (See photograph)

A. I-3 Microscopic Observation of the Polished Section

(1)

<u>Sample No.</u>	<u>Rock Type</u>	<u>Microscopic Observation</u>
IC-705	Cu-Zn-Ha ore (St)	The constituents are hematite, chalcopyrite and sphalerite, as accessory Bi-Pb-S mineral, chalcocite-covellite and argentite. Hematite shows idiomorphic needles and it's aggregates. Chalcopyrite is medium to coarse-grained crystal, closely accompanied with covellite and Pb-Bi-S mineral, and also traversed by Fe-hydroxide veinlets. It is suggested that a very small grained argentite is included in covellite, according to the result of electron microprobe analysis. (See photograph)
IC-802	Zn-Py ore (St)	This ore consists mainly of sphalerite and pyrite, with subordinate amount of chalcopyrite, hematite and galena. Sphalerite includes tiny chalcopyrite dots and idiomorphic pyrite, which is up to 1.0 mm in size. Hematite shows bladed-form and magnetite is a small grained crystal, which is also included in sphalerite.
IC-806	Zn-ore (St)	Main constituent is sphalerite, next in abundance are hematite and chalcopyrite, then magnetite. Sphalerite shows coarse-grained form, accompanied with chalcopyrite dots. Sometimes, sphalerite pseudomorphs after pyrite is observed. Accicular form of hematite, up to 0.4 mm in across, is commonly observed in this ore.
TP-307	Cu-Zn-Mt ore (Ph)	The constituents are magnetite, pyrite and pyrrhotite, with subordinate amount of chalcopyrite. Magnetite chiefly in tabular-shaped aggregates, shows partly pseudomorph after hematite, intimately accompanied with pyrrhotite and pyrite. Pyrite shows xenomorphic form and is replaced largely by gangue minerals. Pyrrhotite is replaced partly by marcasite. Chalcopyrite closely associated with pyrrhotite is dispersed widely in this ore. (See photograph)
TP-312	Zn-Po ore (Ph)	This ore consists of sphalerite and pyrrhotite, with accessory pyrite and magnetite. Sphalerite shows large crystal including a small amount of chalcopyrite dots. Pyrrhotite shows idiomorphic to hypidiomorphic form, and is replaced occasionally by magnetite. Pyrite in idiomorphic to hypidiomorphic form shows aggregated crystals which are replaced partly by marcasite.
CQ-306	Pb-Zn-Py ore (Ph)	The constituents are pyrite, sphalerite and galena, with accessory chalcopyrite. Pyrite shows idiomorphic large crystal, and is up to 4.0 mm in size. Sphalerite including chalcopyrite dots shows xenomorphic form and interstices in gangue minerals. Galena shows coarse-grained and idiomorphic form, and associates closely with pyrite.
CQ-356	Pb-Zn-Py ore (Ph)	This ore consists mainly of pyrite, sphalerite, galena and chalcopyrite, with accessory covellite-chalcocite and arsenopyrite. Pyrite shows idiomorphic and coarse-grained form, and is replaced partly by sphalerite and galena. Sphalerite includes two types of chalcopyrite dots in size. One is several microns in diameter, the other is less than 1 micron. The later occurs irregularly in sphalerite showing spotted appearance, the texture of which is assumed to be a kind of replacement texture. Galena is accompanied intimately with sphalerite and arsenopyrite, and partly alter to cerussite, according to the result of electron microprobe analysis. (See photograph)

<u>Sample No.</u>	<u>Rock Type</u>	<u>Microscopic Observation</u>
CQ-372	Zn-Py ore (Ph)	It is composed mainly of sphalerite, with subordinate amount of galena and pyrite. Sphalerite shows idiomorphic to xenomorphic form and is associated intimately with galena. Sphalerite includes scarcely chalcopyrite dots. Galena shows xenomorphic form, up to 0.6 mm, including a little idiomorphic pyrite.
TO-506	Pb-An ore (St) (Chagapata)	Main constituent is sphalerite, with galena and pyrite as accessory, A lot of chalcopyrite dots is included in sphalerite filling cracks and cavities in irregular shape. Galena shows xenomorphic form and is associated closely with sphalerite and chalcopyrite. Galena lies also in a cavity of the matrix as well as sphalerite. Chalcopyrite is scarce and alters partly to covellite-chalcocite.
NO-643	Pb-Zn-Py ore (St) (Chagapata)	It is composed mainly sphalerite, galena and pyrite, with accessory chalcopyrite. Sphalerite shows xenomorphic form and fills with the interstice of coarse grains of gangue minerals (garnet?). Sphalerite in this ore is scarcely accompanied with chalcopyrite dots. Galena shows xenomorphic to hypidiomorphic form accompanied with sphalerite and pyrite.

A. I-4 -1 Thin Section

Sample No.	Location	Geological Unit	Rock Type
NO-613	G4	Cp	Andesitic tuff
NO-624	G4	Cp	Welded tuff
NO-625	G4	Cp	Andesite
NO-630	G4	Ig	Dacite porphyry
NO-633	G4	Ig	Granodiorite
NO-643	G4	St	Sphalerite-pyrite ore
NO-647	G4	Cp	Welded tuff
NO-652	G4	Ig	Granite porphyry
SO-514	G4	Ig	Dacite
SO-518	G4	Ig	Dacite
SO-523	G4	Ig	Granodiorite porphyry
SO-529	G4	Ig	Altered rock
TO-513	G4	Ig	Dacite
IC-706	IC-3	Ig	Altered rock
IC-901	IC-5	Ig	Altered rhyolite
IC-902	IC-5	Ig	Brecciated rock
CQ-332	CQ	Ph	Garnet skarn
CQ-353	CQ	Ph	Pyroxene skarn
CQ-386	CQ	Ph	Garnet skarn
TP-304	G4	Ph	Magnetite skarn

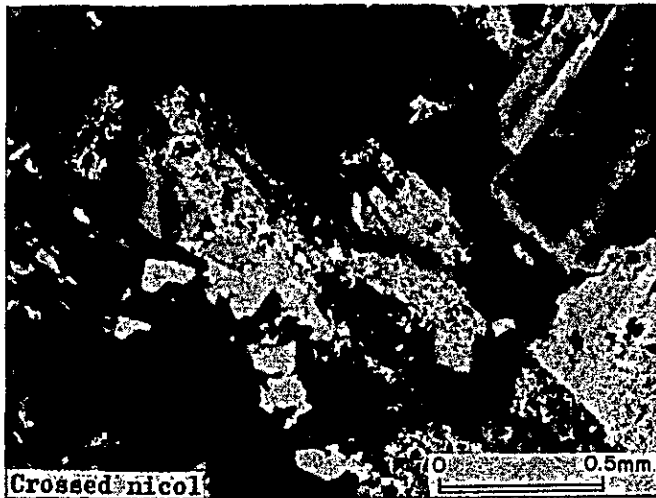
Abbreviations

Bt : Biotite	Kf : Alkali-feldspar
Cal : Calcite	Pl : Plagioclase
Chl : Chlorite	Qt : Quartz
Cpx : Clinopyroxene	Rf : Rock fragment
EP : Epidote	Ser : Sericite
Ga : Garnet	Sp : Sphalerite
Hb : Hornblende	Sph : Sphene



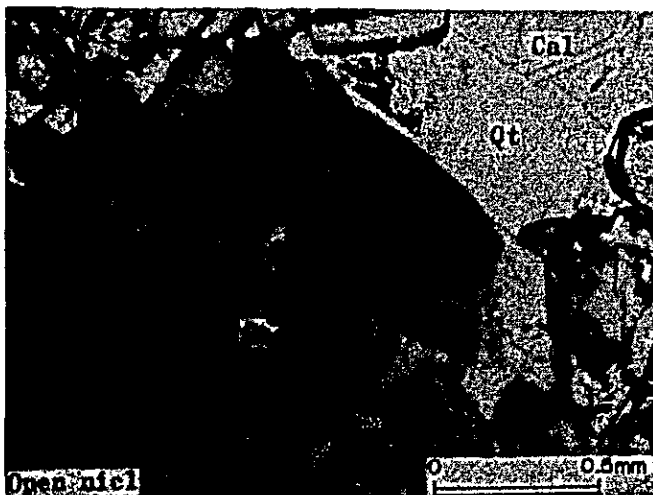
Sample No. NO-625

Rock Type : Andesite



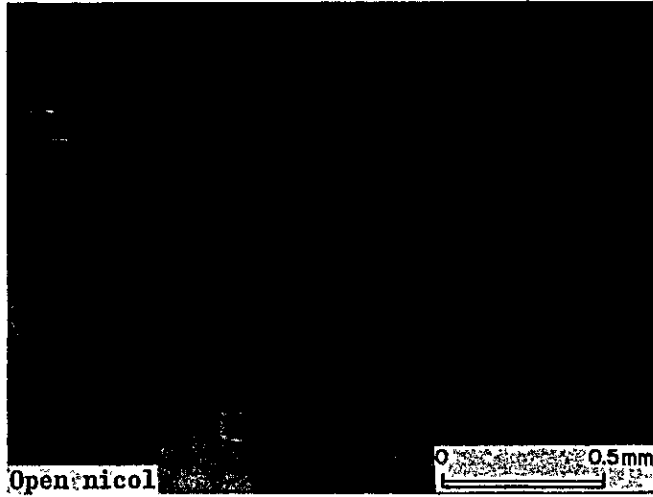
Sample No. NO-633

Rock Type : Granodiorite



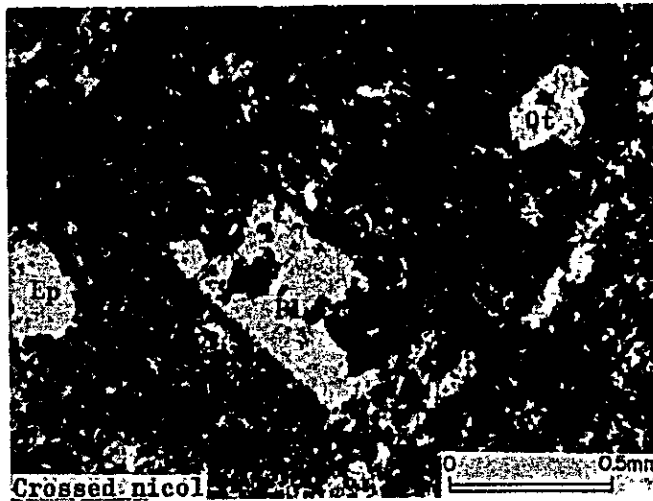
Sample No. NO-643

Rock Type : Sphalerite-
Pyrite ore



Sample No. NO-652

Rock Type : Granite porphyry



Sample No. SO-514

Rock Type : Dacite



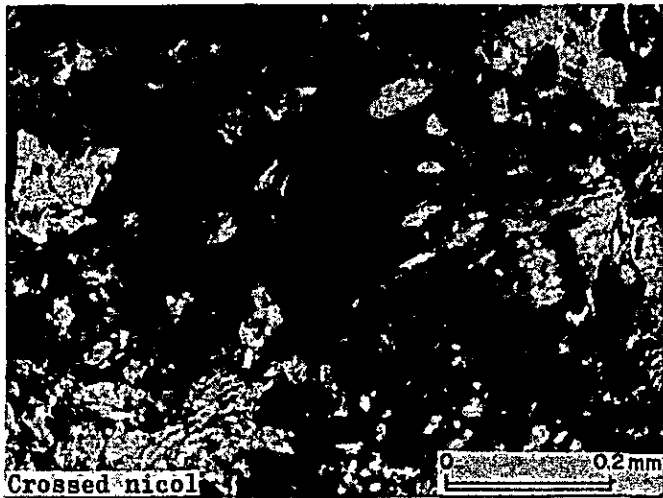
Sample No. SO-523

Rock Type : Granodiorite
porphyry



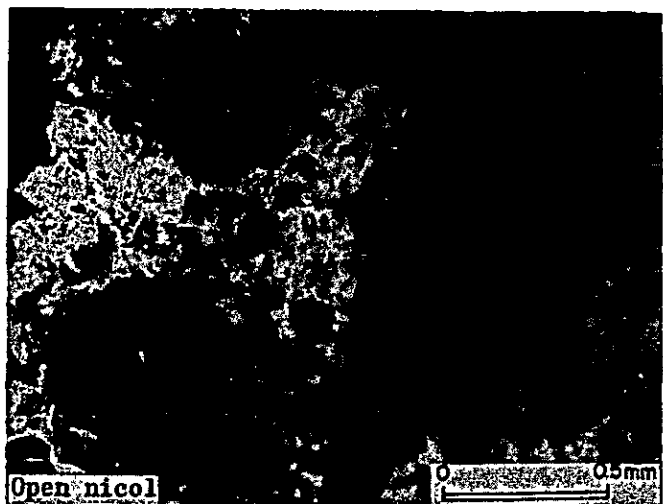
Sample No. IC-902

Rock Type : Brecciated rock



Sample No. CQ-353

Rock Type : Pyroxene skarn



Sample No. CQ-386

Rock Type : Garnet skarn

A. I - 4-2 Polished Section

Sample No.	Location	Geological Unit	Rock Type
NO-643	St	G4	Galena-sphalerite-pyrite ore
TO-506	St	G4	Galena-sphalerite ore
IC-705	St	IC-3	Chalcopyrite-sphalerite-hematite ore
IC-802	St	IC-3	Sphalerite-pyrite ore
IC-806	St	IC-3	Sphalerite ore
CQ-306	Ph	CQ	Galena-sphalerite-pyrite ore
CQ-356	Ph	CQ	Galena-sphalerite-pyrite ore
CQ-372	Ph	CQ	Sphalerite-pyrite ore
TP-307	Ph	G4	Chalcopyrite-sphalerite-magnetite ore
TP-312	Ph	G4	Sphalerite-pyrrhotite ore

Abbreviations

Asp	Arsenopyrite	Hm	Hematite
Bi-Pb	Bi-Pb-S system mineral	Mt	Magnetite
Cc	Chalcocite-Covellite	Po	Pyrrhotite
Cp	Chalcopyrite	Py	Pyrite
Cer	Cerussite	Sp	Sphalerite
G1	Galena		



Sample No. T0-506

Rock Type : G1-Sp ore



Sample No. IC-705

Rock Type : Cp-Sp-Hm ore



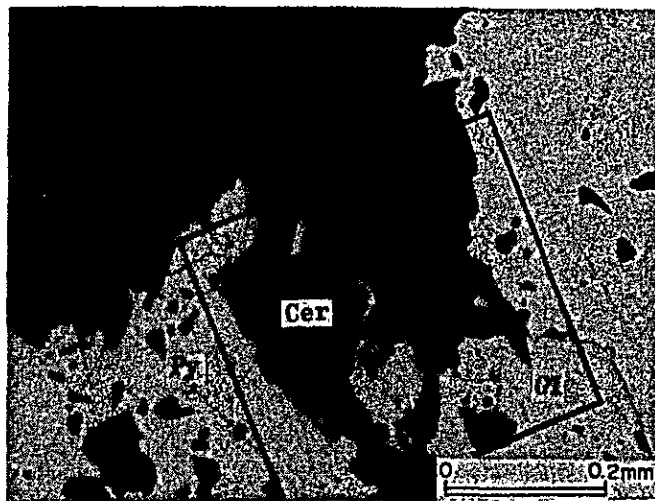
Sample No. IC-705

Rock Type : Cp-Sp-Hm ore



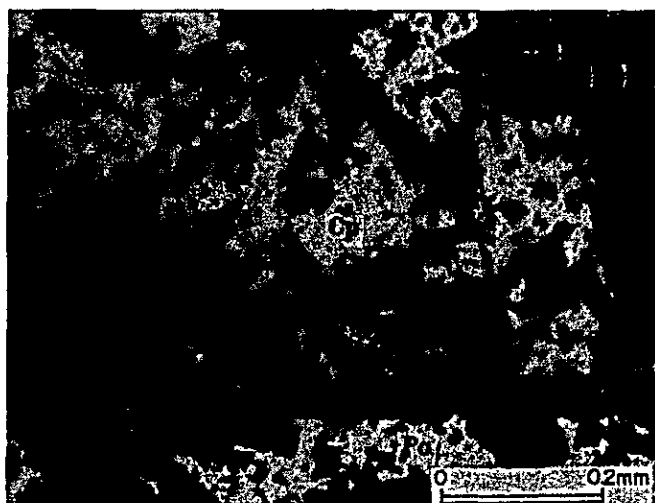
Sample No. CQ-356

Rock Type : G1-Sp-Py ore



Sample No. CQ-356

Rock Type : G1-Sp-Py ore



Sample No. TP-307

Rock Type : Cp-Sp-Mt ore

A. I - 4-3 EPMA Analysis

Sample No.	Result of EPMA Analysis
IC-705	Chalcopyrite-sphalerite-hematite ore
CQ-356(A)	Galena-sphalerite-pyrite ore
CQ-356(B)	Galena-sphalerite-pyrite ore

(EPMA : Electron probe microanalysis)

Abbreviations

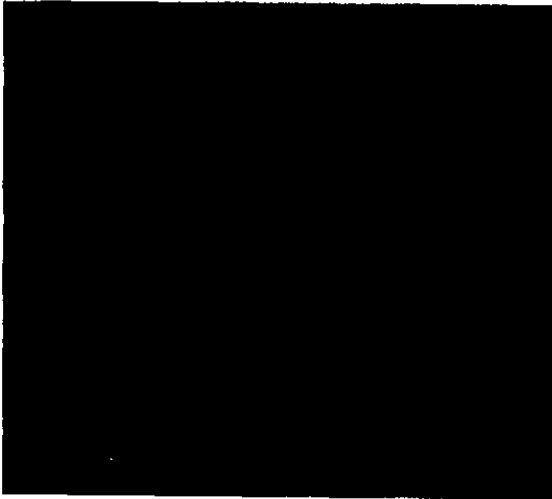
Gl: Galena

Cer: Cerussite

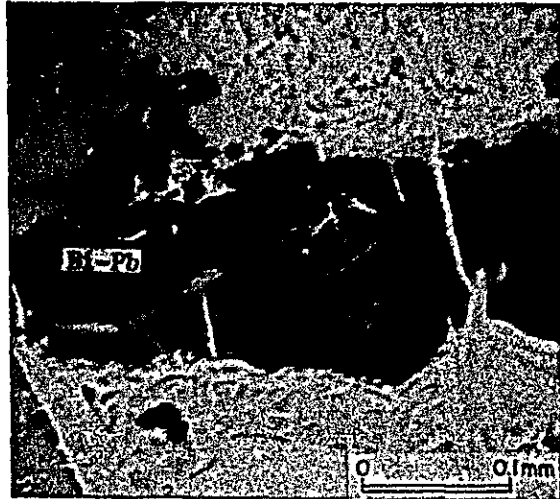
Asp: Arsenopyrite

Py: Pyrite

Bi-Pb: Bi-Pb-S system mineral



Ag X-ray image



Absorbed electron image



Cu X-ray image



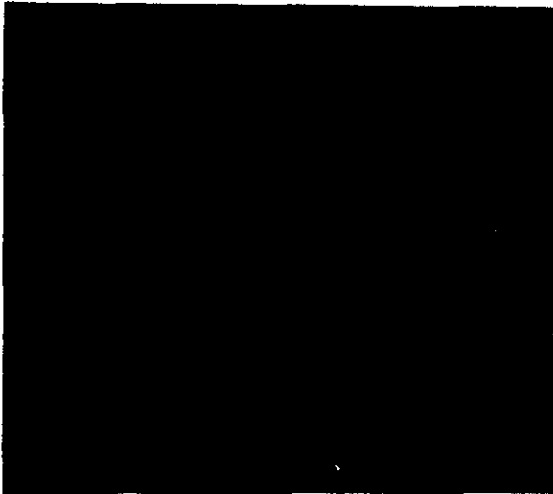
S X-ray image



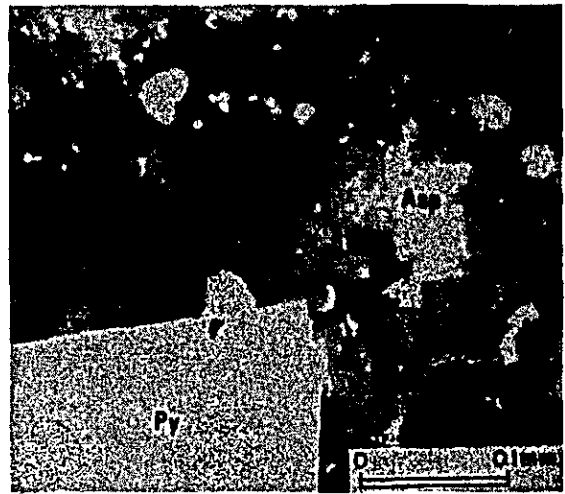
B: X-ray image



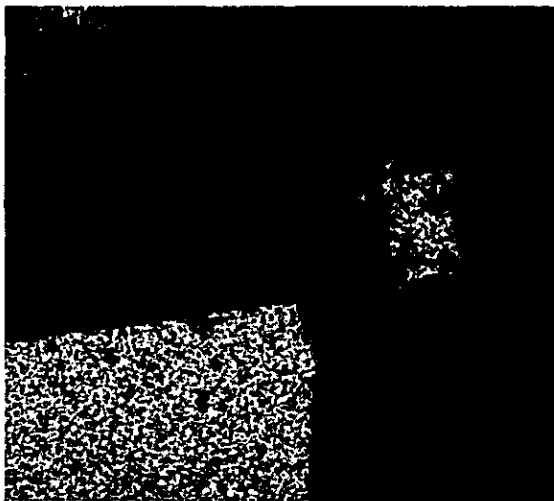
Fe X-ray image



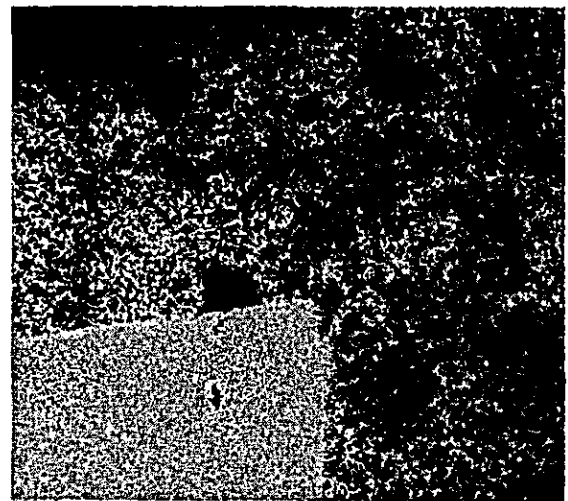
As X-ray image



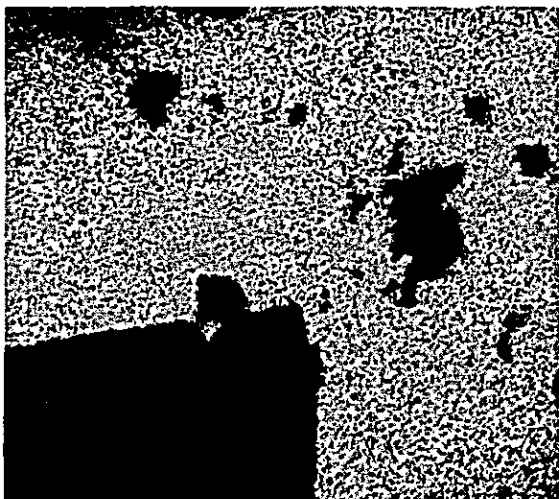
Absorbed electron image



Fe X-ray image

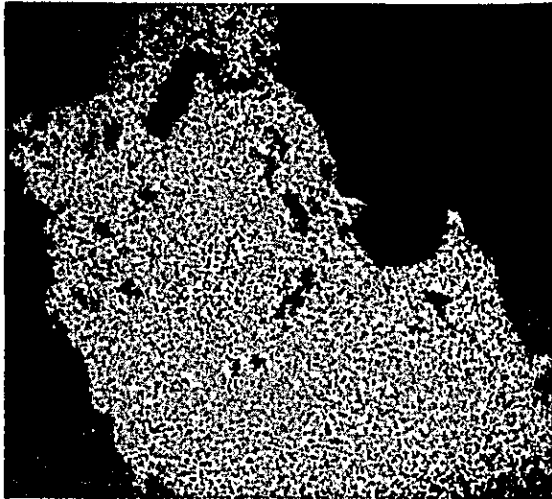


S X-ray image

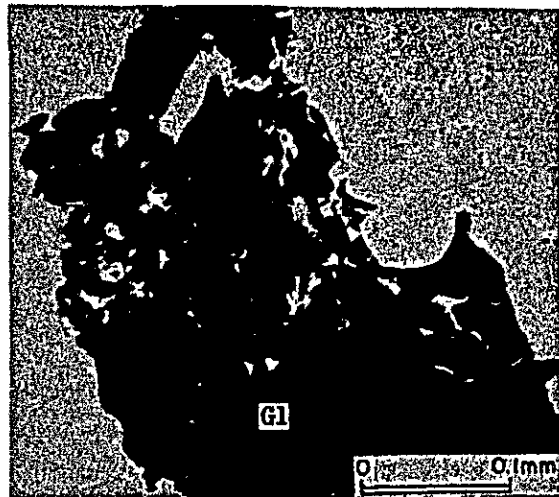


Pb X-ray image

Sample No. CQ-356(B)



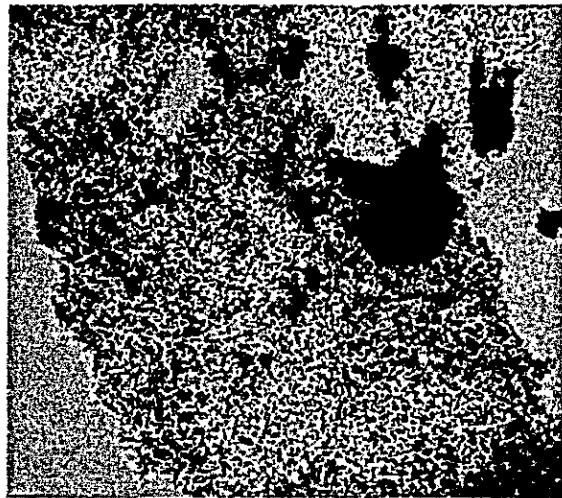
Pb X-ray image



Absorbed electron image



Zn X-ray image



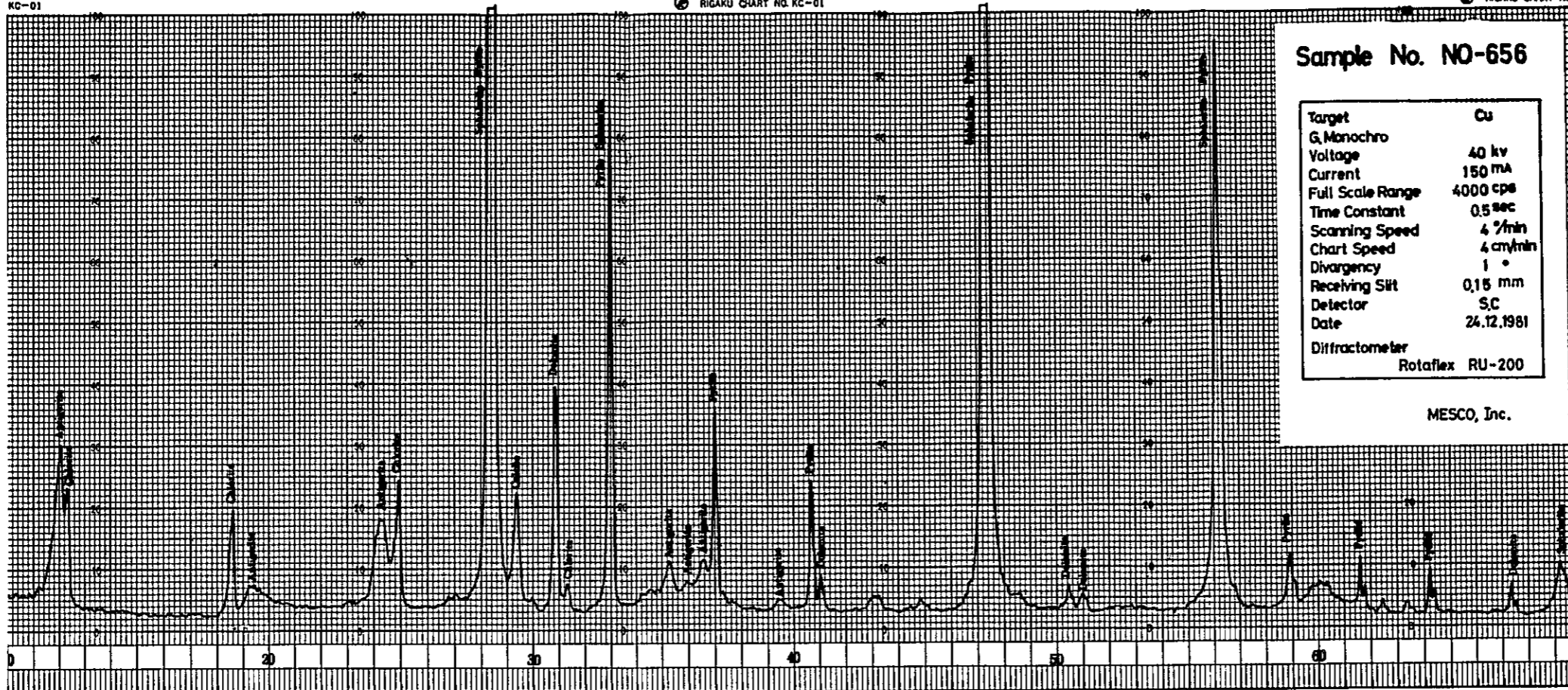
S X-ray image



Fe X-ray image



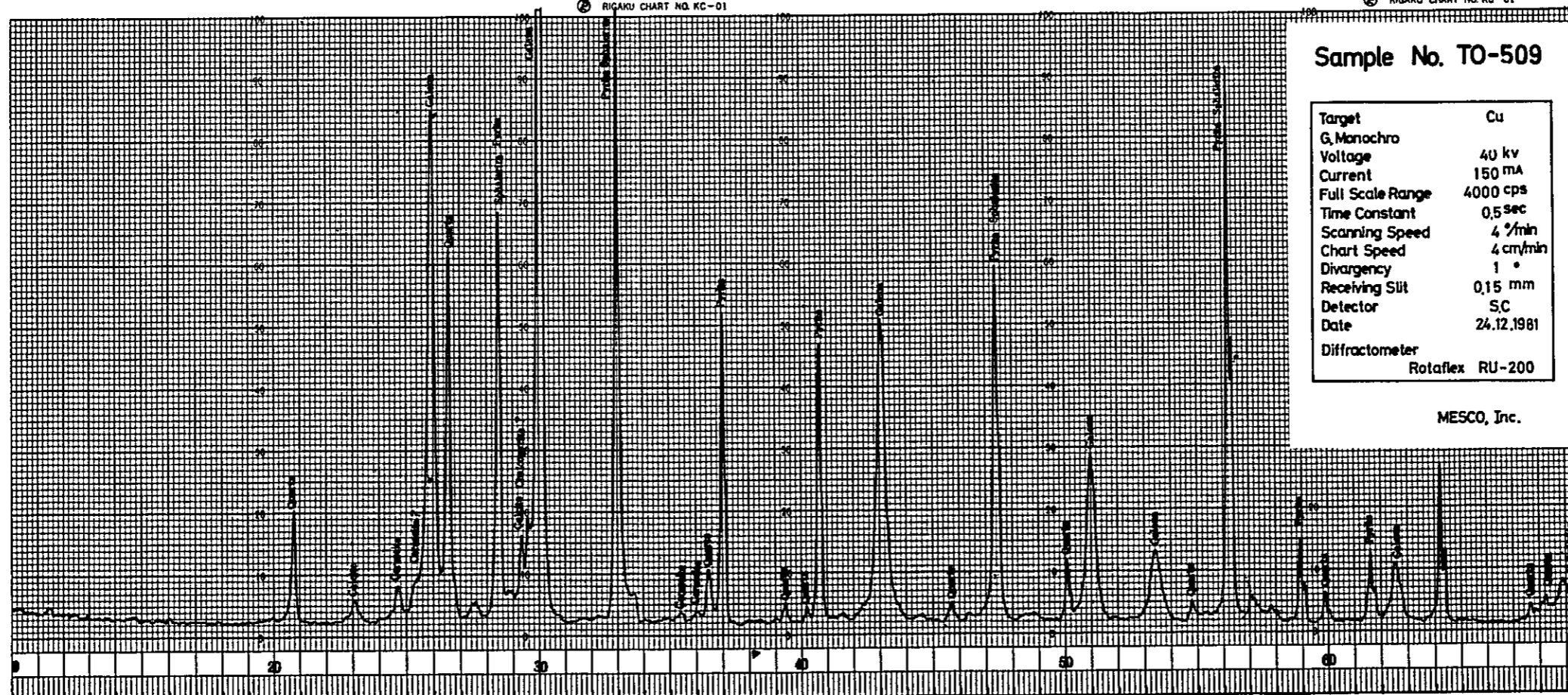
A. I-5 Charts of X-ray Diffraction Test



Sample No. NO-656

Target	Cu
G. Monochro	
Voltage	40 kv
Current	150 mA
Full Scale Range	4000 cps
Time Constant	0.5 sec
Scanning Speed	4 °/min
Chart Speed	4 cm/min
Divergency	1 °
Receiving Slit	0.15 mm
Detector	S.C
Date	24.12.1981
Diffractometer	Rotaflex RU-200

MESCO, Inc.



Sample No. TO-509

Target	Cu
G. Monochro	
Voltage	40 kv
Current	150 mA
Full Scale Range	4000 cps
Time Constant	0.5 sec
Scanning Speed	4 °/min
Chart Speed	4 cm/min
Divergency	1 °
Receiving Slit	0.15 mm
Detector	S.C
Date	24.12.1981
Diffractometer	Rotaflex RU-200

MESCO, Inc.